Propylene by Oxidative Dehydrogenation of Propane over Mixed Metal Oxide Catalysts

BY

Hassan Saeed Al-Asiri

A Thesis Presented to the

DEANSHIP OF GRADUATE STUDIES

KING FAHD UNIVERSITY OF PETROLEUM & MINERALS

DHAHRAN, SAUDI ARABIA

In Partial Fulfillment of the
Requirements for the Degree of

MASTER OF SCIENCE

In

CHEMICAL ENGINEERING

January 2011

KING FAHD UNIVERSITY OF PETROLEUM & MINERALS

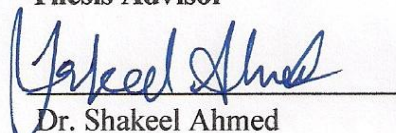# DHAHRAN, SAUDI ARABIA

DEANSHIP OF GRADUATE STUDIES

This thesis, written by **Hassan Saeed Ali Al-Asiri** under the direction of his thesis advisor and approved by his thesis committee, has been presented to and accepted by the Dean of Graduate Studies, in partial fulfilment of the requirements for the degree of MASTER OF SCIENCE IN **CHEMICAL ENGINEERING**

Thesis Committee

_____

Dr. Adnan M. Al-Amer

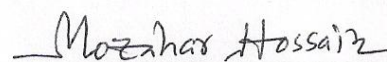**Thesis Advisor**

_____

Dr. Shakeel Ahmed

Co-advisor

_____

Dr. Reyad A. Shawabkeh

Member

_____
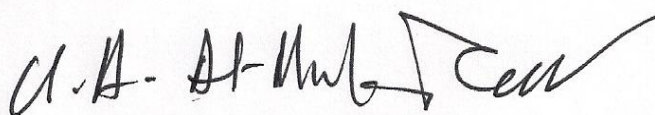
Dr. Eid M. Al-Mutairi

Member

_____

Dr. Mohammad M. Hossain

Member

_____

Dr. Usamah A. Al-Mubaiyedh

Department Chairman

_____

Dr. Salam Zummo

Dean of Graduate Studies

_____29|1|11_____

Date

ii

DEDICATION

This work is detected to my father, mother, wife and son.

ACKNOWLEDGEMENT

TABLE OF CONTENTS

LIST OF TABLES

LIST OF FIGURES

ABSTREACT

Name: **Hassan Saeed ALAsiri**

Thesis Title: **Propylene by Oxidative Dehydrogenation of Propane over Mixed**

Metal Oxide Catalysts

Major Field: **Chemical Engineering**

Date of Degree: January 2011

This research focuses on the oxidative dehydrogenation of propane (ODP) to propylene over molybdenum and vanadium oxide catalysts. The objective of this study is to investigate oxidative dehydrogenation of propane over MoV oxide catalysts and MoV supported on to MCM-41 catalysts and the evaluation of the catalysts in a fixed-bed reactor at temperatures of 350 to 600 °C. For this purpose, several catalysts of MoV oxide catalysts with varied compositions (Mo/V = 1/1, 7/3, 8/2 and 9/1) of molybdenum and vanadium are prepared by using a modified citrate-nitrate auto-combustion method. In addition, MV/MCM-41 catalysts with Mo/V = 1/1 and different metal loadings (5, 10, and 15 %) are prepared by using an impregnation method. The catalysts are characterized by using a BET technique, temperature programmed reduction (TPR), X-Ray Diffraction (XRD), Raman spectroscopy, and UV spectroscopy. The effects of washing and super critical drying (SCD) on unsupported catalyst were investigated. There was an interaction between the molybdenum and vanadium metal in all of the catalysis due to the presence of a peak at 785 cm^{-1} , which was assigned to polymolybdovanadate species V-O-Mo vibration in the Raman study. This interaction could be efficient for alkane activation. In the unsupported catalysts, the better catalyst activity was MoVOx-2 (SCD) with Mo/V ratio 1/1. The comparison between supported and unsupported catalysts that have same ratio of Mo/V (1:1) was studied, and revealed that the supported catalysts are more active than unsupported catalysts. Both type of catalysts showed 100% selectivity for propylene in the range of 350 – 450 °C. However, propylene selectivity decreased with increasing the temperature. The highest yield of 6.05% with 100% propylene selectivity was obtained for 15MV/MCM-41at 450 °C.

Master of Science Degree

King Fahd University of Petroleum & Minerals

Dhahran, Saudi Arabia

January, 2011

خـــلاصــــة الرســـــــالة

اسم الطالب : حسن سعيد العواض العسيري

عنوان الرسالة: البروبيلين بواسطة نزع الهيدروجين من البروبان عن طريق الأكسدة بأستخدام محفز من مزيج مختلط من اكسيد المعدن

التخصص: هندسه كيميائيه

تاريخ الرساله: يناير ٢٠١١م

هذا البحث يركز على نزع الهيدروجين من البروبان عن طريق الأكسدة لأنتاج البروبيلين بأستخدام محفزات أكسيد الموليبدينوم والفاناديوم. الهدف من هذه الدراسة هو تحقيق نزع الهيدروجين من البروبان عن طريق الأكسدة على المحفزات المدعومه وغير المدعومه وتقييم المواد الحفازة في مفاعل عند درجة حرارة ٣٥٠ حتي ٦٠٠ درجة مئوية. لهذا الغرض، تم اعداد عدد من المحفزات التي تحتوي علي الموليبدينوم والفاناديوم بنسب مختلفه باستخدام نترات السيترات للأحتراق الذاتي. بالاضافه الي ذالك تم اعداد عينات اخرى من المحفزات المدعومه بالسلكا تحتوي علي نفس النسبه من الموليبدينوم والفاناديوم باستخدام اسلوب التشريب. تم ايضا دراسة المساحه السطحيه للمحفزات و دراسة المحفزات عن طريق الاختزال الحراري و رامان الطيفي و التحليل الطيفي لأشعه فوق البنفسجيه و الاشعه السينيه. غسل المحفزات الغير مدعومه بالكحول وتجفيفه باستخدام المجفف السوبر اظهرت نتائج كبيره في نشاط المحفزات.المحفز الذي يحتوي علي نفس نسبة الموليبدينوم والفاناديوم هو افضل نشاط محفز من بين المحفزات الغير مدعومه. وأظهرت المقارنه بين المحفزات المدعومه و غير المدعومه بان المحفزات المدعومه اكثر نشاط من غيرها.واظهر النوعان من المحفزات ١٠٠ ٪ من الانتقائيه البروبيلين بين ٣٥٠ و ٤٥٠ درجة مئوية و انخفاض انتقائيه البروبيلين عندي زيادة درجة الحرارة . وافضل انتاجيه كانت للمحفز المدعوم الذي يحتوي علي ١٥٪ من الموليبدينوم والفاناديوم مع١٠٠٪ من الانتقائيه البروبيلين عند ٤٥٠ درجة مئوية.

درجة الماجستير في علوم الهندسه الكيميائيه

جامعة الملك فهد للبترول والمعادن

الظهران- المملكه العربيه السعوديه

يناير ٢٠١١م

CHAPTER 1

1. Introduction

1.1 Introduction

The demand for alkenes (olefins), especially ethylene and propylene, has been growing rapidly, and this demand is most likely to keep on increasing. Alkanes (parffins) are attractive chemical feedstocks because they are relatively inexpensive and abundant. The steam cracking, fluid-catalytic-cracking, and catalytic dehydrogenation are the major processes to produce alkenes from alkanes. These processes have been widely used (Cavani et al., 2007). On the other hand, to meet rising demand for alkenes, an intense research activity is taking place to develop the oxidative dehydrogenation ODH catalysts. There is potential to produce a range of light alkenes by using (ODH) of alkanes (Kumar et al., 2008).

In the case of steam cracking, ethylene is the favored product, but the demand for propylene is rising more rapidly than ethylene (Taylor et al., 2009). Since the 1980s, the catalytic dehydrogenation of propane could be used for producing propylene, which is scientifically attractive (Wolf et al., 2001). However, all of these processes (steam cracking, FCC, and Dehydrogenation) tolerated several limitations such as thermodynamic limit on conversion and selectivity, side reactions, strong endothermic main reaction and requirements to provide heat at high temperature and coke formation. The oxidative dehydrogenation (ODH) of alkanes may overcome some of the restrictions mentioned above. The reaction is attainable at much lower temperatures because it is

exothermic. It minimizes the side reactions, for instance coke formation and cracking of alkanes, over and above overcomes the thermodynamic limitations (Grabowski 2007). Grabowski (2007) divided the type of catalysts used in ODH of light alkanes into three categories:

1. Catalysts based on alkali and alkaline earth ions and oxides

2. Catalysts based on reducible transition metal oxides

3. Other catalysts such as B/P oxides, Ga/zeolite, LaF_3/SmO, and Sn/P.

In recent years, considerable research efforts are focusing on the oxidative dehydrogenation of propane (ODP) to propylene. Propylene is an important chemical feedstock that is in demand mainly for production of polypropylene, acrylic acid acrylonitrile and iso-propanol. In addition, propylene can be used as a fuel for isomerization of isobutane (Wolf et al., 2001). The reactions network of propane (ODP) is shown in Figure1.1. The propane reacts with oxygen to form propylene and CO_x with a rate constant k_1 and k_2, respectively. With the consequent oxidation, the propylene converts to CO_x with a rate constant k_3. High values of k_1 and small values of k_2/k_1 and k_3/k_1 ensure high propylene yields (Argyle et al, 2002).

The scope of this research is to develop MoV oxide catalysts at different compositions of vanadium and molybdenum suitable for oxidative dehydrogenation of propane in a fixed bed reactor.

$$O_2 + C_3H_8 \xrightarrow{\quad k_1 \quad} C_3H_6 + O_2$$
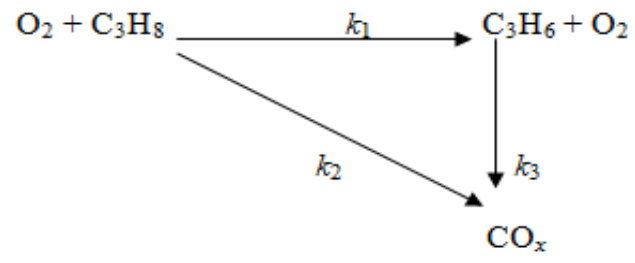
Figure 1.1 Reaction network of propane conversion.

1.2 Objectives

The aim of this study is to develop MoV oxide catalysts suitable for oxidative dehydrogenation of propane. The specific objectives are the following:

- Preparation of MoV oxide catalysts with varied compositions of vanadium and molybdenum and preparation of MoV supported on to MCM-41.

- Characterization of the prepared catalysts by temperature programmed reduction (TPR), BET surface area and pore volume, XRD Raman spectroscopy and UV spectroscopy.

- Performance evaluation of prepared catalyst in a fixed bed reactor.

CHAPTER 2

2. Literature Review

2.1 Literature Review of Catalysts

Various materials have been tested for their potential catalytic improvement of ODP. However, the maximum propylene yield has not exceeded 30%, which makes the oxidative dehydrogenation process continue to fall short from industrial commercialization. A brief overview of the most prominent catalyst materials explored is presented here.

2.1.1   Vanadium Catalyst

In the oxidative dehydrogenation of propane, MCM-41-supported vanadia catalysts were active and selective. The catalytic of MCM-41-supported vanadia samples (V loading from 0.6 to 10 wt %) were tested at a temperature of 550 °C by Solsona (2001). Among the percent of loading, the 2V/MCM showed the highest selectivity, 61.6%, and the yield was 6.8% (Solsona et al., 2001). Vanadium-containing the hexagonal mesoporous silicas (HMS) catalysts were investigated for the oxidative dehydrogenation (ODH) of propane. It has been verified that the vanadium supported HMS catalysts showed greater upper catalytic activity than the literature supports from outcomes obtained over the vanadium supported MCM-41 catalysts in the ODH of propane. In addition, 1.68V-HMS-imp obtained 34.5% conversion of C_3H_8, 34.7% selectivity of C_3H_6 and 11.9% yield at 500 °C (Zhou et al., 2001). The effect of rare earth (Y, La, Ce) oxides on hexagonal mesoporous silicas (HMS) silica supported vanadia

catalysts have been studied. It has been demonstrated that the doping of Y, La oxides into the V-HMS catalyst exhibited a much higher selectivity to propylene than the Ce oxide in the ODH of propane (Zhou et al., 2002). Vanadium oxide, supported by siliceous ITQ-6 catalysts, has been investigated in the oxidative dehydrogenation of propane. It was prepared by a zeolite precursor for the Ferrierite-type structure. The best catalyst was 1V/ITQ6 with 11.2 % yield at 550 °C (Solsona et al., 2006). V-doped zirconia-pillared montmorillonites have been obtained by different methods. The highest values of selectivity and yield for V(Zr)-PILC were 32% and 7.1 %, respectively (Bahranowski et al., 2000).

Vanadium and niobium oxides supported on TiO2 (V- 6Nb/TiO2) were developed in the oxidative dehydrogenation (ODH) of propane. The propylene selectivity, conversion of propane, and yield of propylene were 36.6%, 20.9% and 7.7% respectively at 400 °C (Viparelli et al 1999). V-Nb-O, Mo-Nb-O, Te-Nb-O, and V-Mo-Te-Nb-O mixed metal oxides were studied by Zhao (2003), and their activity increased as follows:

$$V\text{-}Nb\text{-}O > Mo\text{-}Nb\text{-}O > Nb_2O_5 > Te\text{-}Nb\text{-}O$$

The 10% V-Nb-O had 3.03% conversion of propane and 67.6% selectivity of propylene at 400 °C (Zhao et al., 2003). In addition, the effect of various Nb precursors in mixed Nb–V oxide systems was investigated by Sarzi-Amade (2005). To prepare Nb/V mixed oxides systems as probable catalysts for propane ODH, the hydrolytic sol–gel method was used. The 9:1 Nb/V sample showed low activity and higher selectivity to propylene at rising propane conversion, and the 1:1 Nb/V samples showed lower activity and

6

selectivity to propylene than the 4.5:1 Nb/V sample. The highest conversion, selectivity, and yield for the 4.5:1 Nb/V sample were 19.4%, 47.4%, and 9.2%, respectively, at 550 °C (Sarzi-Amade et al., 2005). Also, the mixed oxide systems 1:1 Nb-V, 1:1 Sb-V, 1:2:1 Nb-V Sb, 1:1:1 Nb-V-Mo, and 1:1:5 Nb-V-Si were tested by Pietro Moggi (2003). The 1:1 Sb-V was active in the propane ODH and selective to propylene at 550 °C, and it had 13% yields (Moggi et al., 2003). Stelzer (2005) prepared V/Sb/O-TiO$_2$ by applying different VOx precursors, and the catalysts were calcined in air and nitrogen at 500 °C. The catalytic performance of the catalysts with 10% V and calcined with N$_2$ showed high activity with 11% propylene yields at 25% propane conversion (Stelzer et al., 2005).

Sugiyama (2006) prepared Calcium hydroxyapatites, substituted with vanadate V–CaHAp. The catalytic of vanadate-substituted calcium hydroxyapatites for oxidative dehydrogenation of propane was active, and the conversion for propane and the selectivity for propylene were 16.5% and 54.2%, respectively, on calcium hydroxyapatite (Sugiyama et al., 2006). Cortez (2003) discussed catalytic activity of different potassium loading which was prepared by a different method for the ODH of propane as a function of reaction temperature. With increased potassium content, the yield to propylene reached a maximum yield for 3% Potassium at 475 °C, and the conversion was 23% (Cortez et al., 2003). The catalytic performance of vanadia catalysts supported on Al$_2$O$_3$, TiO$_2$, ZrO$_2$ and MgO and Addition of alkali metals (Li, Na and K) to V$_2$O$_5$/Al$_2$O$_3$ catalyst were tested by Lemonidou (2000). Comparing catalysts on different supports, catalysts supported on titania were most active, and V$_2$O$_5$/Al$_2$O$_3$ was the most selective in propylene. The addition of alkali metals (Li, Na and K) to V$_2$O$_5$/Al$_2$O$_3$ catalyst reduced the catalytic

activity in ODP in the order Li>Na>K and the conversion and the selectivity went down as follows (Lemonidou et al 2000):

$$VAl_2O_3 > VTiO_2 > VZrO_2 > VMgO$$
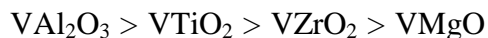
Machli and Lemonidou (2005) studied the effect of magnesia loading in the vanadia on titania catalyst, and it showed interesting results in terms of selectivity to the desired product propylene. The selectivity significantly increased with the existence of MgO on vanadia catalyst. At low loading of magnesia, the loss in activity could be decreased, and also the series of Mg introduction affected the activity. The best catalytic Performance was the 5 wt% vanadia on titania catalyst promoted with 1.9 wt% MgO (5V–1.9Mg–Ti) which was prepared by sequential deposition of first MgO and then V_2O_5 on TiO_2 (Machli & Lemonidou, 2005).

Ni–V–O catalysts for the oxidative dehydrogenation (ODH) of propane were investigated by Zhaorigetu (2004). The $Ni_{0.9}V_{0.1}O_Y$ catalyst showed the highest activity at 425 °C with 49.9% selectivity of C_3H_6 and the 19.4% conversion C_3H_8 (Zhaorigetu et al., 2004). V–Mg–O catalysts were prepared by solid reaction (the mix-VMg catalysts) or from mesoporous precursors (the meso-VMg catalysts), and they were used in a fixed-bed tubular flow reactor at 350 and 450 °C. The meso-VMg catalysts had higher selectivities and yields to propylene than the mix-VMg. At 450 °C, a C_3H_6 selectivity of 80.61% was observed on meso-VMg-3 at a C_3H_8 conversion of 11.50 % with 9.27% yields (Chao & Ruckenstein, 2004).

The catalytic behavior of samarium VO_4 ($SmVO_4$) impregnated with vanadium in the oxidative dehydrogenation of propane were developed by Barbero and Cadus (2003).

Catalysts with 3% vanadium (3-V/SmVO$_4$) were highly active; the conversion to propane was 31.27 %, and the selectivity and yield to propylene were 26.86 % and 8.40%, respectively, at 500 °C (Barbero & Cadus 2003). Zinc-modified, γ-Al$_2$O$_3$ supported vanadium oxides for the oxidative dehydrogenation of propane was investigated and were prepared by dry impregnation and co-precipitation methods. For VZnO/Al by impregnation method at 350 °C, the conversion of propane was 8.7 % and the yield and selectivity of propylene were 3.5% and 40.7 %, respectively (Mattos et al., 2002). A series of ceria-supported vanadium catalysts was studied by Daniell (2002). The ceria support material itself yielded the maximum propane conversion, while this showed, basically, no selectivity towards propylene. The best result was obtained on 6wt% V$_2$O$_5$/CeO$_2$ catalyst with yields of 4.2% (Daniell et al., 2002).

A VO$_X$/CeO$_2$ catalyst was prepared and was experimentally tested with different vanadium loading by Taylor (2009), and this percent difference of V loading on the ceria support influenced the propane conversion. The performance of catalyst depended on the V loading. At 2.5% V/CeO$_2$ (with high dispersion V species), the highest yield was obtained (3.7%). The conversion and selectivity were 4.2 and 89 respectively. For 30% V/CeO$_2$ (formation of a mixed cerium–vanadium phase), the highest selectivity obtained (97%). The conversion and yield are 3.7 and 3.6 respectively. A poor result was obtained at 10% V/CeO$_2$ (Taylor et al., 2009).

Mishakov (2009) synthesized VOx/MgO aerogel catalysts by using three different preparation methods: by mechanical mixing VO$_x$/MgO-AP(MM), by impregation VO$_x$/MgO-AP(imp-20), and by aerogel method [VO$_x$/MgO]-AP. From this study, the catalyst that was prepared by mechanical mixing VO$_x$/MgO-AP(MM) showed a lower

activity than VO_x/MgO-AP(imp-20) and $[VO_x/MgO]$-AP. Although, VO_x/MgO-AP(imp-20) catalyst obtained high activity, it had less selectivity and propane conversion. The $[VO_x/MgO]$-AP had the best results when it was compared with the other results. For $[VO_x/MgO]$-AP, when the temperature increased, the conversion increased also, but the selectivity of C_3H_6 decreased because the propene was converted on surface acid sites to carbon oxides to form the desired reaction. At higher temperature the yield increased, and the highest yield was 8.4 at T = 550 C (Mishakov et al., 2009).

In 2009, Karakoulia et al. used vanadia catalysts supported on mesoporous silicas, and the results showed that activity was

4V-HMS >4V-MCF» 4V-SiO2

The HMS exhibited much higher activity compared to the 4V-SiO$_2$ due the lower degree vanadia dispersion in 4V-MCF and 4V-SiO$_2$ because of the partial destruction of the mesopore structure and respective loss of surface area during the preparation of the catalysts. Selectivity of propene decreased with increasing propane conversion due to the consecutive oxidation of the olefin to a mixture of CO and CO_2 (Karakoulia et al., 2009).

Sugiyama (2008) discussed the oxidative dehydrogenation of propane over vanadium catalyst supported on calcium and strontium hydroxyapatites at different loading percentages of vanadium ($VO_x/CaHAp$ and $VO_x/SrHAp$), and they were compared with $Mg_2V_2O_7$. 5%$VO_x/SrHAp$ catalyst, revealing the highest conversion, selectivity and yield (13%), (60.7%), and (7.9%), respectively, when it was compared with other different loading, also with the groupings of $VO_x/CaHAp$ and $Mg_2V_2O_7$. The

higher loading vanadate increased the activity of VO$_x$/CaHAp catalyst (Sugiyama et al., 2008).

The vanadium oxide supported on mesocellulous silica foams (MCF) for the oxidative dehydrogenation of propane was prepared with a different percent of vanadium by the Yong- Liu group (2006), and it was also compared with other catalysts (2.8V-SBA, 4.5V-MCM and 1.8V-SiO$_2$) that were done by the same group. The 4.2V-MCF catalyst had the best result when it was compared with other V loading percentages, in addition to 2.8V-SBA, 4.5V-MCM and 1.8V-SiO$_2$. It had the highest yield (27.9), and the conversion and selectivity were 40.8 and 68.5, respectively (Liu et al., 2006).

The best catalysts performances in each study are summarized in Table 2.1 which contains the name of catalyst, temperature, selectivity, and conversion of vanadium catalysts.

Table 2.1 Catalyst, temperature, selectivity, and conversion of vanadium catalysts.

No.	Catalyst	T(°C)	C_3H_8 Conversion (%)	C_3H_6 Selctivity (%)	CO_2 Selctivity (%)	CO Selctivity (%)	C_3H_6 Yield (%)	References
1	2V/MCM	550	11.1	61.6	8.9	16.9	6.8	Solsona et al., 2001
2	1V/ITQ6	550	21.1	53.1	11.2	22	11.2	Solsona et al., 2006
3	V(Zr)-PILC	420	22	32	NA	NA	7.1	Bahranowski et al., 2000
4	10% V-Nb-O	400	3.03	67.6	NA	NA	2	Zhao et al., 2003
5	4.5:1 Nb/V	550	19.4	47.4	NA	NA	9.2	Sarzi-Amade et al., 2005
6	1:1 Sb-V	500	34	38	39	NA	13	Moggi et al., 2003
7	10%V/Sb/O-TiO$_2$	500	24.5	43.6	18.2	30.9	10.7	Stelzer et al., 2005
8	V–CaHAp	450	16.5	54.2	NA	NA	8.9	Sugiyama et al., 2006
9	V–3%K–O/Al$_2$O$_3$	470	23	47.8	4	7	11	Cortez et al., 2003
10	VAl2O$_3$	500	20.3	39.8	Co$_x$ = 60.2		8.1	Lemonidou et al., 2000
11	VTiO$_2$	500	30.4	22.8	Co$_x$ = 77.0		6.9	Lemonidou et al., 2000
12	5V–1.9Mg–Ti	500	28	44	NA	NA	12.3	Machli and Lemonidou 2005
13	V- 6Nb/TiO$_2$	400	20.9	36.6	21.1	41.8	7.7	Viparelli et al., 1999
14	Ni0.9V0.1OY	425	19.4	49.9	13	3	9.7	Zhaorigetu et al., 2004
15	meso-VMg-3	450	11.5	80.61	0	0	9.27	Chao and Ruckenstein 2004
16	1.68V-HMS-imp	500	34.5	34.7	29.6	31.7	11.9	Zhou et al., 2001
17	3-V/SmVO4	500	31.27	26.86	NA	NA	8.4	Barbero and Cadus 2003
18	VZnO/Al	350	8.7	40.7	36.5	22.1	3.5	Mattos et al., 2002
19	6wt% V$_2$O$_5$/ CeO$_2$	400	11.4	36.8	NA	NA	4.2	Daniell et al., 2002
20	2.5% V/CeO$_2$	450	4.2	89	NA	NA	3.7	Taylor et al., 2009
21	[VOx/MgO]-AP	550	30	28	Co$_x$ = 70		8.4	Mishakov et al., 2009
22	4V-HMS	600	40	47	NA	NA	19	Karakoulia et al., 2009
23	5%VO$_x$/SrHAp	450	13	60.7	22.6	16.7	7.9	Sugiyama et al., 2008
24	4.2V-MCF	550	40.8	68.5	Co$_x$ = 21.1		27.9	Liu et al., 2006

2.1.2 Molybdenum Catalysts

A series of chlorine-modified molybdenum catalysts supported on silica and titania (Si:Ti) mixed oxides have been prepared and characterized for ODH of propane by a modified sol–gel technique. At a temperature of 550∘C, the results showed that the highest catalytic yield (25.7%) was attained with the 10%Mo/Si:Ti = 1:1 and Cl/Mo = 2, with a propylene of selectivity 45.0% and the conversion of propane 57.2% (Liu et al., 2006). Alumina-supported chromium– molybdenum oxides catalysts were prepared to test the performance of the catalysts for the oxidative dehydrogenation (ODH) of propane. In addition, the effect of Alkali metals (Li, K, Cs) addition to catalyst samples was also studied. Catalyst (Cs/CrMo = 0.125) was active, and the conversion to propane was 15.1% , and the selectivity to propylene was 64.5% at 420 °C (Jibril et al., 2003a). Catalytic oxidative dehydrogenation of propane to propylene research has studied the effect of potassium loading on the structural and catalytic properties of $MoO_x/ZrO2$ catalysts. The catalysts were prepared by modified sol–gel method, and the addition of potassium prevented crystalline $Zr(MoO_4)_2$ formation. One of the catalysts (K015 MoO_x/ZrO_2) was shown propane conversion of 43% and yield to propylene of 10.9% at 530 °C (Koc et al., 2005). The effects of 3 vol. % of CO_2 added in the gas feed on $NiMoO_4$ catalysts for oxidative dehydrogenation of propane was investigated. The propane conversion was 12.8%, and selectivity to propylene was 29.7% at 450 °C for $NiMoO_4$ catalyst without adding CO_2 (Dury et al., 2003). Catalysts based on a physical mixture of Ga_2O_3 and MoO_3 were investigated in the oxidative dehydrogenation of propane (ODP) to propene. This work shows that Ga_2O_3/MoO_3 calcined was among the most promising catalysts reported for propane oxidative dehydrogenation. Both

propylene selectivity and yield were 62 % and 5.7 %, respectively, at 470 °C (Davies & Taylor, 2004). Alumina-supported chromium oxide and binary mixed oxide catalysts of the form Cr–Mo-Al$_2$O$_3$ have been prepared and evaluated for ODP at reaction temperature range (300–450 °C). The CrMo(4 : 1) catalysts demonstrated propane yields greater than 5 % with propane conversion of 10.1% and propylene selectivity at 51.2% (Jibril et al., 2003b). Mo/Al$_2$O$_3$ catalysts with 13wt% of MoO$_3$ and promoted with Cr were found to catalyze the oxidative dehydrogenation of propane. Catalytic activity measurements have been carried out between 350 and 500 °C under atmospheric pressure. It was observed that the conversion was 31.9% and the selectivity was 23.4 % at 500 for 3CrMo/Al$_2$O$_3$ catalyst. It also exhibited a propylene yield of 7.5% (Abello et al., 2003). Oxidative dehydrogenation of propane has been studied on Mg-Mo-O catalysts by Cadus. At 550 °C, the conversion was 5.8% in addition to the selectivity to propene, which was 94.4% for (1/1)MgMoO (Cadus et al., 1996).

The best catalysts performances in each study are summarized below in Table 2.2, which contains the name of catalyst, temperature, selectivity, and conversion of molybdenum catalysts.

Table 2.2 Catalyst, temperature, selectivity, and conversion of molybdenum catalysts.

No.	Catalyst	T(°C)	C_3H_8 Conversion (%)	C_3H_6 Selctivity (%)	CO_2 Selctivity (%)	CO Selctivity (%)	C_3H_6 Yield (%)	References
1	10%Mo/Si:Ti = 1:1 Cl/Mo = 2	550	57.2	45	NA	NA	25.7	Liu et al., 2006
2	Cs/CrMo = 0.125	425	15.1	64.5	NA	NA	9.7	Jibril et al., 2003a
3	K015 MoOx/ZrO2	530	43	25.3	NA	NA	10.9	Koc et al., 2005
4	$NiMoO_4$	450	12.8	29.7	52.9	NA	3.8	Dury et al., 2003
5	Ga_2O_3/MoO_3	470	9.9	62	NA	NA	5.7	Davies & Taylor 2004
6	CrMo(4 : 1)	350	10.1	51.2	48	14.9	5.2	Jibril et al., 2003b
7	3CrMo/Al2O3	500	31.9	23.4	37	38.2	7.5	Abello et al., 2003
8	(1/1)MgMoO	550	5.8	94.4	5.6	0	5.5	Cadus et al., 1996

2.1.3   Vanadium and Molybdenum Catalysts

The catalytic performance of vanadia and molybdena catalysts with monolayer coverage supported on alumina and titania have been investigated to explain the differences in catalytic behavior in the oxidative dehydrogenation of propane to propene. The activity of metal oxide and the support used decreases as shown in the following series:

5VTi>14VAl > 5MoTi > 15MoAl.

Figure 2.1 shows the Propene selectivity as a function of propane conversion at 500 °C (Heracleous et al., 2005).
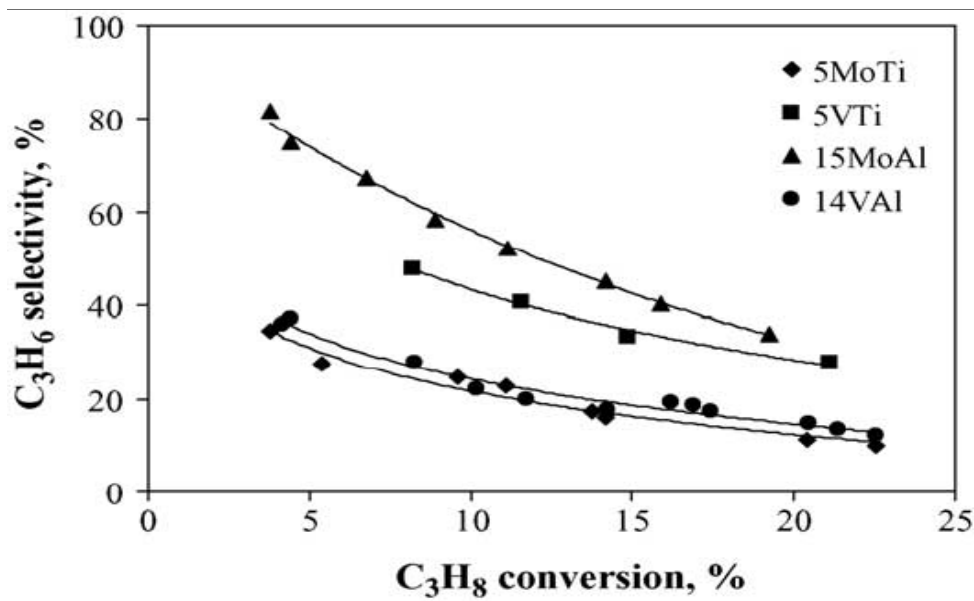
Figure 2.1 Selectivity conversion profiles at 500 °C (Heracleous et al., 2005).

The catalytic performance of vanadia dispersed on alumina containing a nominal polymolybdate monolayer in the oxidative dehydrogenation (ODH) of propane was studied. The catalyst activity and selectivity for propane ODH to propene increased as the dispersion of VOx on alumina containing a monolayer equivalent of molybdena because the formation of V–O–Mo bonded between the dispersed vanadia and the molybdena layer (Dai et al., 2004).

The oxidative dehydrogenation (ODH) of propane was investigated for the interactions between Mo and V on alumina. The activity and selectivities on these catalysts were compared with those on vanadium and molybdenum dispersed on alumina. All catalyst were prepared at a constant Mo/V = 1 atomic ratio with different Mo + V loadings, and the catalysts were xMoVAl, or xMoAl or xVAl, where x the summation of

(Mo + V) monolayer. The performances of these catalysts are shown in Figure 2.2 (Banares & Khatib, 2004).
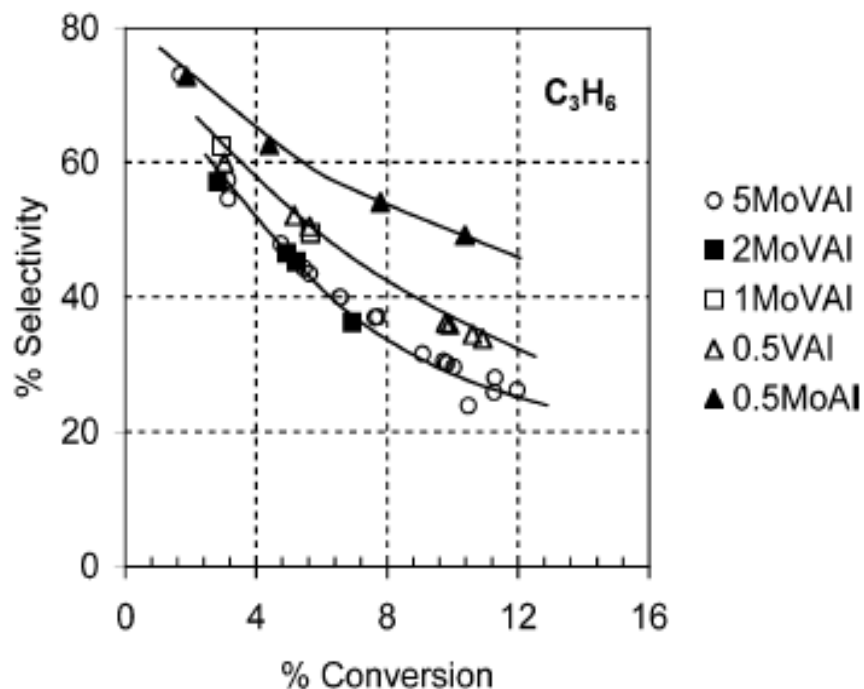
Figure 2.2 Propene selectivity as a function of propane conversion (Banares & Khatib 2004).

The mixed catalysts between Mo and V on alumina were studied for the oxidative dehydrogenation (ODH) of propane. Alumina-supported Mo–V catalysts were prepared with different Mo + V loadings by using the impregnation method. Figure 2.3 shows that a conversion of propane increases with increasing the concentration of Mo for

$V_{1.4}Mo_x/Al_2O_3$. At the same time, olefins selectivity reaches a maximum for $V_{1.4}Mo_x/Al_2O_3$ (Murgia et al., 2008).
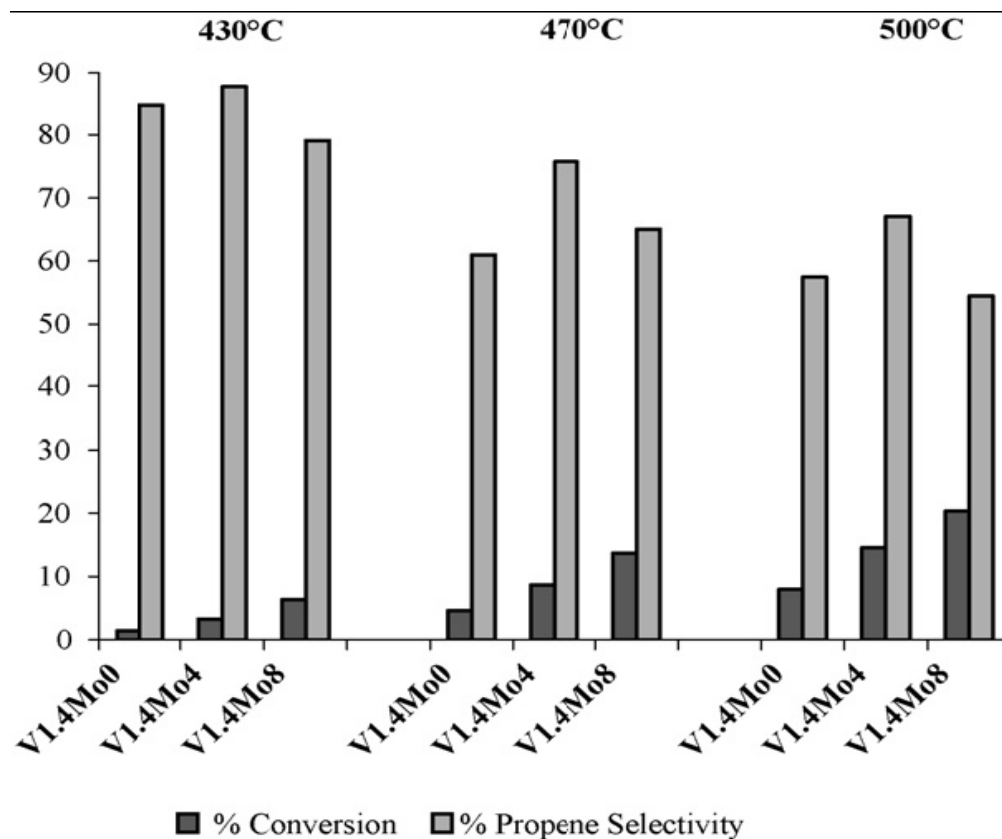
Figure 2.3 Variation of propene selectivity with propane conversion for V1.4Mox/Al2O3 (Murgia et al., 2008).

The mixed catalysts obtained by the incipient wetness coimpregnation method of Mo and Von TiO_2 supports conformed a potentially attractive system to achieve dehydrogenation of propane. The activity and selectivity depended on the Mo/V ratio used. In this work, researchers studied the effect of the concentration and the nature of

18

the acid sites on the catalyst surface for this reaction. Catalyst with high V and low Mo concentrations (3.42V0.6MoTi) was preferred because it had the highest activity and provided the best propene yield at iso-conversion. Figuer 2.4 shows the results for all the tests at 400 °C (Malleswara Rao et al., 2008).
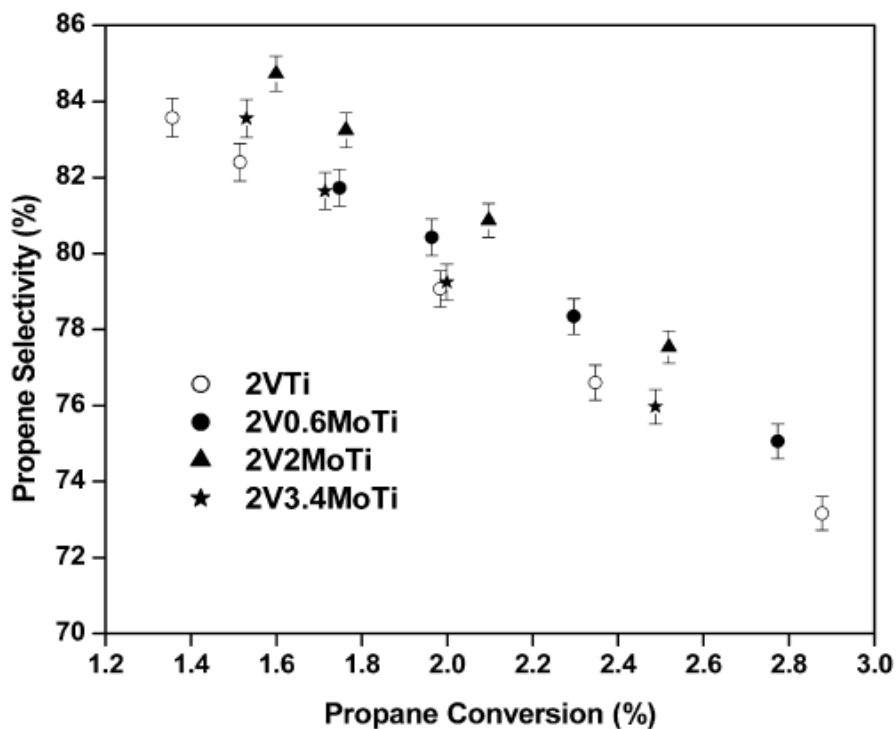
Figure 2.4 Propene selectivity and propane conversion at T = 400 °C (Malleswara Rao et al., 2008).

The composition for achieving maximum propene yields during the propane ODH reaction over supported vanadia–alumina and vanadia–titania catalysts with and without molybdena modifier catalysts were studied. The molybdena modified vanadia catalysts superior to unmodified vanadia catalysts because they had the highest activity and

selective for propene formation. Figure 2.5 and Figure 2.6 show the results for all the tests (Nayak et al., 2010).
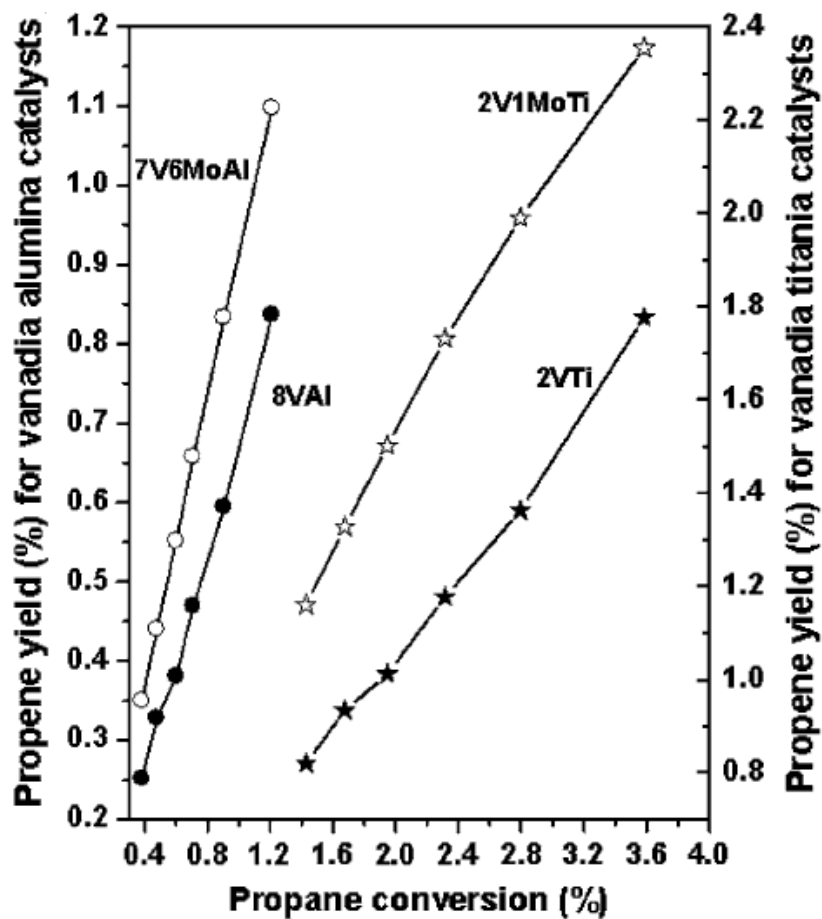
Figure 2.5 Propene yield as a function of propane conversion for alumina and titania supported modified and unmodified vanadia catalysts T = 380 °C (Nayak et al., 2010).
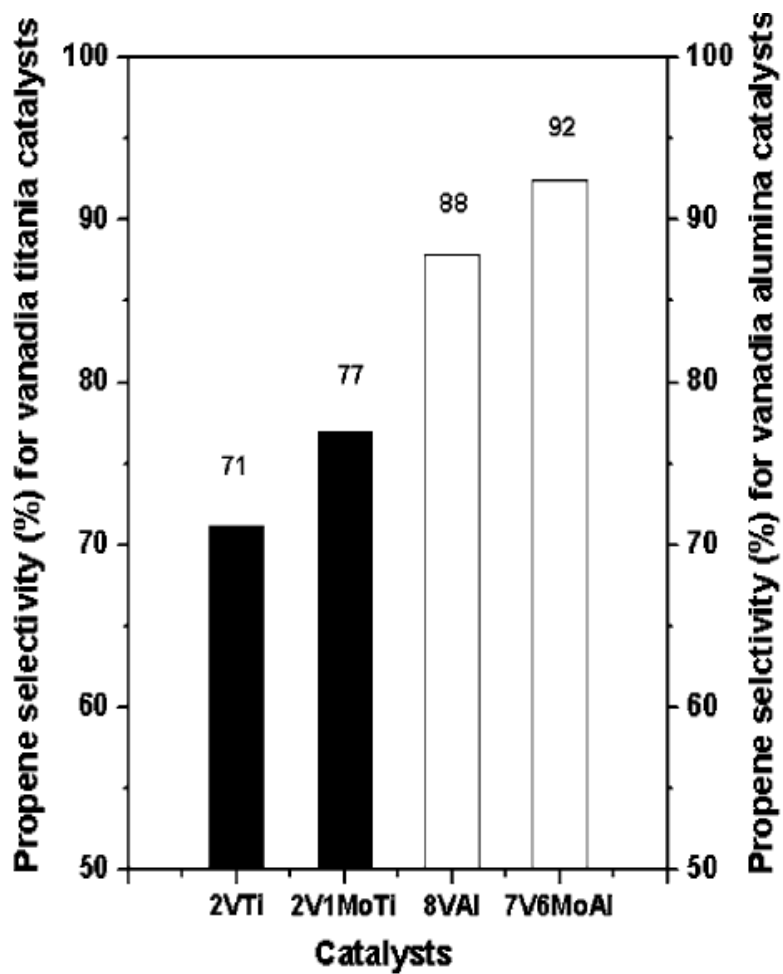
Figure 2.6 Propene selectivity for the vanadia–alumina catalysts 0.75% propane conversion and for the vanadia– titania catalysts 2% propane conversion (Nayak et al., 2010).

2.1.4   Additional Types of Catalysts

The oxidative dehydrogenation (ODH) of propane was investigated on Ce–Ni–O catalysts of different Ni content which were prepared by co-precipitation and impregnation methods. The $CeNi_1$ precipitated catalysts were active at low reaction temperatures (at 300 °C) and presented relatively good selectivity to propylene (60%) with 11% yield of propylene. The addition of potassium to the Ni/Ce impregnated sample increased the selectivity to propylene but lowered the conversion for oxidative dehydrogenation of propane to propylene. The activity decreased with the increased loading of Ni/Ce ratio (Boizumault-Moriceau et al., 2003). Oxidative dehydrogenation of propane has been discussed on zeolite Na-Y, stabilized zeolite Y (USY) and ZSM-5 by Kubacka (2000). In the ODE of propane, the activity of Zeolite Na-Y with boron species was low. An inert component like oxide boron species was not active with the zeolitic support. At 10% conversion of propane, the selectivity was increased in the following order:

$$Ca\text{-}Y \sim Mg\text{-}Y < In < In,Ga < Ga \sim Mg \sim Sn \sim Sb \sim Ca < Ga\text{-}H\text{-}ZSM\text{-}5$$

When the amount of framework aluminium in zeolitic is decreased, the selectivity went up in the following order (Kubacka et al., 2000):

$$zeolite\ Y < stabilized\ zeolite\ USY\text{-}ex < ZSM\text{-}5$$

Mesocellular silica foams supported chromium catalysts were studied by Liu (2006) in oxidative dehydrogenation of propane (ODH). The systems were found to be active and highest catalytic performance at temperatures 550 °C for the 1.0Cr–MCF. The yield of propylene amounted to 13.8% with the selectivity of about 41.8% (Liu et al.,

2006). Ce_mNi_nO catalysts were prepared by the gel-co precipitation of oxalate precursor method by Liu group, and they were compared with reference samples like Ce_mNi_nO-OC, Ce_mNi_nO-KC, and Ce_mNi_nO-imp. The experiment was done at different Ce/Ni molar ratios. Liu (2009) reported that $CeNi_2O$-OG catalyst with ½ molar ratio of Ce/Ni was the highest conversion, selectivity, and yield (12.8%), (82.7%) and (10.6%), respectively, among the other molar ratios or other techniques (Ce_mNi_nO-OC, Ce_mNi_nO-KC and Ce_mNi_nO-imp). Regarding the $CeNi_2O$-OG catalyst, it could be noted that the activity temperature (250 °C) was lower than V or Mo oxides catalysts which have shown to be active and selective for the reaction at high temperatures (500 °C). The role of ceria-based material was to increase the attention in the area of heterogeneous catalysts because of the unique redox properties. The high activity and selectivity of $CeNi_2O$-OG catalyst due to the more reducible and dispersed of NiO species and this can be increase the concentration of surface reactive oxygen species (Liu et al., 2009).

The effects of various supports (Al_2O_3, TiO_2, SiO_2, and MgO) chromium oxide catalysts were synthesized, characterized and studied for the propane ODH reaction. In these catalysts, 10 wt. % chromium oxide on alumina presented the best performance. The propane ODH reaction studies revealed that were more active and selective; propylene was 54.1%, and conversion was 16.7% at 450 °C (Jibril 2004). The nCrSiAl and nCrSiZr catalysts have been tested and found to be active in propane oxidative dehydrogenation. Selectivities for propylene production were found to be extremely poor. On the 10CrSiZr, the propane degree of conversion was 5% and the selectivity to C_3H_6 was 18.3% at 400 °C (Fujdala & Tilley, 2003).

A series of $Cs_xH_{3-x}PW_{12}O_{40}$ (x = 0.9–3.0) samples were tested as the catalysts for oxidative dehydrogenation of propane (ODP). The best yield of propylene (7.3 %) could only be achieved over the $Cs_{1.5}H_{1.5}PW_{12}O_{40}$ catalyst, this catalyst could operate at 380 $^{\circ}$C and 38% propene selectivity could be reached at a 19% propane conversion (Zhang et al., 2010).

Oxidative dehydrogenation of propane has been studied on Chromium-loaded hydroxyapatite catalysts Cr(x)/CaHAp (0.1 ≤ x ≤ 3.7 wt. % Cr). The best performance of catalysts was achieved over the x ≥ 2.9 wt.% catalyst, which possessed a selectivity near 40% propylene and conversion of propane > 16% (Boucetta et al., 2009). Several alumina-supported chromium oxide catalysts were tested in propane oxidative dehydrogenation. Catalysts were prepared by varying the chromium oxide loading. These supported chromium oxide catalysts were active for the oxidative dehydrogenation (ODH) of propane, and propene was the major product. The activity and selectivity towards propene was improved when loaded up to monolayer limits and decreased for upper loading. The best catalyst performance was recorded for 15% CrAl-600 at 500 $^{\circ}$C (selectivity 87%, propylene yield 5.2%) (Cherian et al., 2002).

The best catalysts performances in each study are summarized below in Table 2.3, which contains the name of catalyst, temperature, selectivity, and conversion of previous study catalysts.

Table 2.3 Catalyst, temperature, selectivity, and conversion of different type of catalysts

No.	Catalyst	T(°C)	C_3H_8 Conversion (%)	C_3H_6 Selctivity (%)	CO_2 Selctivity (%)	CO Selctivity (%)	C_3H_6 Yield (%)	References
1	Ga-H-ZSM-5	500	10	40.4	NA	NA	4	Kubacka et al., 2000
2	15% CrAl-600	500	6	87	NA	NA	5.2	Cherian et. al., 2002
3	CeNi1 precipitated	300	19.2	59.1	NA	NA	11.3	Boizumault-Moriceau et al., 2003
4	10CrSiZr	400	5	18.3	70.2	11.5	0.9	Fujdala &Tilley 2003
5	Cr/Al2O3	450	16.7	54.1	1	41	9	Jibril 2004
6	1.0Cr–MCF	550	32.9	41.8	24	16.4	13.8	Liu et al., 2006
7	CeNi2O-OG	275	12.8	82.7	17.3	NA	10.6	Liu et al. 2009
8	Cr(3.7)/CaHAp	500	16	39	NA	NA	6.4	Boucetta et. al., 2009
9	$Cs_{1.5}H_{1.5}PW_{12}O_{40}$	380	19	38	7.6	42	7.3	Zhang et. al., 2010

Table 2.4 shows the best catalyst performance in tables 2.1, 2.2 and 2.3. The highest conversion of propane was 40.8 % for 4.2V-MCF at 550 °C. The highest selectivity of propylene was 94.4 % for (1/1)MgMoO at 550 °C. For CeNi2O-OG catalyst, it could be noted that the activity temperature (250 °C) was lower than V or Mo oxides catalysts. The selective of propylene was 82.7%, and conversion of propane was 12.8%.

Table 2.4 Catalyst, temperature, selectivity, and conversion of best catalyst performance in table 2.1, 2.2 and 2.3

No.	Catalyst	T(°C)	C_3H_8 Conversion (%)	C_3H_6 Selectivity (%)	CO_2 Selctivity (%)	CO Selectivity (%)	C_3H_6 Yield (%)	References
1	(1/1)MgMoO	550	5.8	94.4	5.6	0	5.5	Cadus et al., 1996
2	10%Mo/Si:Ti = 1:1	550	57.2	45	NA	NA	25.7	Liu et al., 2006
3	4.2V-MCF	550	40.8	68.5	Cox = 21.1		27.9	Liu et al., 2006
4	4V-HMS	600	40	47	NA	NA	19	Karakoulia et al., 2009
5	CeNi2O-OG	275	12.8	82.7	17.3	NA	10.6	Liu et al. 2009
6	2.5% V/CeO2	450	4.2	89	NA	NA	3.7	Taylor et al., 2009

2.2 Catalyst Preparation Methods

A suitably designed catalyst should have the necessary attributes of activity, stability, selectivity, and regenerability. These can be linked to the physical and chemical properties of the catalyst, which in turn can be related to the variable parameters inherent in the method used for the preparation of the catalyst. A summary of the combustion synthesis (CS) and impregnation method techniques is given below, which describes a review and the method steps.

2.2.1   Combustion Synthesis (CS)

Combustion synthesis (CS) is a useful, low-priced method for production of various industrially valuable materials such as advanced ceramics (structural and functional), catalysts, composites, alloys, intermetallics, and nanomaterials (Patil et al., 2002). Presently, CS is an attractive method for the manufacture and preparation of nanomaterials, and it has been applied globally in 65 countries (Aruna & Mukasyan, 2008).

Nanocrystalline $Ni_1Co_{0.2}Mn_{1.8}O_4$ powders were successfully prepared by a gel auto-combustion process of nitrate citrate gels method using Analytical grade Ni $(NO_3)_26H_2O$, $Co(NO_3)_26H_2O$, $Mn(NO_3)_2(50\%)$, citric acid, and ethylene glycol (EG) as starting materials. The flow chart for the process is shown in Figure 3.7. $Ni_1Co_{0.2}Mn_{1.8}O_4$ was dissolved in a minimal quantity of water and the pH of the resulting solution was adjusted from 3.0 to 6.0, using ammonia. After that, amount of ethylene glycol (EG) was added to the solutions. This homogeneous solution was heated at 80 $^{\circ}$C on a hot plate

until it formed the sol. By keeping the solution at a temperature of 130 ⁰C under constant

stirring, the solution became a dried gel. The solution was converted into powder by

igniting it, with the air at room temperature. The powders were calcined at 300–800 ⁰C
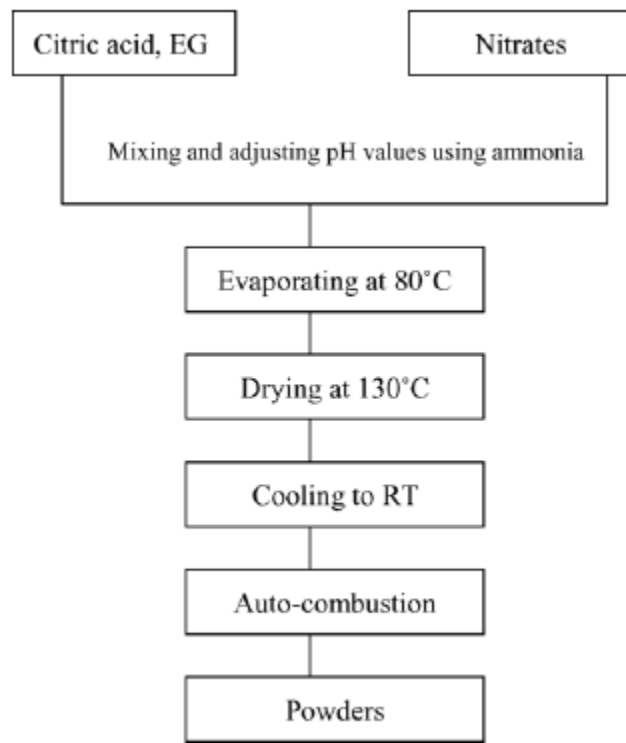
(Wang et al., 2007).

Figure 2.7 Flow chart for sucrose combustion synthesis of Ni1Co0.2Mn1.8O4 (Wang et al., 2007).

Three important factors could have affected the catalyst when it was prepared by using auto-combustion method. These factors are acid/metal nitrates ratio (C/M), the fuel/oxidant ratio (F/O), and pH. Deganello (2009) studied these factors to prepare an iron, a cobalt, and a cerium-perovskite with (C/M) = 1 – 4, (F/O) = 0.4-1.6 and pH = 1-11. In Figure 2.8, the surface area reduces with F/O ratio until reaching a minimum after that rises with an upper F/O ratio. The combustion process becomes stronger by rising pH and a negative effect on the final powder morphology can be seen at low pH. The effecting of C/M ratio is shown in Table 2.4. At C/M = 1.2, the surface area was extremely low. When increasing the C/M to 2, the surface area increased and the surface area was again decreased at C/M = 4 (Deganello et al., 2009).
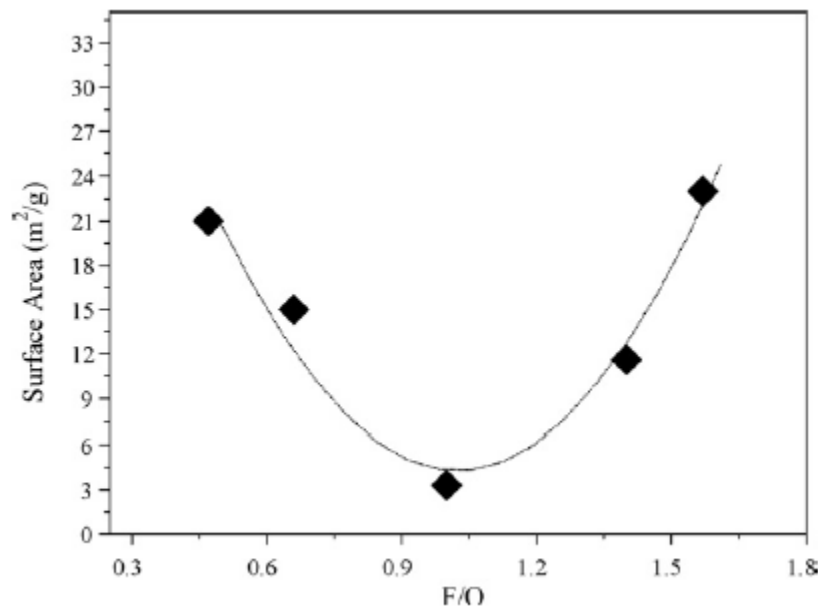
Figure 2.8 The surface area (BET method) versus the F/O ratio with C/M = 4; pH 9; calcined at 1000 ∘C/5 h (Deganello et al., 2009).

Table 2.5 Morphological properties at different C/M ratios (Deganello et al., 2009).

C/M	Particle size (nm)	Crystal size (nm)	Agglomeration degree (particle size/crystal size)	Surface area (m^2/g)
1.2	234	69	3.4	5
2	200	116	1.7	33
4	209	91	2.3	21

2.2.2   Impregnation Method

The most useful preparation method for heterogeneous catalysts is impregnation. The most important advantage of this method is its simplicity. Figure 2.9 shows the steps of the impregnation method. Impregnation appears to be a suitable method for the application of precursors of active phase(s) inside the mesopores because MCM-41 offers a relatively large pore volume. The most attractive fact about the material MCM-41 is that MCM-41 opens an opportunity for the design of catalytically active sites inside the uniform channels with controllable nano-order pore diameter (Wang et al., 2005; Caponetti et al., 2008; Kim et al., 1995; Higashimoto et al., 2005).
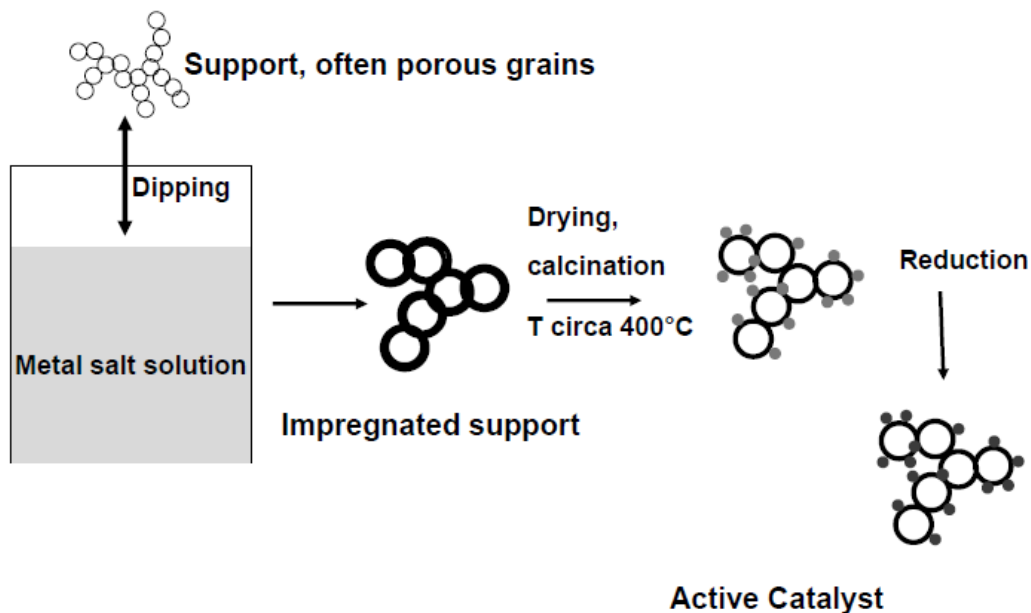
Figure 2.9 The steps of impregnation method (Stark 2010).

2.3 Catalyst Characterization

The following section is a brief discussion of catalysts characterization that includes the following methods: BET technique for surface area measurements, temperature programmed reduction (TPR), X-Ray Diffraction (XRD), Raman spectroscopy, and diffuse reflectance UV-V spectroscopy.

2.3.1 BET Surface Area

Table 2.5 summarizes the surface areas obtained from BET analysis for Mo and V catalyst samples. The surface areas of metal oxides were extremely low. On the other hand, the support catalysts usually showed high surface area. For example, the MCM-41 (support materials) had a 1086.5 m^2/g surface area. When metals were loaded on the support, the surface area decreased.

Table 2.6 The surface areas obtained from BET analysis.

Samples	S_{BET} $(m^2 g^{-1})$	References
MCM-41	1086.5	Higashimoto et al., 2005
Mo-MCM-41	1007.6	
Mo-MCM-41	1002.4	
Mo-MCM-41	987.7	
Mo-MCM-41	945.4	
imp-Mo/MCM-41	672	
Pure MCM-41	1025	Wang et al., 2005
V-MCM-41 (Si/V= 64)	1010	
V-MCM-41 (Si/V= 32)	850	
V-MCM-41 (Si/V= 16)	830	
V-MCM-41 (Si/V= 8)	962	
MoV2O8	2.2	Vuk et al., 2002
MoVNb-3	24	Concepcion et al., 2004
MoVSb-4	9	
MoV-orth-1	6.1	Katou et al., 2004
MoV-orth-2	9.3	
MoV-amor-1	10.3	
MoV-amor-2	7.6	
MoVTe-orth-1	5.8	

2.3.2   Temperature Programmed Reduction (TPR)

The reduction profile for 12Mo/Al l showed single peak at about 710 K, followed by a broad feature at higher temperatures; the peak at 710 K was attributed to reduction of Mo^{6+} to Mo^{4+}, while the feature at higher temperature reflected the reduction of Mo^{4+} to Mo^0. The reduction profile for 10.5V/Al showed peak at about 710 K, which was attributed to the reduction of V^{5+} to V^{3+}. The addition of vanadia to 12Mo/Al provided a sharp feature appeared at 690 K and it shifts to 720 K with increasing vanadia content.

Temperature-programmed reduction (TPR) results are shown in Figure 2.10 (Dai et al., 2004). Temperature-programmed reduction (TPR) data of 10VAl, 12MoAl, 10V12MoAl, 12CrAl, 10V12CrAl, 10V12MoAl and 12Mo10VAl are shown in Figures 2.11 and 2.12 and Table 2.6 (Yang et al., 2005).

The reduction profile for undoped sample showed two peaks; the first peak (315 ^oC very small) and the second peak (575 ^oC broad) were attributed to isolated tetrahedral vanadium species in amorphous and crystalline magnesium orthovanadate. The addition of increasing amounts of Mo to VMg led to a shift of the peak at 575 ^oC to higher temperatures, and its intensity also decreased with the Mo content. The new peak at 685 ^oC and 780 ^oC appear in Mo-doped samples corresponds to the reduction of Mo^{6+} -ions. The Temperature-programmed reduction (TPR) results are plotted in Figure 2.13 (Dejoz et al., 1999).
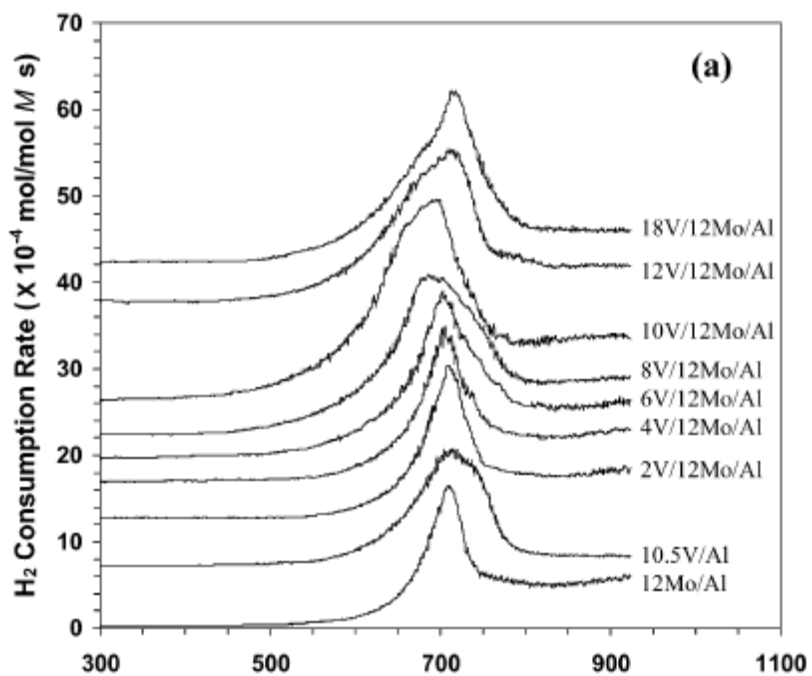
Figure 2.10 TPR profiles of 12Mo/Al, 10.5V/Al, and xV/12Mo/Al (x = 2–18) (Dai et al., 2004).
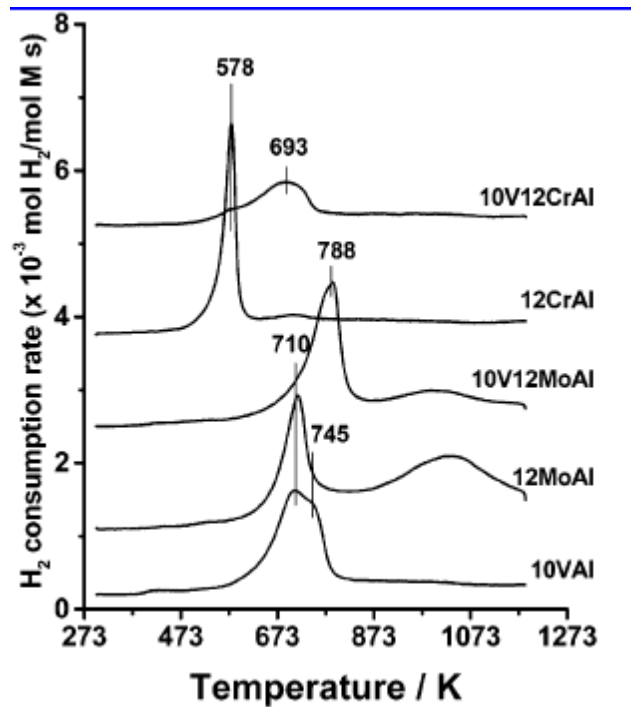
Figure 2.11 TPR spectra of 10VAl, 12MoAl, 10V12MoAl, 12CrAl, and 10V12CrAl catalysts (Yang et al., 2005).
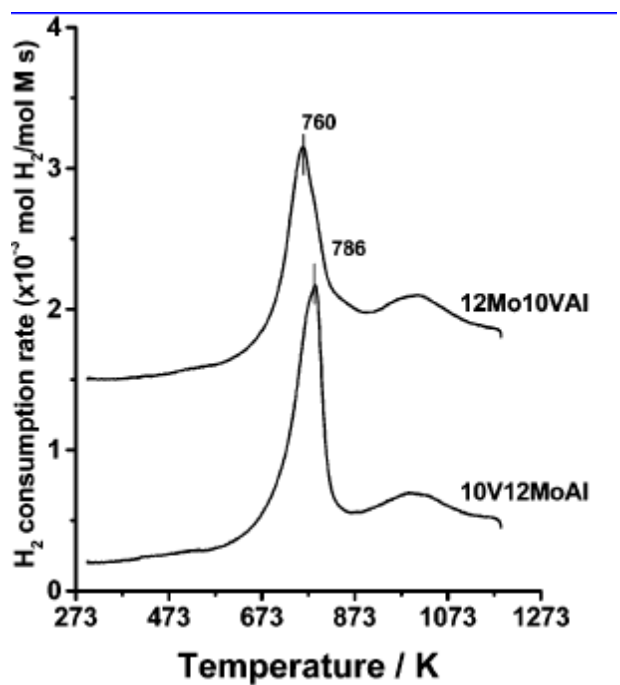
Figure 2.12 TPR spectra of 10V12MoAl and 12Mo10VAl (Yang et al., 2005).

Table 2.7 TPR Results reported in Figures 2.11 and 2.12 (Yang et al., 2005)

sample	reduction peak temperature (K)	assignment	H_2/M ($M = V$, Mo, or Cr) (theoretical values are given in parentheses)
10VAl	710–745	$V^{5+} \rightarrow V^{3+}$	0.92 ($H_2/V = 1$)
12MoAl	710	$Mo^{6+} \rightarrow Mo^{4+}$	0.86 ($H_2/Mo = 1$)
	1053	$Mo^{4+} \rightarrow Mo^0$	2.02 ($H_2/Mo = 2$)
12CrAl	578	$Cr^{6+} \rightarrow Cr^{3+}$	0.91 ($H2/Cr = 1.5$)
10V12MoAl	786	$V^{5+} \rightarrow V^{3+}$ $Mo^{6+} \rightarrow Mo^{4+}$	0.99 ($H_2/(V + Mo) = 1$)
	1053	$Mo^{4+} \rightarrow Mo^0$	1.9 ($H_2/Mo = 2$)
12Mo10VAl	760	$V^{5+} \rightarrow V^{3+}$ $Mo^{6+} \rightarrow Mo^{4+}$	0.89 ($H_2/(V + Mo) = 1$)
	1053	$Mo^{4+} \rightarrow Mo^0$	2.1 ($H_2/Mo = 2$)
10V12CrAl	572	$Cr^{6+} \rightarrow Cr^{3+}$	0.12 ($H_2/Cr = 1.5$)
	693	$V^{5+} \rightarrow V^{3+}$	1.08 ($H_2/V = 1$)
12Cr10VAl	572	$Cr^{6+} \rightarrow Cr^{3+}$	0.29 ($H_2/Cr = 1.5$)
	712	$V^{5+} \rightarrow V^{3+}$	0.91 ($H_2/V = 1$)
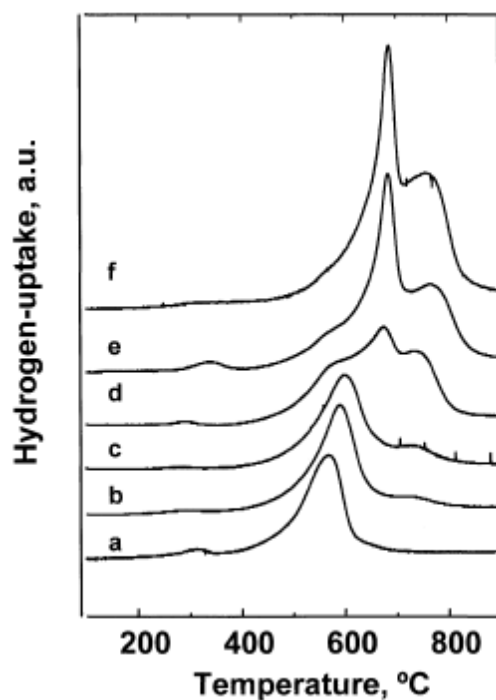
Figure 2.13 TPR profiles of undoped and Mo-doped catalysts: (a) VMgO; (b) 0.1MoVMg; (c) 0.2MoVMg; (d) 0.6MoVMg; (e) 1.0MoVMg; (f) 1.4MoVMg (Dejoz et al., 1999).

2.3.3   UV Spectroscopy

The absorption spectra (UV) of Mo-MCM-41 with varying Mo content (0.5–4.0 wt %) are displayed in Figure 2.14. An intense and broad absorption in 220–240 nm and 260–300 nm on the entire sample region was registered and could be related to the charge transfer from O^{2-} to Mo^{6+}. Catalysts with higher Mo content showed high intensity of the absorbance. None of the samples showed absorption longer than 340 nm region because of the existence of MoO_3 (Higashimoto et al., 2005).

The absorption spectra of Mo_3V_6, Mo_3V_6Te, Mo_6V_3 and Mo_6V_3Te samples are shown in Figure 2.15. The absorption bands appearing at 200–400 nm region was registered and could have been related with the presence of Mo^{6+} and V^{5+} species absorption bands near 290–350 and 350–450 nm assigned to Mo^{6+} and V^{5+} species in octahedrical coordination, respectively. The width of the band absorption increased with increasing vanadium content (Guerrero-Perez et al., 2008).
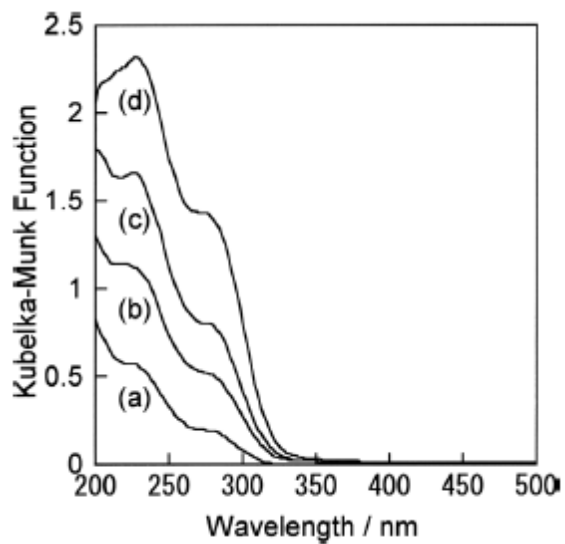
Figure 2.14 UV spectra of Mo-MCM-41 with different Mo contents of (a) 0.5, (b) 1.0, (c) 2.0, and (d) 4.0 wt% (Higashimoto et al., 2005).
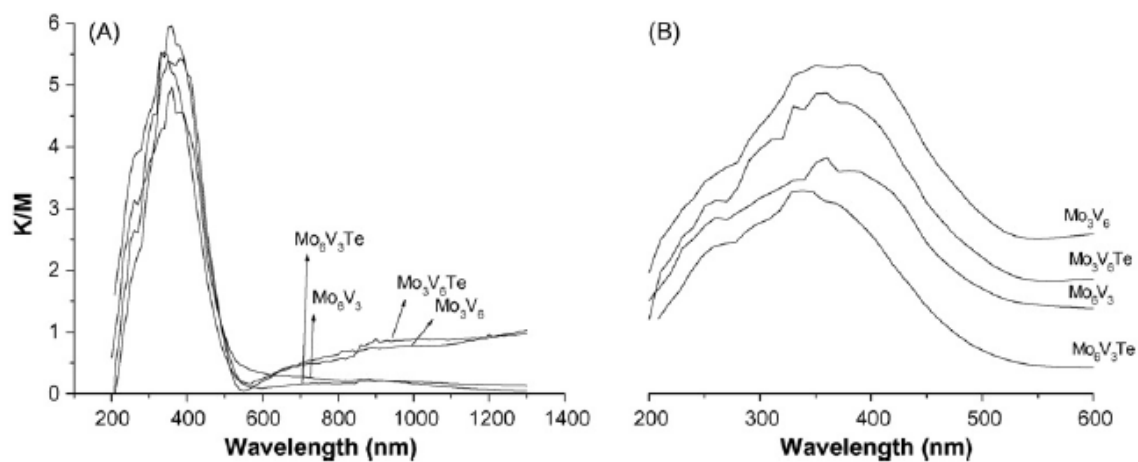
Figure 2.15 Diffuse reflectance UV–vis spectra of samples (A) and 200–600 nm region (spectra have been shifted respect absorbance axis) (B) (Guerrero-Perez et. al., 2008)

2.3.4   X-Ray Diffraction (XRD)

Jibril and Shakeel (2005) analyzed MCM-41 by X-Ray Diffraction (XRD) as seen in Figure 2.16. XRD of MCM-41 exhibited a higher order of pore structure and four low-angle peaks in the region of $2\theta = 1.5\text{-}10^{\mathbf{o}}$. These peaks related to hkl values of (100), (110), (200), and (210) reflections (Jibril & Shakeel, 2006).

Figure 2.17 shows variable temperature in situ XRD patterns of $H_7PV_4Mo_8O_{40}$/APTS/SBA-15 and XRD indexed results of MoO_3 and V_2O_5 are summarized in Table 2.7. The sample shows signs of amorphous $H_7PV_4Mo_8O_{40}$ inside the channels due to no characteristic diffractions. Also shown is a hump centered around 23° corresponding to diffraction of the amorphous SBA 15. Researchers noticed that crystalline MoO_3 took place during oxidation of the organics. On the other hand, XRD detected no diffractions of crystalline vanadium oxide, confirming that vanadium species are finely dispersed (Bin et al., 2005). Figure 2.18 shows the X-ray diffraction of Metal oxides ($Mg_{2.5+x}V_{1+2x}Mo_{1-2x}O_8$) that are synthesized at 823 K by the sol–gel method (Pless et al., 2004). Alumina-supported V–Mo–O mixed oxide catalysts are analyzed with the X-ray diffraction in Figure 2.19 (Khatib et al., 2006).

38
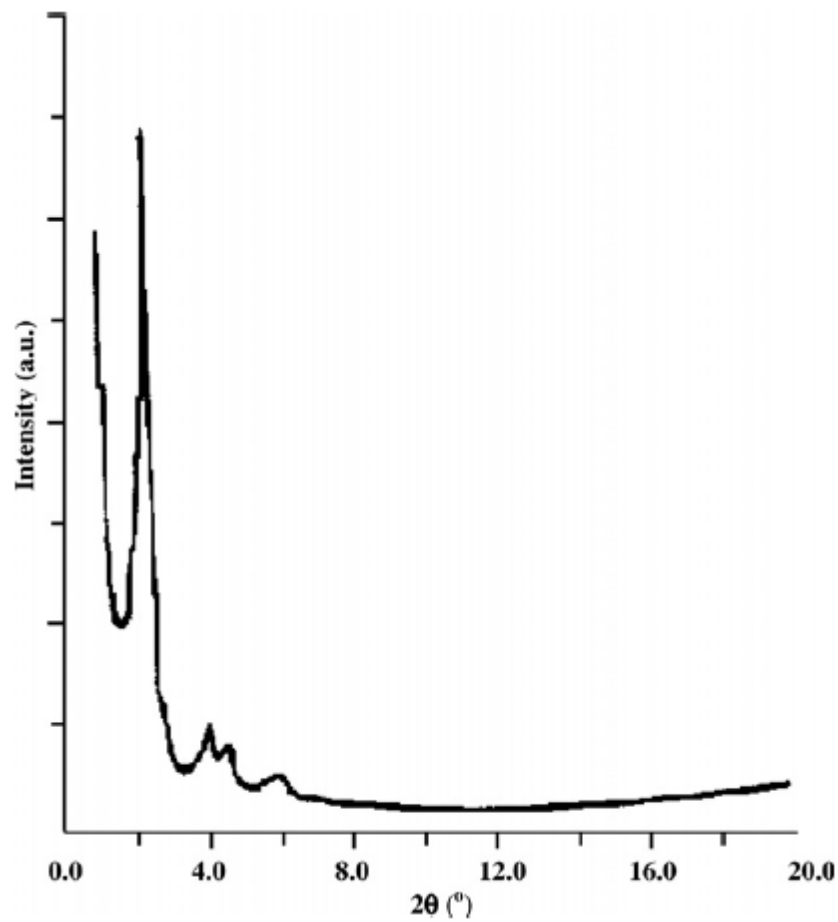
Figure 2.16 XRD of MCM-41 (Jibril & Shakeel, 2006).
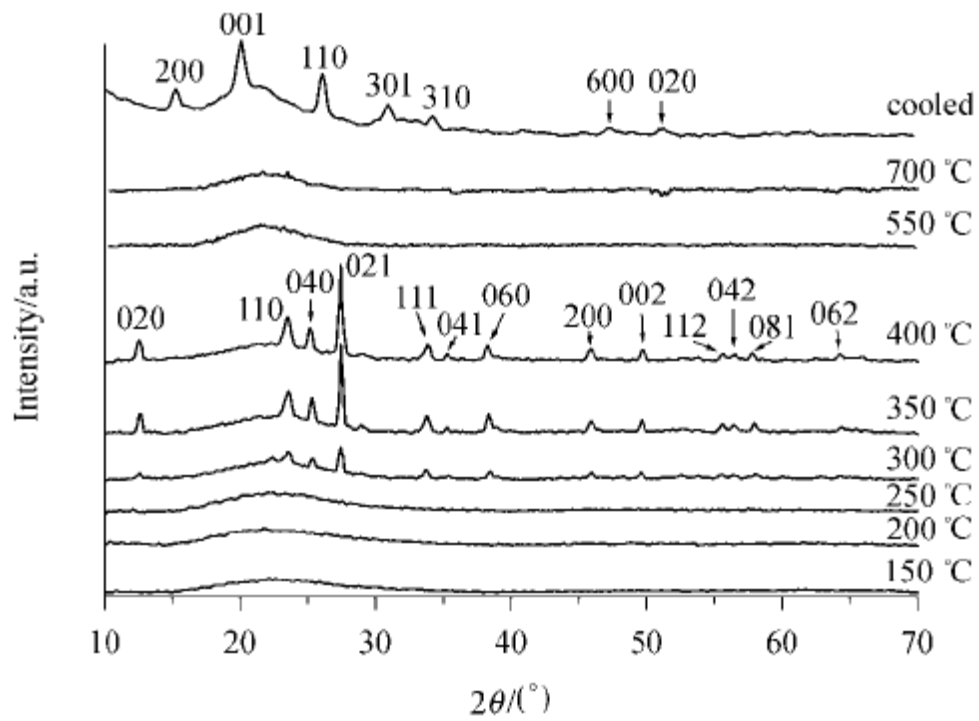
Figure 2.17 XRD patterns of H7PV4Mo8O40/APTS/SBA-15 (Bin et al., 2005).

Table 2.8 XRD indexed results of MoO3 and V2O5 (Bin et al., 2005)

			MoO$_3$					V$_2$O$_5$	
h	k	l	JCPDS 5-508 $2\theta/(°)$	Found $2\theta/(°)$	h	k	l	JCPDS 41-1426 $2\theta/(°)$	Found $2\theta/(°)$
0	2	0	12.76	12.58	2	0	0	15.35	15.27
1	1	0	23.33	23.50	0	0	1	20.26	20.18
0	4	0	25.70	25.17	1	1	0	26.13	26.12
0	2	1	27.33	27.42	3	0	1	31.00	30.93
1	1	1	33.73	33.83	3	1	0	34.28	34.19
0	4	1	35.50	35.25	6	0	0	47.32	47.21
0	6	0	38.98	38.25	0	2	0	51.21	51.24
2	0	0	45.74	45.83					
0	0	2	49.24	49.75					
1	1	2	55.19	55.67					
0	4	2	56.36	56.50					
0	8	1	58.80	58.83					
0	6	2	64.53	64.25					
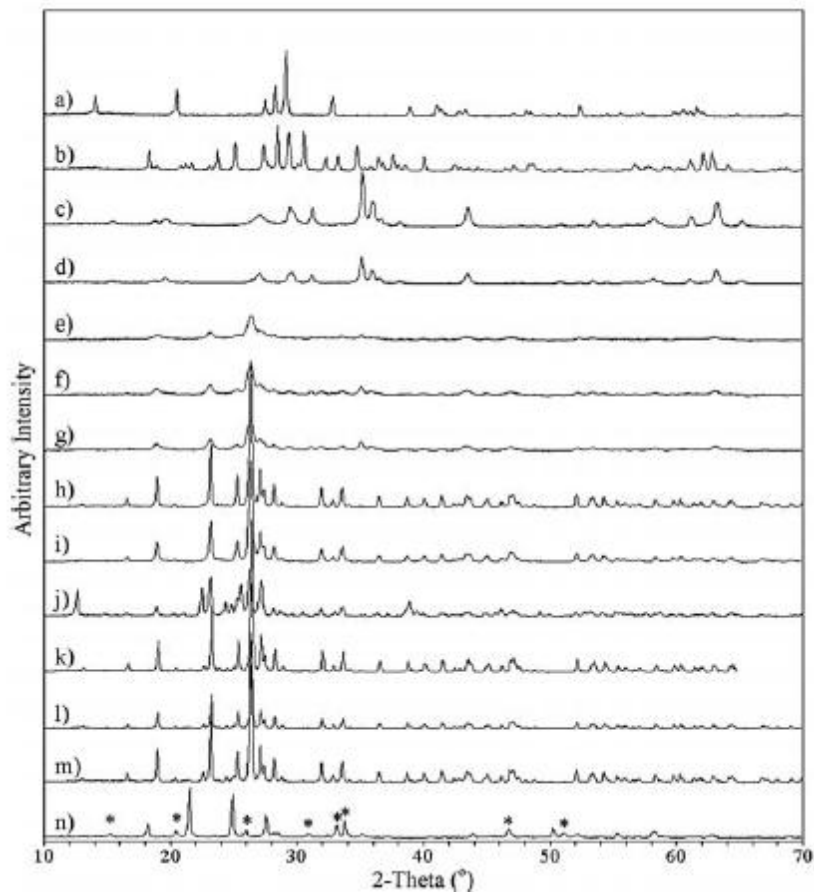
Figure 218 XRD patterns of (a) MgV_2O_6; (b) $Mg_2V_2O_7$; (c) $Mg_3(VO_4)_2$; (d) $Mg_{2.98}(V_{0.98}Mo_{0.02}O_4)_2$; (e) 37.0% $Mg_3(VO_4)_2/MgMoO_4$; (f) 1:2 $Mg_3(VO_4)_2/MgMoO_4$; (g) 29.9% $Mg_3(VO_4)_2/MgMoO_4$; (h) $Mg_{0.992}MoO_{3.992}$; (i)$Mg_{1.015}MoO_{4.015}$; (j) $MgMo_2O_7$; (k) 2% V_2O_5 on $MgMoO_4$; (l) 1.86% V_2O_5, 0.14% MoO_3 on $MgMoO_4$; (m) 1.72% V_2O_5, 0.28% MoO_3 on $MgMoO_4$; (n) MoV_2O_8, impurity V_2O_5 (*). Diffraction patterns were taken at room temperature in air (Pless et al., 2004).

42
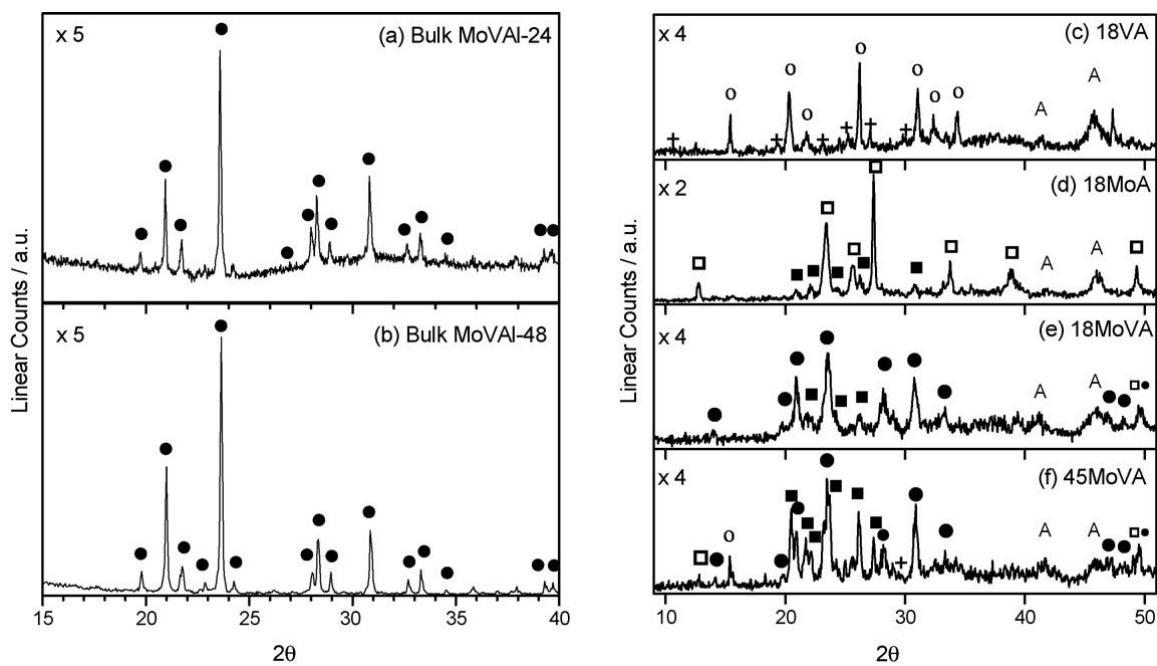
Figure 2.19 XRD patterns of (a) bulk-MoVAl-24; (b) bulk-MoVAl-48 (c) 18VA; (d) 18MoA; (e) 18MoVA; (f) 45MoVA. Phase identification: (o), V_2O_5; JCPDS file: 77-2418; (+), AlV_3O_9; JCPDS file: 49-694; (□), α-MoO_3; JCPDS file: 35-609; (■), $Al_2(MoO_4)_3$; JCPDS file: 23-764; (●), $AlVMoO_7$; JCPDS file: 46-687(Khatib et al., 2006).

2.3.5   Raman Spectroscopy

The Raman spectra of dehydrated 0.5VAl, 0.5MoAl and xMoVAl catalysts are shown in Figure 2.20. For 0.5MoAl catalyst, the Raman band at 996 cm^{-1} is assigned to the Mo=O stretching mode of surface monooxo molybdenum oxide species. The spectrum for 0.5VAl catalyst showed band at 1031 cm^{-1}. This band is attributed to of surface vanadium oxide species (V=O stretching mode) and the band at 850 cm^{-1} is attributed to stretching modes of V–O–V. The band 999, 820, 672, 383, 342, 290, 250, 163 cm^{-1} were assigned to alpha-MoO$_3$ and The band 994, 701, 525, 409, 295, 285, and 143 cm^{-1} are assigned to V$_2$O$_5$. 1MoVAl, 2MoVAl and 5MoVAl showed new Raman bands appear at 962, 783 and 763 cm^{-1}. The bands located at 965 and 786 cm^{-1} are related to alpha-MoO$_3$. These bands are shifted by ca. 30 cm^{-1} because of an additional distortion of the species of molybdenum superficial oxides which result from the interaction with vanadium cations. On the other hand, the Raman band at 763 cm^{-1} might have corresponded to the mixed Mo–V–O phase (Banares & Khatib, 2004).
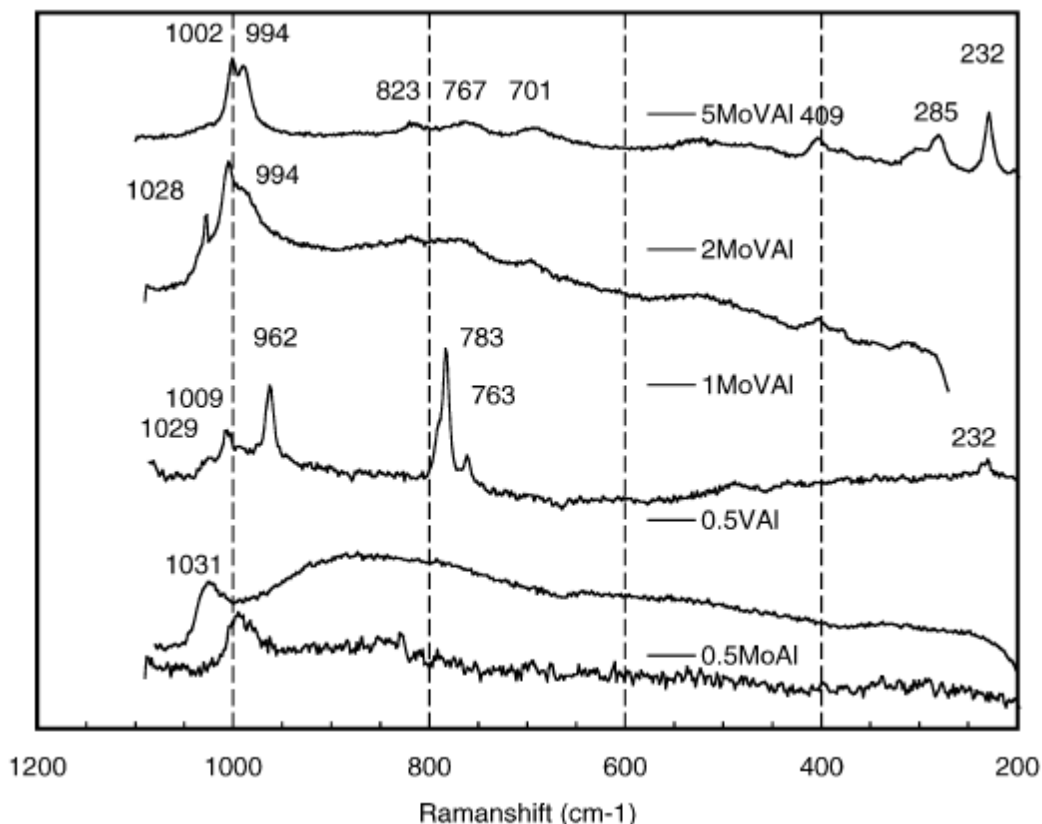
Figure 2.20 Raman spectra of dehydrated fresh catalysts (0.5MoAl, 0.5VAl, 1MoVAl, 2MoVAl, and 5MoVAl) (Banares & Khatib 2004).

Figure 2.21 shows the Raman spectra for $V_{1.4}Mo_x/Al_2O_3$ and Figure 2.22 shows the Raman spectra for Mo_4V_x/Al_2O_3. For $V_{1.4}Mo_x$, The Raman bands at 1033, 939 and 847 cm^{-1} corresponded to symmetrical stretching mode V=O, stretching mode of bridges M–O–M and antisymmetrical stretching modes of Mo–O–Mo, respectively. For Mo_4V_x/Al_2O_3, The band bands were observed at 1039 and 911 cm^{-1} due to the vibration modes of Mo=O and Mo–O–Mo, respectively (Murgia et al., 2008). Table 2.8 lists Raman Band Positions of V-Nb-O, and Mo-Nb-O, mixed metal oxides catalyst (Zhao et al., 2003).

45
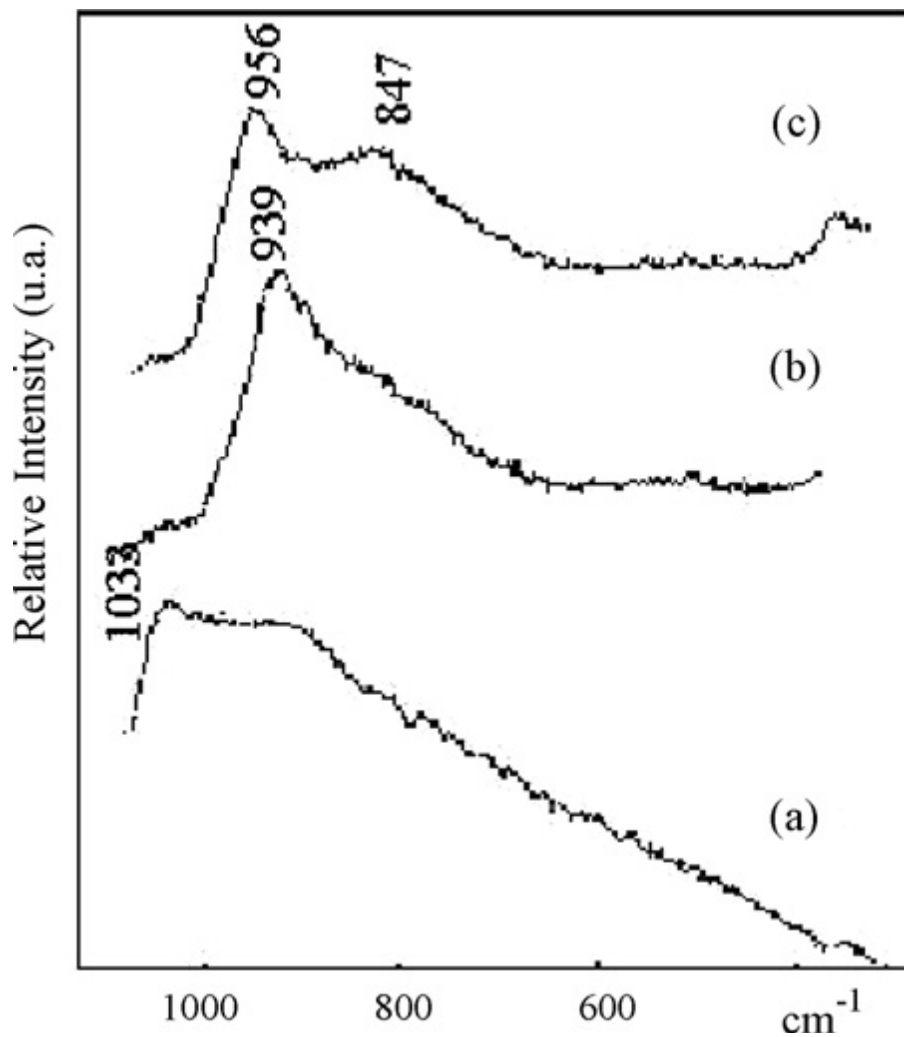
Figure 2.21 Raman spectra of (a) $V_{1.4}Mo_0/Al_2O_3$, (b) $V_{1.4}Mo_4/Al_2O_3$ and (c) $V_{1.4}Mo_8/Al_2O_3$ (Murgia et al., 2008).
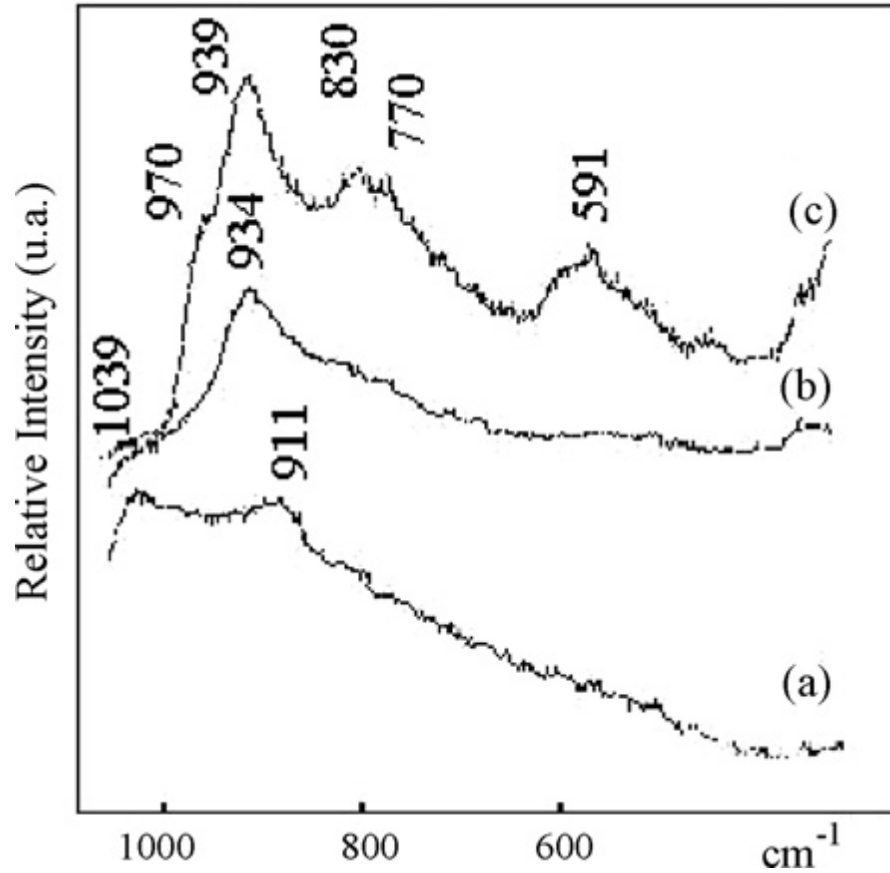
Figure 2.22 Raman spectra of (a) $Mo_4V_0/$ Al_2O_3, (b) $Mo_4V_{1.4}/$ Al_2O_3 and $Mo_4V_{2.8}/$ Al_2O_3 (Murgia et al., 2008).

Table 2.9 Raman Band Positions of V-Nb-O, and Mo-Nb-O (Zhao et al., 2003).

sample	band position M=O (cm^{-1})	structure	substrate or support
Nb_2O_5 (bulk)	not detected	polymeric NbO_5/NbO_6	Nb_2O_5 (TT)
1% V−Nb−O	not detected		$Nb_{2-x}V_xO_5$ (TT)
5% V−Nb−O	980	polymeric VO_6	$Nb_{2-x}V_xO_5$ (TT)
10% V−Nb−O	1020 (~1025)[a]	polymeric VO_4	$V_4Nb_{18}O_{55} + Nb_{2-x}V_xO_5$
20% V−Nb−O	1020 (~1025)[a]	polymeric VO_4	$V_4Nb_{18}O_{55} + Nb_{2-x}V_xO_5$
surface NbO_x/Nb_2O_5[56]	~986	polymeric NbO_5/NbO_6	Nb_2O_5 (TT)
surface VO_x/V_2O_5	~1020	Not known (polymeric VO_4 ?)	V_2O_5
1% V_2O_5/Nb_2O_5[5,54]	1031[a]	isolated VO_4	Nb_2O_5
5% V_2O_5/Nb_2O_5[5,54]	1033[a]	isolated VO_4	Nb_2O_5
1% Mo−Nb−O	not detected		$Nb_{2-x}Mo_xO_5$ (TT)
5% Mo−Nb−O	~985 (very weak)	MoO_6	$Nb_{2-x}Mo_xO_5$ (TT)
10% Mo−Nb−O	987	MoO_6	$Nb_{2-x}Mo_xO_5$ (TT)
20% Mo−Nb−O	987	MoO_6	$Nb_{2-x}Mo_xO_5$ (TT)
5% MoO_3/Nb_2O_5[36]	996	MoO_6	Nb_2O_5 (TT)

CHAPTER 3

3. Experimental

3.1 Experimental Plan

For successful achievement of the present research work, the experiments were designed as follows:

- ❖ Preparation of oxide catalysts with different mole ratios by using modified citrate-nitrate auto-combustion method

- ❖ Preparation of molybdenum and vanadium supported catalysts with different percent loading by using impregnation method

- ❖ Preparation of one catalyst by physical mixing of commercial vanadium oxide and molybdenum oxide.

- ❖ Use of MCM-41 as a support (prepared in our lab)

- ❖ Characterization of the prepared catalyst by Temperature-Programmed Reduction (TPR), BET surface area and pore volume, XRD, Raman spectroscopy, and UV spectroscopy

- ❖ Evaluation of these catalysts in a fixed bed reactor for oxidative dehydrogenation of propane to propylene by using gas mixture consisting of N_2, air and propane as a feed

- ❖ Selection of the best catalyst performance and examination of its life time

3.2 Catalyst Preparation

3.2.1 Catalyst Composition

Eight catalysts were prepared for this work as seen in Table 3.1. These catalysts were divided into three groups:

- Commercial molybdenum vanadium oxide catalyst (MoVOx-1)

- Molybdenum vanadium oxide without support (MoVOx-2 (SCD), MoVOx-3 (SCD), MoVOx-4 (SCD) and MoVOx-5 (SCD))

- Molybdenum and vanadium support catalysts (5MV/MCM-41, 10 MV/MCM-41 and 15 MV/MCM-41).

The first group (MoVOx-1) was prepared with 1:1 mole ratio of Mo:V. The second group was unsupported catalysts. The metal oxide catalysts were designed with an increase in the molybdenum and a decrease in the vanadium. The mole ratios of Mo:V in the oxide catalyst were (1:1), (0.7:0.3), (0.2:0.8) and (0.9:0.1) for MoVOx-2 (SCD), MoVOx-3 (SCD), MoVOx-4 (SCD), and MoVOx-5 (SCD), respectively. The third group was supported catalysts that were made with a 1:1 mole ratio of Mo:V and different amount of meta loading %. The type of support was MCM-41. The loading % were 5%, 10%, and 15% for 5MV/MCM-41, 10 MV/MCM-41, and 15 MV/MCM-41, respectively.

Table 3.1 Code and composition of prepared catalysts.

Catalyst Code	Mole %			Type
	Mo/V	Mo	V	
MoVOx-1	1/1	1	1	Unsupported (physical mixing)
MoVOx-2(SCD)	1/1	1	1	Synthesized unsupported
MoVO-3 (SCD)	0.7/0.3	0.7	0.3	Synthesized unsupported
MoVO-4 (SCD)	0.8/0.2	0.8	0.2	Synthesized unsupported
MoVO-5 (SCD)	0.9/0.1	0.9	0.1	Synthesized unsupported
5MV/MCM-41	1/1	1	1	supported on to 5% loading
10MV/MCM-41	1/1	1	1	supported on to 10% loading
15MV/MCM-41	1/1	1	1	supported on to 15% loading

3.2.2   Catalyst Preparation Procedure

I- Commercial molybdenum vanadium oxide catalyst

The MoVOx-1 catalyst was prepared from Commercial V_2O_5 and MoO_3 with a 1:1 mole ratio of Mo:V. Next, 4 g of V_2O_5 and 1.6 g of MoO_3 were mixed and ground to gather for 60 minutes. The mixture was calcined at 550 °C for 4 h with a heating rate of 5 °C/min.

II- Molybdenum vanadium oxide catalysts without support

Nanocrystalline MoVOx-X powders were successfully prepared by using a modified auto-combustion process of nitrate citrate gels method, using Ammonium heptamolybdate tetrahydrate $(NH_4)_6Mo_7O_{24}\cdot4H_2O$, Ammonium vanadate(V) NH_4VO_3 , Ammonium nitrate, citric acid, and diethanolamin as starting materials (Deganello et al., 2009). The flow chart for the modified auto-combustion process is shown in Figure 3.1. Molybdenum solution was prepared by dissolving Ammonium heptamolybdate tetrahydrate in distilled water. However, vanadium solution was prepared by dissolving Ammonium vanadate in distilled water, and diethanolamin was added to the vanadium solution. The molybdenum solution and vanadium solutions were mixed together. A solution of citric acid and Ammonium nitrate were mixed with the Molybdenum and vanadium solution. To adjust the pH, Ammonium solution was added. This homogeneous solution was heated at 80 °C on an oil bath for 24 h under constant stirring; the solution
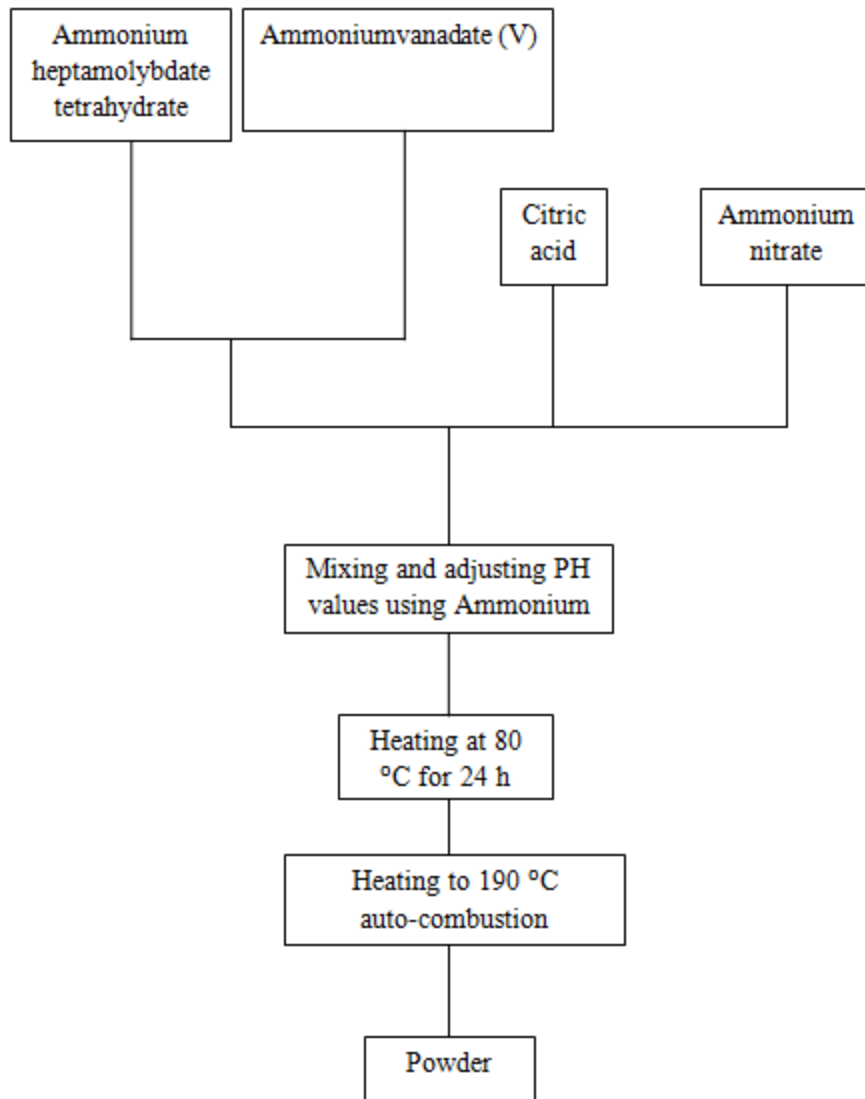
Figure 3.1 Flow chart for process combustion synthesis of MoVOx-X catalysts.

became dried gel. The temperature of the oil bath was increased to 190 ^{o}C, and finally the decomposed gel self-ignited as seen in Figure 3.2. The product was ground and crushed to convert it into powder. The powders were calcined at 550 ^{o}C for 6 h with a heating rate of 1 ^{o}C/min. After calcinations, catalysts were washed with alcohol and dried by using super critical drying (SCD). All catalysts were prepared under these conditions: the citric acid/metal nitrates ratio (C/M) was 2. Ammonium nitrate was added to regulate the fuel/oxidant ratio (F/O), represented by the citric acid/total nitrate ions ratio, which was 0.4. Finally, ammonia solution was slowly added to adjust the pH to 9.

III- Washing and super critical drying (SCD) procedure

Catalysts were washed by alcohol after calcinations and were placed in an ultrasound bath water for 30 minutes. The solution was filtered by using micro-filters that were put inside the super critical drying (SCD) equipment (Autosamdri-815B, Series A). Autosamdri-815B has 6 cycles which are cool, fill, purge, heat, bleed and vent. The following is a description of each cycle:

- **Vent:** After switching "ON" the Autosamdri-815B, the vent mode was started to indicate that the process was in standby. Autosamdri-815B was set to vent mode for 3-5 minutes to warm-up. The vent button was pressed and the pure alcohol was released into the chamber. The filters were placed into the chamber. The chamber lid was put in place and secured. Before proceeding, the process was adjusted for the time of purge as follows:
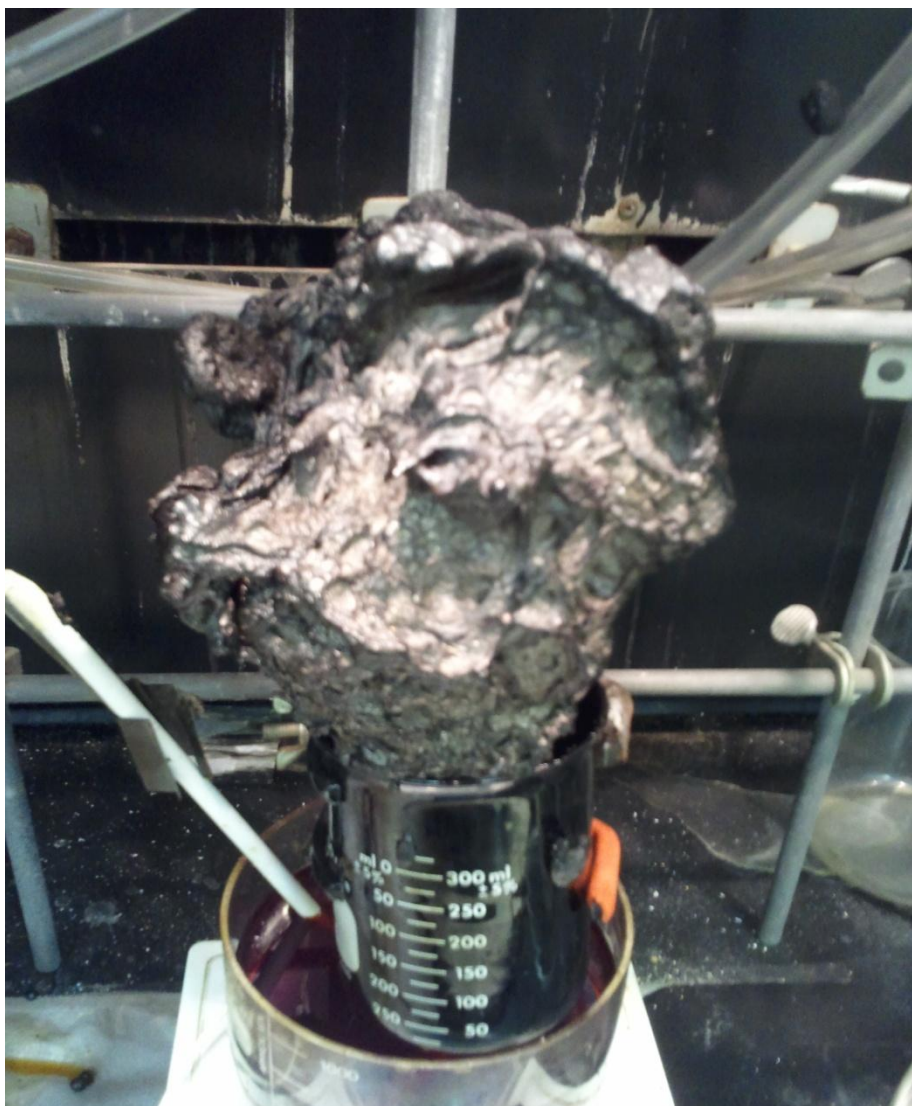
Figure 3.2 Photo of the catalyst after self-ignition at 190 ⁰C.

♦ 1/4 chamber =10 minute purge time

♦ 1/2 chamber =15 minute purge time

♦ 3/4 chamber =10 minute purge time

- **Cool:** The "Cool" button was pressed to stop the vent and start the cool cycle. When the chamber temperature was decreased, liquid CO_2 was circulated through the unit. After the chamber reached the operational temperature, the cool mode was automatically stopped.

- **Fill:** The "Fill" button was pressed to fill the chamber with liquid CO_2 and this cycle was run for 8 minutes. Through the fill mode, the cool cycle was ON/OFF to automatically keep the chamber temperature below 10 ^oC.

- **Purge:** After the fill mode, the purge cycle was automatically started and this mode remained based on the purge time pre-set. The waste alcohol and CO_2 were collected in the SOTER condenser.

- **Purge-fill:** The purge-fill mode was automatically run after the purge cycle was finished. In this process, the chamber was filled with liquid CO_2 for 4 minutes.

- **Heat:** At the end of purge-fill mode, the heat cycle was automatically started. The pressure and temperature were increased to reach the critical point. The pressure was stabilized in the range of 1350 psi ± 5%. The unit was reached the critical point as the temperature was achieved 31 ^oC. In this stage, the tousimis equilibrium was started for 4 minutes.

- **Bleed:** When the tousimis equilibrium period was finished, the bleed cycle was automatically started. (The rate of the chamber should be maintained at 100-150 psi/min.)

- **Vent:** At approximately 400 psi, the bleed mode was changed to vent mode. In this mode, the pressure was reduced to atmospheric pressure in approximately 5 minutes. Finally, the samples were removed from the chamber.

IV- Molybdenum vanadium catalysts support by MCM-41

The MV-MCM-41 catalysts were prepared by impregnation method from Ammonium heptamolybdate tetrahydrate $(NH_4)_6Mo_7O_{24} \cdot 4H_2O$, Ammonium vanadate(V) NH_4VO_3 , citric acid, and MCM-41. First of all, the support MCM-41 was placed in the oven at 200 ^oC for 30 minutes with a heating rate of 5 ^oC/min.. Then, the MCM-41 was cooled in the dissector. The incipient volume of the MCM-41 was measured, and it was 2 ml/g. For the 2g of catalyst that was prepared, 4 ml of water were needed. Ammonium vanadate(V) was mixed with 4 ml of water. Citric acid was added to the vanadium solution with a ratio of one mole of V: one mole of citric acid to dissolve the vanadium into the water. Ammonium heptamolybdate tetrahydrate was mixed with the solution. The support MCM-41 was added to the solution, and it was kept at room temperature for one hour. The result was dried overnight at 110°C. The dried powder was crushed and calcined at 550°C for 6 h with heating rate 1 ^oC/min.

3.3 Characterizations of Prepared Catalysts

The catalysts were characterized by using the BET technique for surface area measurements and porosity studies and temperature programmed reduction (TPR) to find the most efficient reduction conditions. X-Ray Diffraction (XRD) and Raman spectroscopy were used for the fingerprint characterization of crystalline materials and the determination of their structure, and diffuse reflectance UV-V was used to analyze the effect of the metal inserted into the solid network.

3.2.1   Temperature Programmed Reduction (TPR)

Temperature-Programmed Reduction (TPR) was carried out in a quartz gas flow reactor, under a stream of 5% H_2 in Ar with rate 20 ml/min at atmospheric pressure, measuring the hydrogen consumption by a Thermal Conductivity Detector (TCD). The weight of supported catalyst and unsupported catalyst were 0.03 and 0.05g, respectively. The heating rate was 15°C/min., and the end temperature was 800°C.

3.2.2   BET surface area and pore volume

The N_2 was used as gas adsorption for determining the internal surface area of a mesoporous material. This method is based on the adsorption and condensation of N_2. The partial pressure of N_2 above the sample is gradually increased and the amount of N_2 adsorbed at each pressure increment is recorded. The process is then reversed, i.e., the pressure is gradually decreased. In the present study, specific surface areas were measured according to the BET theory. The weight for each sample was approximately 100mg for supported catalysts and 200mg for unsupported. Samples were degassed under vacuum at 300°C for 3 h before being analyzed.

3.2.3 Raman Spectroscopy

Raman spectra of VMo oxide catalysts supported and unsupported catalysts were recorded using a fiber optic RamanStation from Avalon equipped with a near-infrared laser (785 nm). The spectra were recorded with the laser power at 100 mW with 50 second exposure times and 10 scans. All spectra were recorded over the wavenumber range of 3000-250 cm^{-1} at 2 cm^{-1} resolution with the probe held ~ 5 mm above the powder samples. No further sample preparation was required.

3.2.4 UV Spectroscopy

Diffuse reflectance UV-V spectra were recorded using a Harrick Praying Mantis diffuse reflectance attachment fitted in a Perkin Elmer Lambda 650S spectrometer with an integrating sphere detector. The spectra were recorded over wavelength range 800-200 nm, with MgO used as the white reference material. The unsupported catalysts were diluted with MgO with a ratio of 1:10 catalyst and MgO respectively.

The spectra are displayed in F(R), Kubelka-Munk units

$$F(R) = \frac{(1-R)^2}{2R} = \frac{k}{S}$$

where k and S are the absorption and scattering coefficients.

3.2.5 X-Ray Diffraction (XRD)

The crystallinity and phase purity of synthesized catalysts can be obtained using powder X-ray diffraction (XRD), where every crystalline material has its own characteristic XRD pattern. It is diffracted by the crystalline phase in the specimen

according to the well known "Bragg's Equation," ($n\lambda=2d\sin\theta$). The fine powder was packed into a sample holder and the surface of the packed sample was smoothed with a flat glass. The powder X-ray diffraction spectra samples were recorded under the following operation conditions:

- Cu X-ray radiation from a broad focus tube at 40 KV and 30mA

- Divergence slit with 1 degree scatter slit and a receiving slit of 0.1 mm

- Scanning speed and interval of data collection was 2 degree 2θ/min.

- Angle scanned from 2-80 degree 2θ

- Scan mode was continuous Scan

3.3 Catalyst evaluation

The catalysts prepared in this study were evaluated by using fixed bed reactor (FBR) system. The sample of feed mixture gases that consisted of N_2, air and propane were introduced into the reactor with ratio 2:1 of propane and O_2, respectively. The experiments were performed over a temperature range of 350-600 °C.

3.3.1 Reaction systems

Figure 3.3 shows the reaction system that consists of three major parts. The first part is gas mixing. The second part consists of a high temperature furnace, three temperature controllers, and temperature monitor. The reactor is the final part.
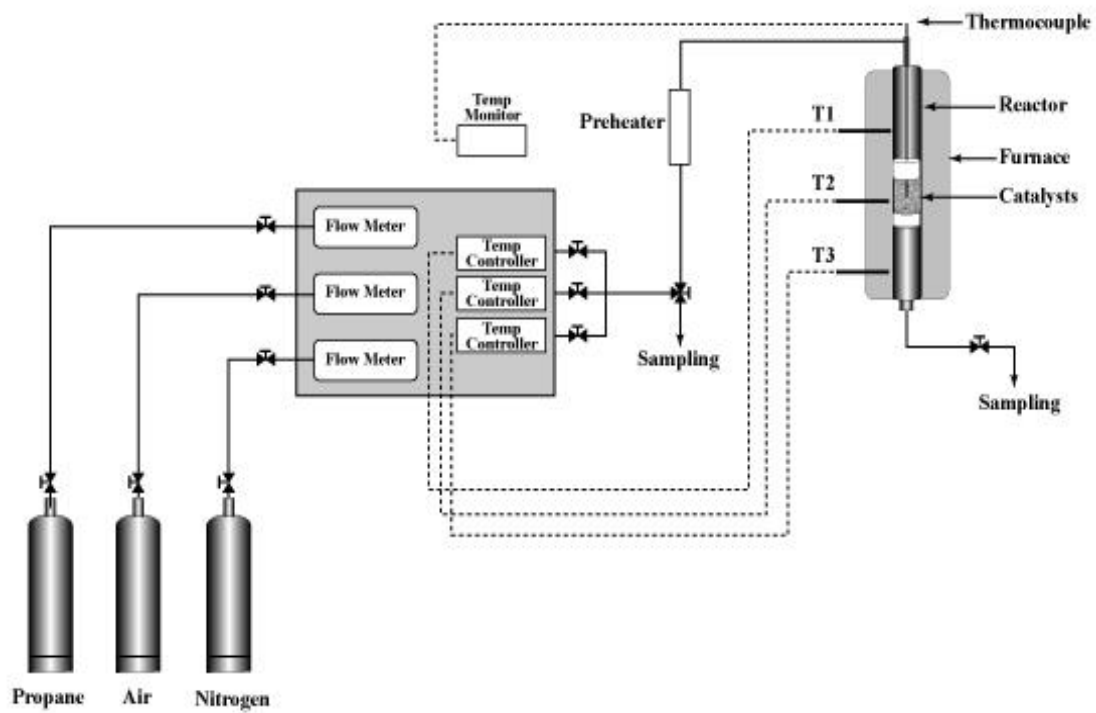
Figure 3.3 Schematic diagram of the reaction system.

3.3.2   Experimental set-up and procedure

The FBR system consists of three precise mass flow meters. They were connected to the gas cylinders, and they were used for metering the reactant gases as shown in Figure 3.3. In each line, three valves were placed to control the flow. The leak test was conducted after the connections were completed. Using the soap bubble-meter, the flow meters were calibrated with the same gas. To make sure no change in calibrations, the calibrations were checked in the beginning and the end of each experiment. The reactor is a half meter long stainless steel tube, and the ID diameter is one centimeter. The reactor furnace was divided into three equal zones and each of these zones was connected by temperature controllers that were used for increasing the temperature of the reactor.

The catalyst was placed in the middle of the reactor, and the thermocouple that was used for measuring the catalyst temperature was placed in the middle of the catalyst bed. The diameter of the thermocouple was 0.3 cm. The lower part of reactor was filled with calcium carbide and the quartz wool was put above the calcium carbide. Then, 0.5 grams of catalyst sample was filled in the middle of the reactor above the quartz wool, and another amount of the quartz wool was put above the catalyst. After that, the calcium carbide was filled the upper part of the reactor. To prevent blocking of the reactor or generating back pressure, all the packing was fixed properly. Finally, the reactor was fixed into the system.

To determine the final concentrations of hydrocarbons, CO_2, CO, O_2, and N_2, the gases were analyzed by three GCs with FID and TDC detectors. To begin the reaction, the mixture gases were fed to the reactor. By using temperature controllers, the

temperature of the reaction was increased. Initially, the temperature fluctuated before reaching the set point temperature, and the catalyst-bed temperature was monitored. The temperature was raised to 350, 400, 450, 500, 550 and 600 $^{\circ}$C. The product sample was collected in a special plastic bag after the catalyst temperature stabilized for 60 minutes. After that, the product was analyzed by GC. The product stream was circulated through the chiller to condense any liquid products. A CO detector was used during the experiments to detect any CO leak in the laboratory. The exhaust of the reaction was connected to the hood because CO is highly poisonous and H_2 is highly filmable. The same procedure was applied for each catalyst with the following reaction conditions:

- Feed gases consisted of N_2, air and propane with ratio 2:1 of propane and O_2

- Temperature range of 350-600 $^{\circ}$C.

- 0.5 grams of catalyst.

- Product sample collected in a special plastic bag after the catalyst temperature stabilized for 60 min.

CHAPTER 4

4. Results and Discussion

4.1 Characterization

4.1.1 BET Surface Area and Pore Volume

The surface area and pore volume were determined for unsupported catalysis (MoVOx-1, MoVOx-2 (SCD), MoVOx-3 (SCD), MoVOx-4 (SCD), and MoVOx-5 (SCD)) and supported catalysis (5MV/MCM-41, 10MV/MCM-41, and 15MV/MCM-41). In this section, the results of the surface area and pore volume are discussed.

BET Surface Area of Unsupported catalysts

The surface areas of catalysts with different mole ratios of Mo/V are presented in Table 4.1 and in Figure 4.1. The surface area of oxide catalyst usually is small. MoVOx-1 catalyst that was prepared by physical mixing from V_2O_5 and MoO_3 showed extremely low surface area (0.043 m^2/g). The other unsupported catalysts were prepared by a modified auto-combustion process of nitrate citrate gels method followed by super critical drying (SCD). The results shows that the surface area increased with an increase of the mole ratio of Mo/V, as illustrated in Figure 4.1. The surface area of MoVOx-2 (SCD) and MoVOx-3 (SCD) was 1.89 and 1.88 m^2/g, respectively. For MoVOx-4 (SCD), the surface area increased to 2.30 m^2/g. When the mole of molybdenum was 0.9 for MoVOx-5 (SCD), the surface area was 2.83 m^2/g.

Table 4.1 Surface area of unsupported catalysts.

Catalyst Code	Mo/V	Surface area (m^2/g)
MoVOx-1	1/1	0.043
MoVOx-2 (SCD)	1/1	1.89
MoVO-3 (SCD)	0.7/0.3	1.88
MoVO-4 (SCD)	0.8/0.2	2.30
MoVO-5 (SCD)	0.9/0.1	2.83
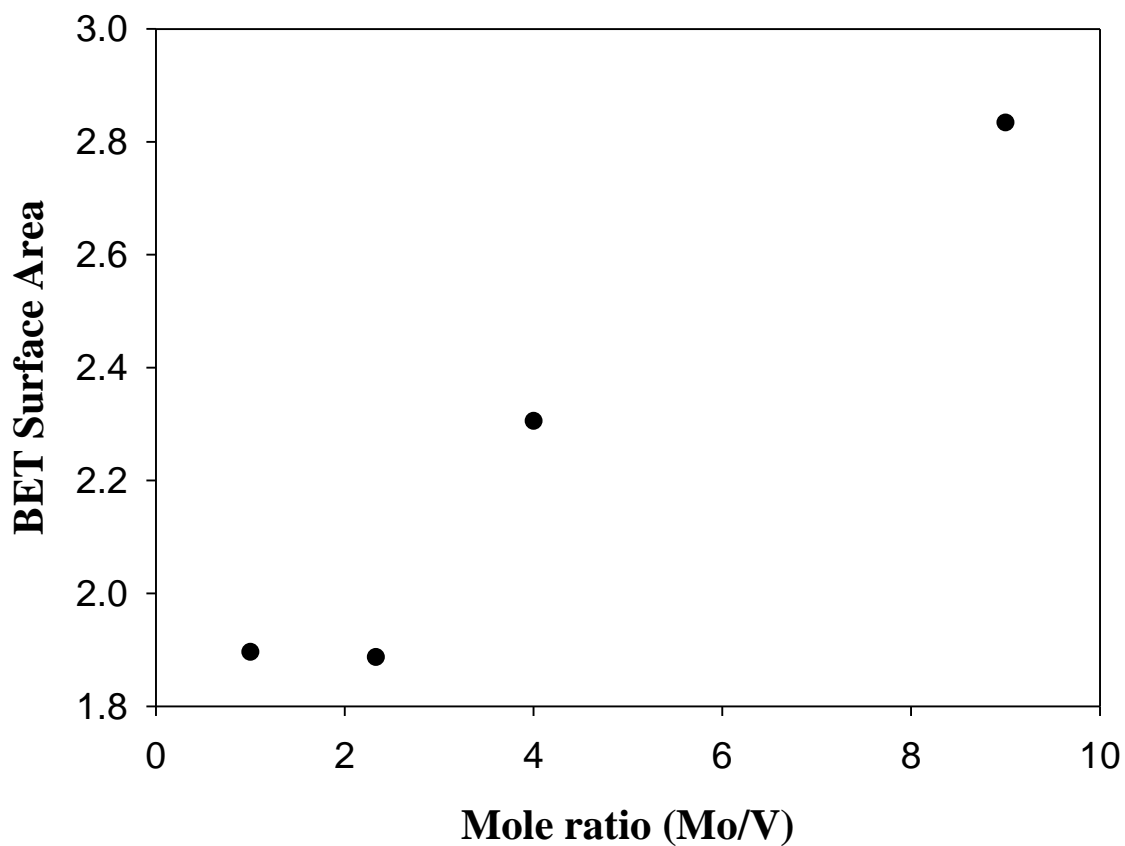
Figure 4.1 Surface area as function of mole ratio of Mo/V.

Table 4.2 and Figures 4.2 and 4.3 show the surface area of catalysts and pore volume of the support MCM-41 and xMV/MCM-41catalysts (x= 5, 10 and 15) that were prepared by the impregnation method. The surface area of MCM-41 was 1084 m^2/g, and the pore volume was 0.9 cm^3/g. The surface area was decreased with increasing of the metal loading, as illustrated in Figure 4.2. The surface area of the support was reduced by 40.4, 44.6 and 62.2 % with loadings of 5%, 10%, and 15%, respectively. The surface area of xMV/MCM-41catalysts were compared with literature values (Higashimoto et al. 2005; Wang et al., 2005) and it shows that the reduction in this catalysts higher than literature values. This reduction is because using the citric acid in the preparation steps. In addition, the pore volume decreased with the increasing of the metal loading, as presented in Figure 4.3. For example, the pore volume of support was reduced by 61.0% with 15% loading (15MV/MCM-41). The reduction in surface area and pore volume is due to the blockage of the pores of the support. The adsorption-desorption isotherm of MCM-41 and xMV/MCM-41catalysis (x= 5,10 and 15) are shown in Figures 4.4 and appendix A. The adsorption-desorption isotherm of xMV/MCM-41 catalysts did not change the type of porosity of the MCM-41. The capillary condensation occurred at a relative pressure of 0.45 and above and appeared to be leveling off near the saturation pressure. Capillary evaporation was shifted to relative pressures of over 0.05 lower than capillary condensation. The isotherm is known as a type IV isotherm, according to the IUPAC classification representing a mesoporous material with pores in the range of 2 to 50 nanometers.

Table 4.2 Surface area and pore volume of supported catalysis

Catalyst Code	Mo/V	Surface area (m^2/g)	Pore Volume (cm^3/g)
MCM-41	-	1084	0.90
5MV-MCM-41	1/1	646	0.63
10MV-MCM-41	1/1	601	0.55
15MV-MCM-41	1/1	410	0.35
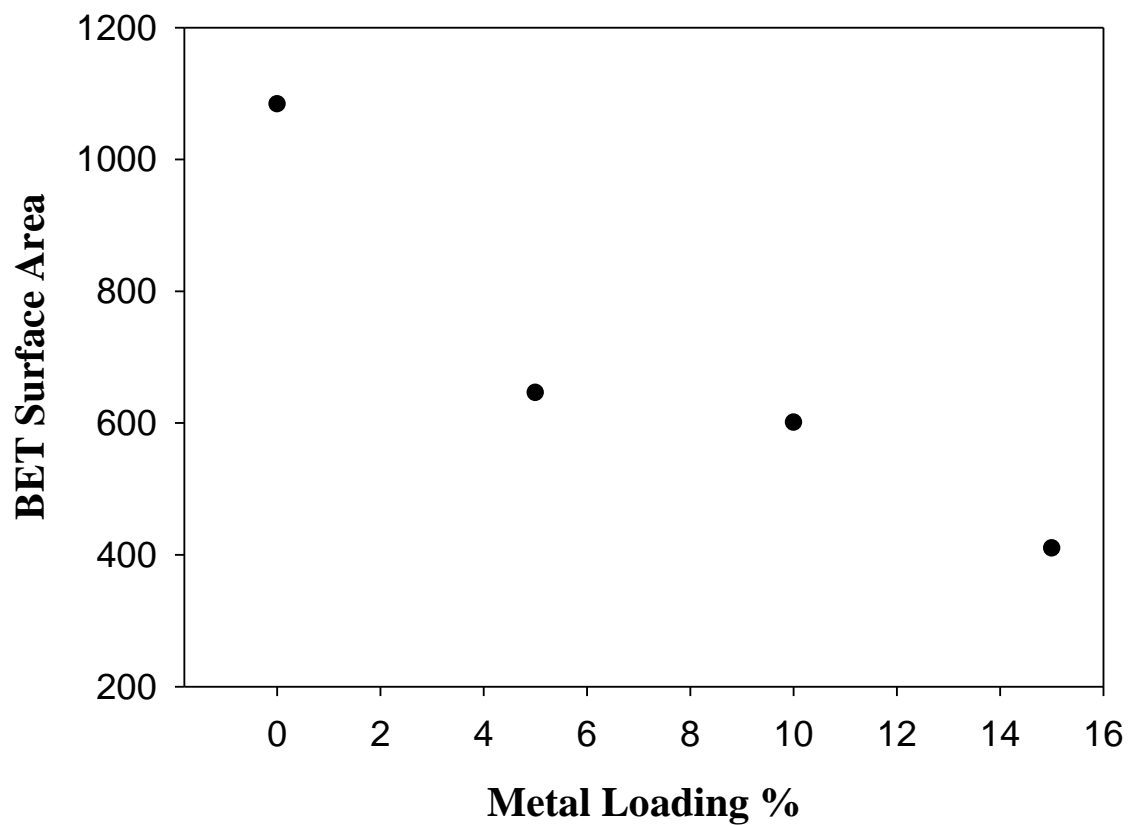
Figure 4.2 Surface area as function of metal loading %.
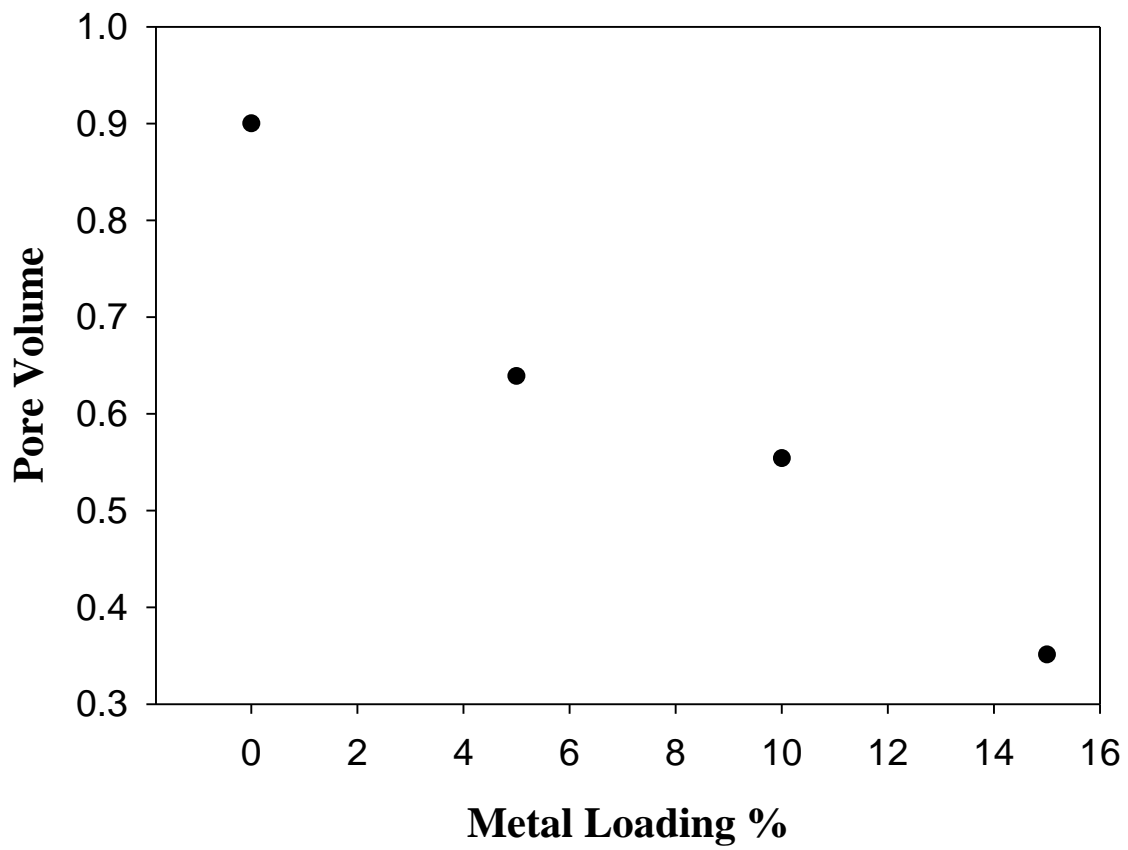
Figure 4.3 Pore volume as function of metal loading %.
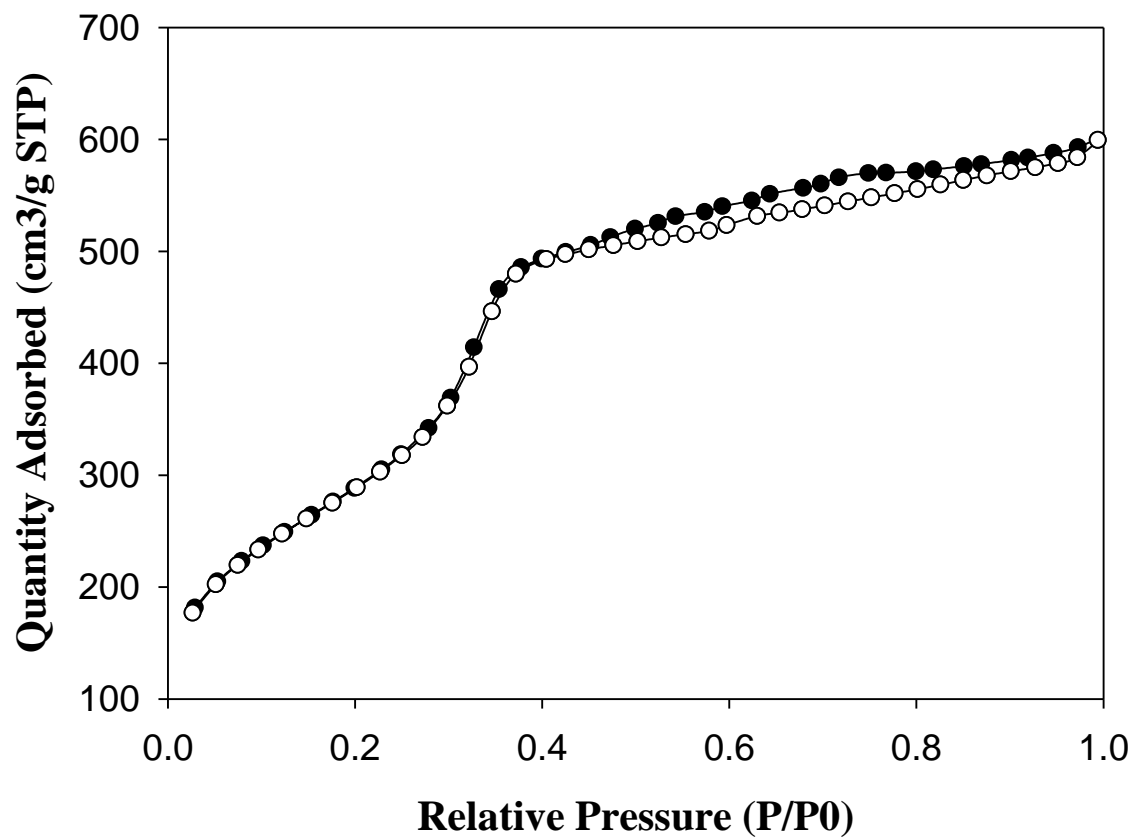
Figure 4.4 Adsorption-desorption isotherm of MCM-41.

4.1.2   Temperature Programmed Reduction (TPR)

Temperature Programmed Reduction (TPR) of unsupported catalysts

The temperature-programmed reduction (TPR) results of MoVOx-2 (SCD), MoVOx-3 (SCD), MoVOx-4 (SCD), and MoVOx-5 (SCD)   are plotted in Figure 4.5. The reduction profile for all samples shows two peaks. The first peak at 606 ^{o}C corresponds to simultaneous reduction of Mo^{6+} to Mo^{4+} and V^{5+} to V^{3+} and this peak is overlap reduction peak for Mo and V. The second peak at 731 ^{o}C is attributed to reduction of Mo^{4+} to Mo^{0} (Yang et al., 2005; Dai et al., 2004). The peak at 606 ^{o}C was reduced with   decreasing of vanadium content. On the other hand, the peak at 731 ^{o}C was increased with an increase of the molybdenum content.

Temperature Programmed Reduction (TPR) of supported catalysts

Temperature-programmed reduction (TPR) data of 5MV/MCM-41, 10MV/MCM-41 and 15MV/MCM-41 are shown in Figure 4.6. All catalysis show two peaks at β_Z and α_Z where Z = 5-7. The peaks at β_Z are assigned to reduction of Mo^{6+} to Mo^{4+} and V^{5+} to V^{3+}. The peaks at α_Z correspond to reduction of Mo^{4+} to Mo^{0} (Yang et al., 2005; Dai et al., 2004). At 5MV/MCM-41 catalysts, a shoulder at $\gamma_5 = 485$ ^{o}C is attributed to reduction of V^{5+} to V^{3+} and it disappears with an increase of the metal loading %. Furthermore, the hydrogen consumption diminishes with raising the metal loading %. The temperature of β_Z (Z = 5-7) peak goes up and the temperature of α_Z (Z = 5-7) peak declines with

increasing the metal loading %. Table 4.3 summarizes the TPR results reported in Figures 4.5 and 4.6.
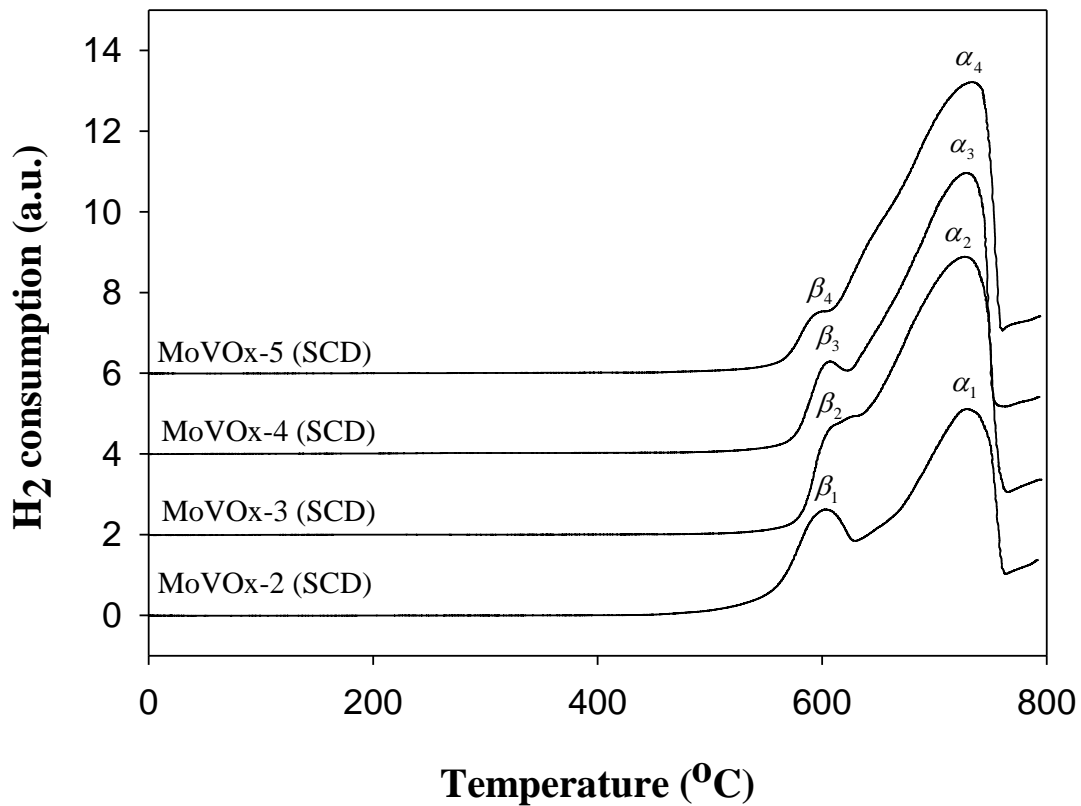
Figure 4.5 TPR profiles of MoVOx-2 (SCD), MoVOx-3 (SCD), MoVOx-4 (SCD) and MoVOx-5 (SCD).
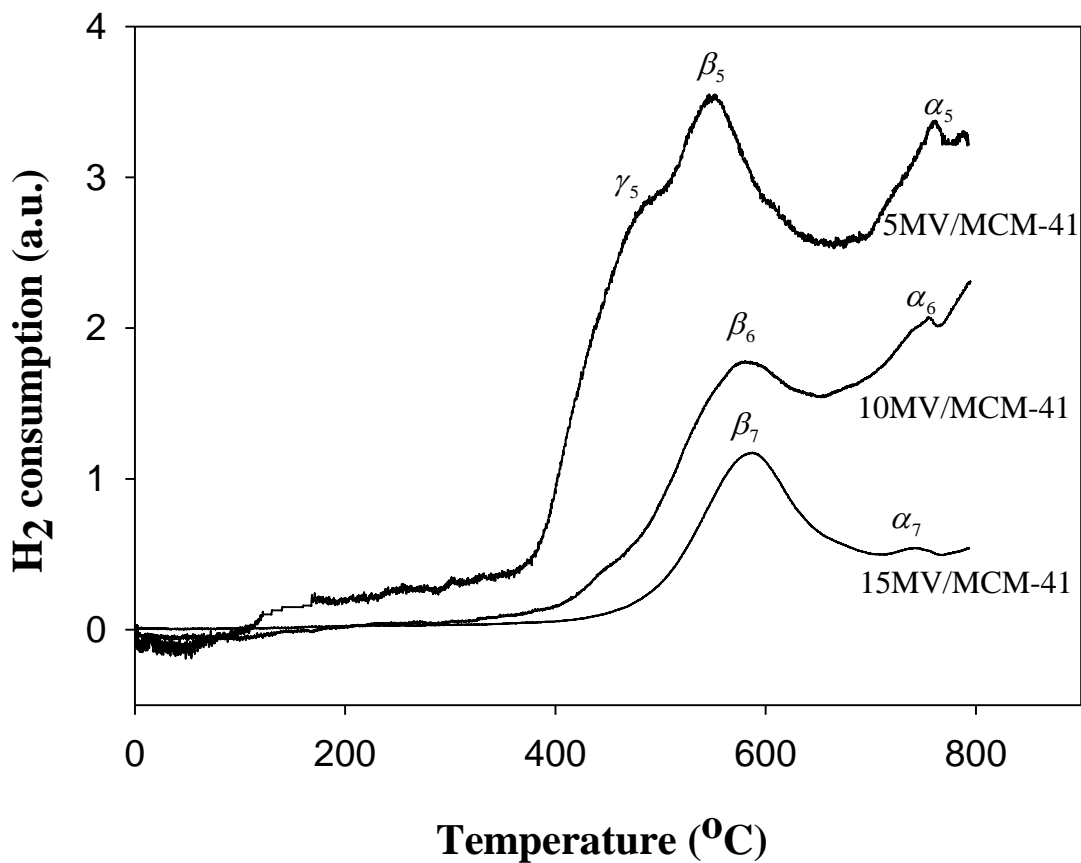
Figure 4.6 TPR profiles of 5MV/MCM41, 10MV/MCM41 and 15MV/MCM41.

Table 4.3 TPR Results Reported in Figures 4.5 and 4.6.

catalyst code	Z	β_Z °C	assignment	α_Z °C	assignment
MoVOx-2 (SCD)	1	606		731	
MoVO-3 (SCD)	2	606		731	
MoVO-4 (SCD)	3	606	$V^{5+} \longrightarrow V^{4+}$ $Mo^{6+} \longrightarrow Mo^{4+}$	731	$Mo^{6+} \longrightarrow Mo^{4+}$
MoVO-5 (SCD)	4	600		731	
5MV/MCM-41	5	550		760	
10MV/MCM-41	6	580		756	
15MV/MCM-41	7	586		746	

4.1.3   UV Spectroscopy

UV Spectroscopy of unsupported catalysts

The absorption spectra (UV) of MoVOx-2 (SCD), MoVOx-3 (SCD), MoVOx-4 (SCD), and MoVOx-5 (SCD) are displayed in Figure 4.7. An intense and broad absorption in 200–260 nm and 260–400 nm on the entire samples region are registered and could be related to charge transition of Mo^{6+} and V^{5+}. For the MoVOx-2 (SCD) catalyst, the absorption bands that appear at 400–500 nm regions are registered for V^{5+}, but it vanishes for other catalysts. The breadth of the band absorption decreases with an decrease of the molybdenum content (Guerrero-Perez et. al., 2008; Higashimoto et. al., 2005).

UV Spectroscopy of supported catalysts

The absorption spectra of 5MV/MCM41, 10MV/MCM41, and 15MV/MCM41 samples are shown in Figure 4.8. The absorption bands that appear at 200–400 nm regions are recorded and could be correlated to the presence of Mo^{6+} and V^{5+} species. For 5MV/MCM41 catalyst, the maximum is appeared at 235 nm when coverage is half monolayer and it presents lower than 10MV/MCM41 and 15MV/MCM41 catalysis. The maximum band for 10MV/MCM41 and 15MV/MCM41 is 340 nm. The amount of absorption increases with rising metal loading. This absorption is indicative of an electronic interaction between Mo and V oxide centers (Guerrero-Perez et. al., 2008; Higashimoto et. al., 2005).
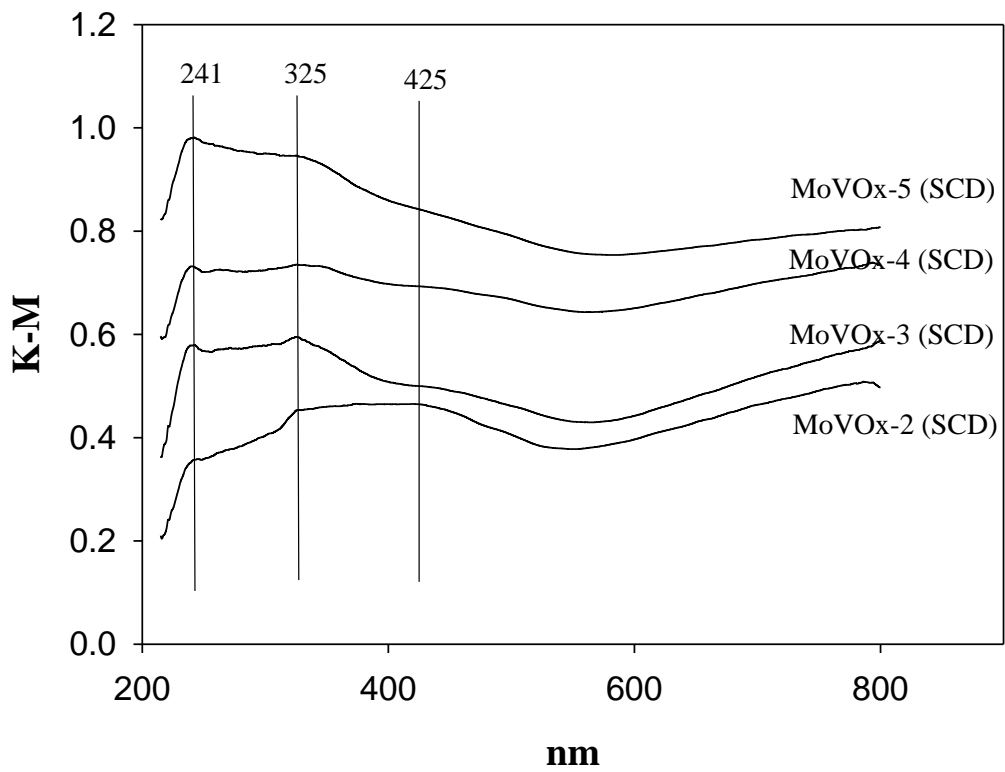
Figure 4.7 UV spectra of MoVOx-2 (SCD), MoVOx-3 (SCD), MoVOx-4 (SCD) and MoVOx-5 (SCD).
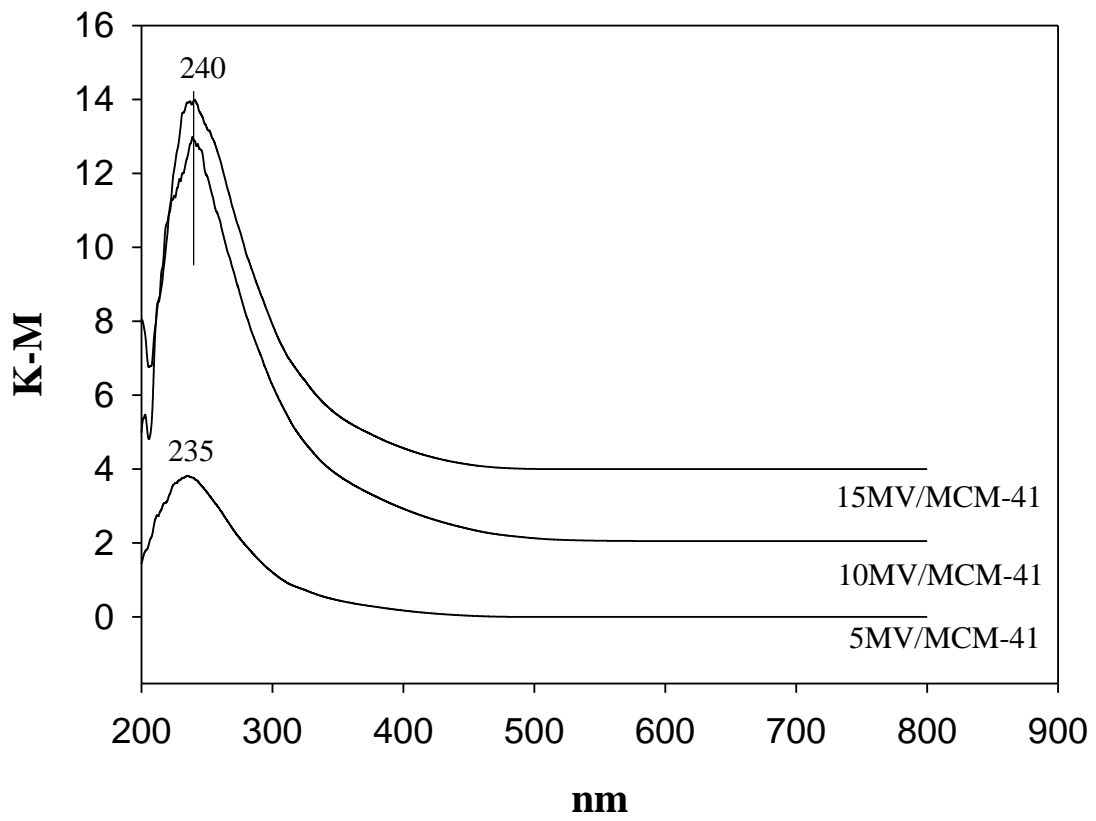
Figure 4.8 UV spectra of 5MV/MCM41, 10MV/MCM41 and 15MV/MCM41.

4.1.4   X-Ray Diffraction (XRD)

X-Ray Diffraction (XRD) of unsupported catalysts

Table 4.4 summarizes the results of 2θ for MoVOx-2 (SCD), MoVOx-3 (SCD), MoVOx-4 (SCD), and MoVOx-5 (SCD) that are shown in Figure 4.9.   They are compared with the results that were investigated in the Bin (2005) study. The crystallization of the catalyst increased with an increase in the molybdenum content. Some of the peaks can be affected by increasing the molybdenum content and decreasing the vanadium content. The peaks at $2\theta =18.2^{o}$ and 25.0^{o} are related to MoV_2O_8 and the peak at $2\theta =21.6^{o}$ corresponds to V_2O_5 (Takehira et al., 2004). The XRD results show two new peaks: the first peak at $2\theta =44.2^{o}$ could be attributed to V_2O_5 because it appears only in the MoVOx-2 (SCD) at high vanadium content and the second peak at $2\theta =67.5^{o}$ could be attributed to MoO_3 because it comes into view with rising molybdenum content.

Figure 4.10 and Table 4.5 show the XRD results of MoVOx-1, and they are compared with the XRD peaks that were examined in the Bin (2005) study. The catalyst MoVOx-1 is Crestline material, and it shows new peaks, such as $2\theta = 29.8^{o}$ and 39.7^{o}. The peak at $2\theta =21.6^{o}$ corresponds to V_2O_5, and the peak at $2\theta =57.9^{o}$ is assigned to MoV_2O_8 (Takehira et al., 2004). The peak at $2\theta =67.7^{o}$ could be related to MoO_3.
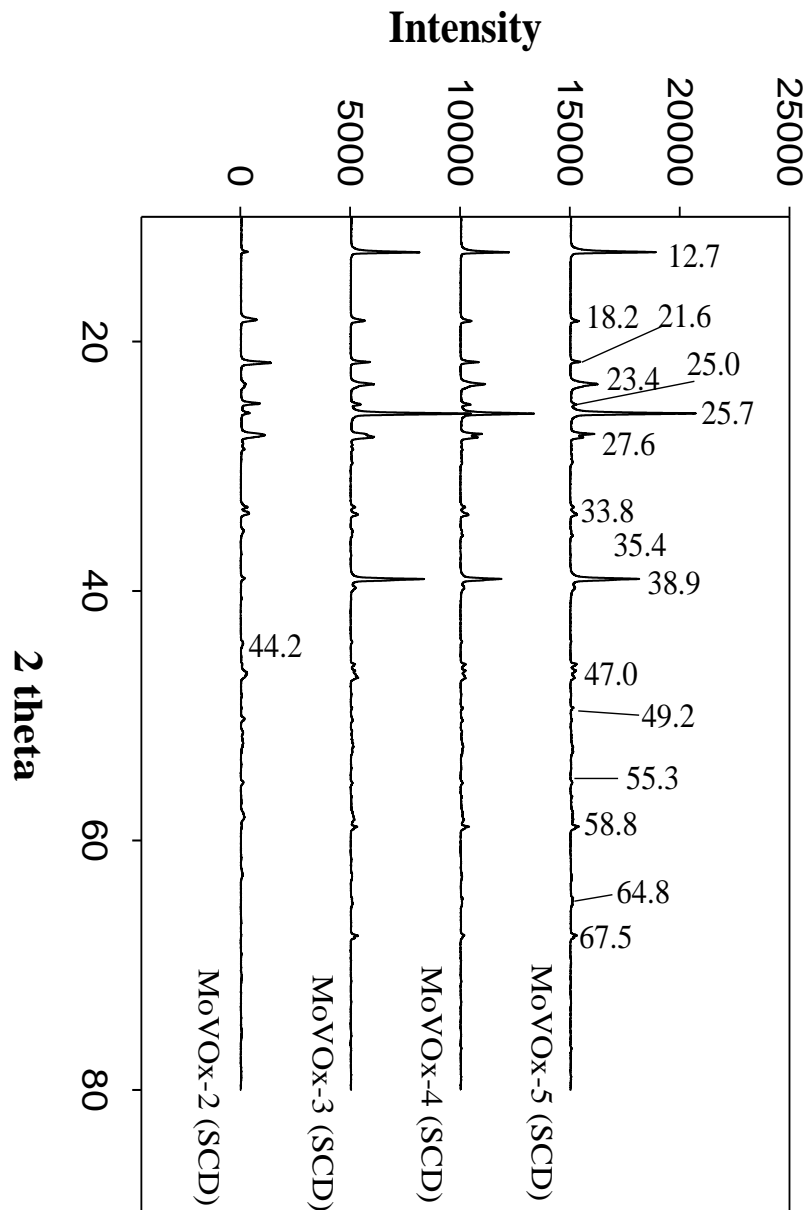
Figure 4.9 XRD patterns of MoVOx-2 (SCD), MoVOx-3 (SCD), MoVOx-4 (SCD) and MoVOx-5 (SCD).

Table 4.4 XRD indexed results of MoO3 and V2O5 for MoVOx-2 (SCD), MoVOx-3 (SCD), MoVOx-4 (SCD), and MoVOx-5 (SCD).

MoO_3 2θ		
Found	JCPDS 5-508	Bin et al., 2005
12.7	12.76	12.76
23.4	23.33	23.33
25.7	25.7	25.7
27.6	27.33	27.33
33.8	33.73	33.73
35.4	35.5	35.5
38.9	38.98	38.98
49.2	49.24	49.24
55.3	55.19	55.19
58.8	58.8	58.8
64.8	64.53	64.53
V_2O_5 2θ		
Found	JCPDS 41-1426	Bin et al., 2005
47	47.32	47.32
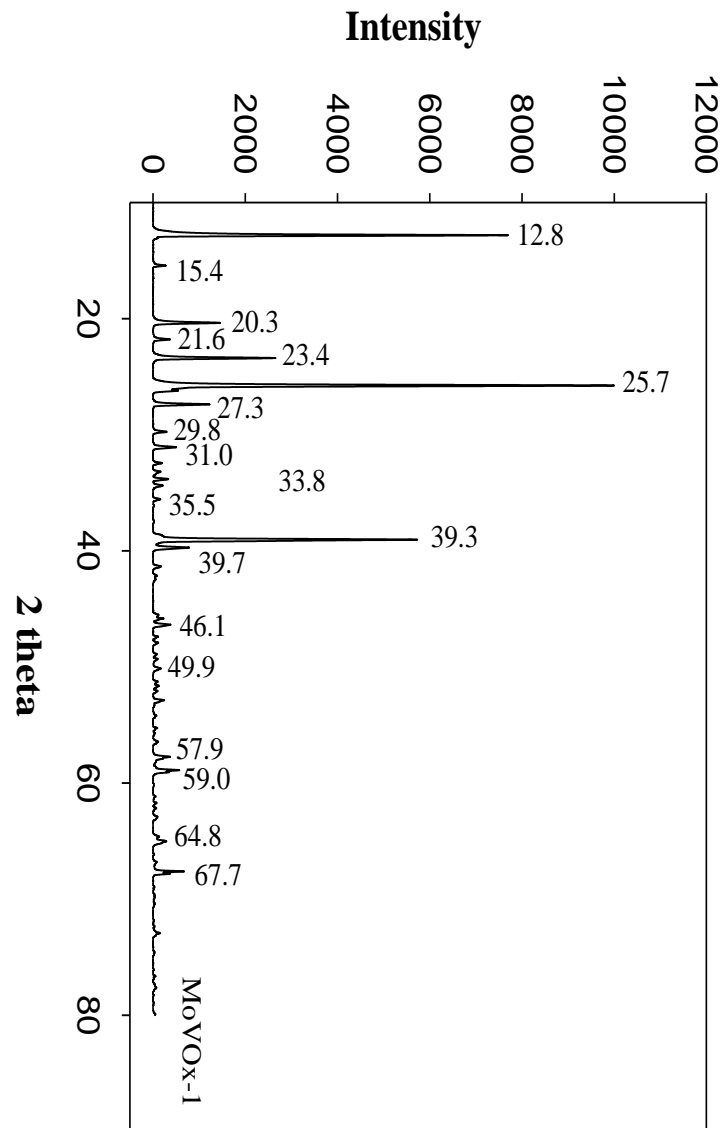
Figure 4.10 XRD patterns of MoVOx-1.

Table 4.5 XRD indexed results of MoO_3 and V_2O_5 for MoVOx-1.

MoO$_3$		
Found	JCPDS 5-508	Bin et al., 2005
12.8	12.76	12.76
23.4	23.33	23.33
25.7	25.7	25.7
27.3	27.33	27.33
33.8	33.73	33.73
35.5	35.5	35.5
39.3	38.98	38.98
46.1	45.74	45.74
49.9	49.24	49.24
59	58.8	58.8
64.8	64.53	64.53
V$_2$O$_5$		
Found	JCPDS 41-1426	Bin et al., 2005
15.4	15.35	15.35
20.3	20.26	20.26
31	31	31

<u>X-Ray Diffraction (XRD) of supported catalysts</u>

MCM-41, 5MV/MCM-41, 10MV/MCM-41, and 15MV/MCM-41 at low (2θ= 1.8^o to 10°) and high (2θ= 10° to 80°) 2θ is analyzed by X-Ray Diffraction (XRD) as presented in Figures 4.11 and 4.12, respectively. It is clear from the results of XRD that all samples are amorphous material. At low 2θ, MCM-41, 5MV/MCM-41, 10MV/MCM-41, and 15MV/MCM-41 show diffraction in the range $2\theta = 3.2^o$ - 5.5^o, and the intensity of the diffraction decreases with increasing metal loading %. This might be attributed to V–O (~1.5893 Å) and Mo–O (~1.658 Å) longer bonding length with oxygen than Si–O (~1.509 Å) (Selvaraj & Lee, 2005). At high 2θ, the humps centered at 23° for all samples are due to the diffraction of the amorphous silica. The peak at 77.5^o is related to the support MCM-41. For 5MV/MCM-41, the peak at 44.4^o could be related to V_2O_5. The peaks appear with increasing metal loading %. For example, the peaks at 23.4^o, 25.9^o, 27.6^o for 15MV/MCM-41 are assigned to MoO_3 (Bin et al., 2005) and the peaks at 21.9^o and 30.6^o for 15MV/MCM-41 correspond to V_2O_5 (Bin et al., 2005; Takehira et al., 2004).
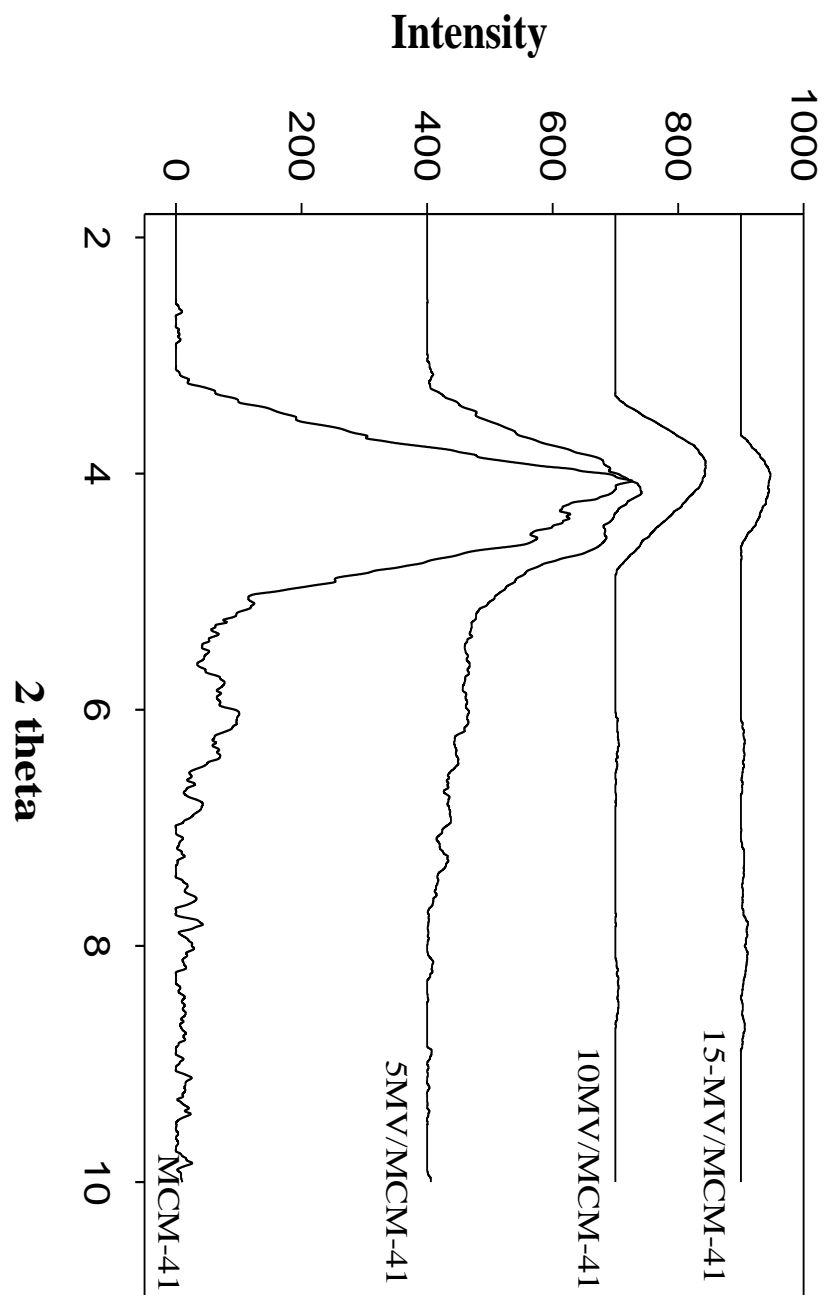
Figure 4.11 XRD patterns of MCM41, 5MV/MCM-41, 10MV/MCM-41 and 15MV/MCM-41 at low 2θ.
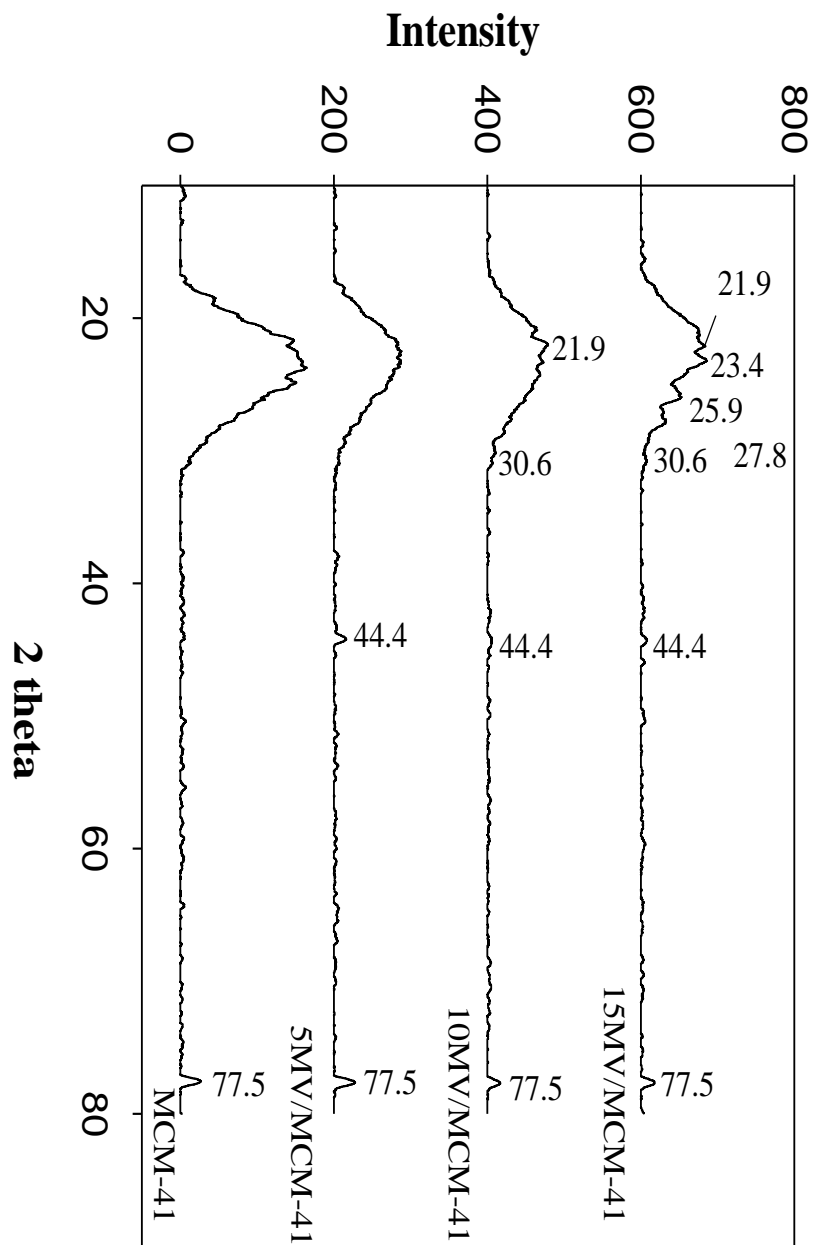
Figure 4.12 XRD patterns of MCM-41, 5MV/MCM-41, 10MV/MCM-41 and 15MV/MCM-41 at high 2θ.

4.1.5   Raman Spectroscopy

Raman Spectroscopy of unsupported catalysts

Figure 4.13 shows Raman spectra for MoVOx-2 (SCD), MoVOx-3 (SCD), MoVOx-4 (SCD), and MoVOx-5 (SCD). When the molybdenum content increases, the crystallization of the catalyst increases because the intensity of the peaks rises (this is in line with XRD results). The peaks at 291, 338, 380, 668, 820 and 995 cm^{-1} have been attributed to MoO_3 crystals (Kornelak et al., 2007). The peaks at 488 and 600 cm^{-1} have been assigned to V_2O_5 crystals (Yang et al., 2005). The peak at 600 cm^{-1} shifted by 60 cm^{-1}, and this could be inductive of a destroyed V_2O_5 by some Mo cations. The Raman spectrum catalysts show a peak located at 785 cm^{-1}. This peak is assigned to polymolybdovanadate species V-O-Mo vibration, and these phases appear to be efficient for alkane activation. The Raman spectrum shows the peak characteristic of M-O-M bands (where M = Mo or V) located at 933 cm^{-1} (Murgia et al., 2008), and this peak at 933 cm^{-1} appears only in MoVO-5 (SCD) catalyst.

84
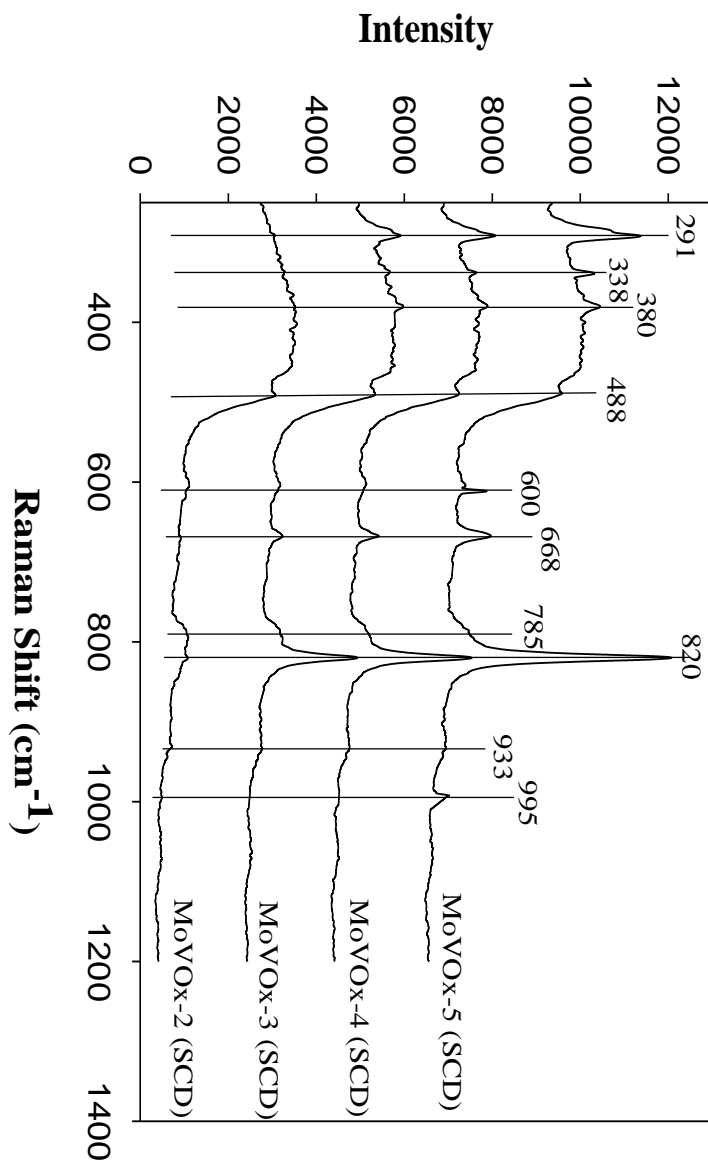
Figure 4.13 Raman spectroscopy of MoVOx-2 (SCD), MoVOx-3 (SCD), MoVOx-4 (SCD) and MoVOx-5 (SCD).

Raman Spectroscopy of supported catalysts

Raman spectroscopy of MCM-41, 5MV/MCM-41, 10MV/MCM-41, and 15MV/MCM-41 are shown in Figure 4.14. The Raman results for support catalysis prove that all catalysts are amorphous materiel due to the absence of sharp peaks. The peaks at 380 and 830 cm^{-1} are assigned to MoO_3 crystals (Kornelak et al., 2007) while the peaks at 489 and 600 cm^{-1} are assigned to V_2O_5 crystals and V-O-V (polymeric surface vanadate oxide species) stretch mode on the surface of the support, respectively (Yang et al., 2005). There is also a peak present at 910 cm^{-1} and 950 cm^{-1} which are assigned to Mo-O-Mo (polymeric surface molybdenum oxide species) and V-O-V (polymeric surface Vanadium oxide species) stretch mode on the surface of the support respectively. The peaks at 1009 and 1055 cm^{-1} represent the Mo=O stretching mode of the surface monooxo molybdenum oxide species and the monovanadate species V=O (stretching mode), respectively. The presence peak at 785 cm^{-1} is assigned to polymolybdovanadate species V-O-Mo vibration and indicates that Mo and V interact, forming Mo-O-V phases above monolayer coverage. This interaction could be efficient for alkane activation (Murgia et al., 2008). The peak at 600 cm^{-1} assigned to V_2O_5 crystals and shifted by 60 cm^{-1} because of destroyed V_2O_5 by some Mo cations as discussed previously.
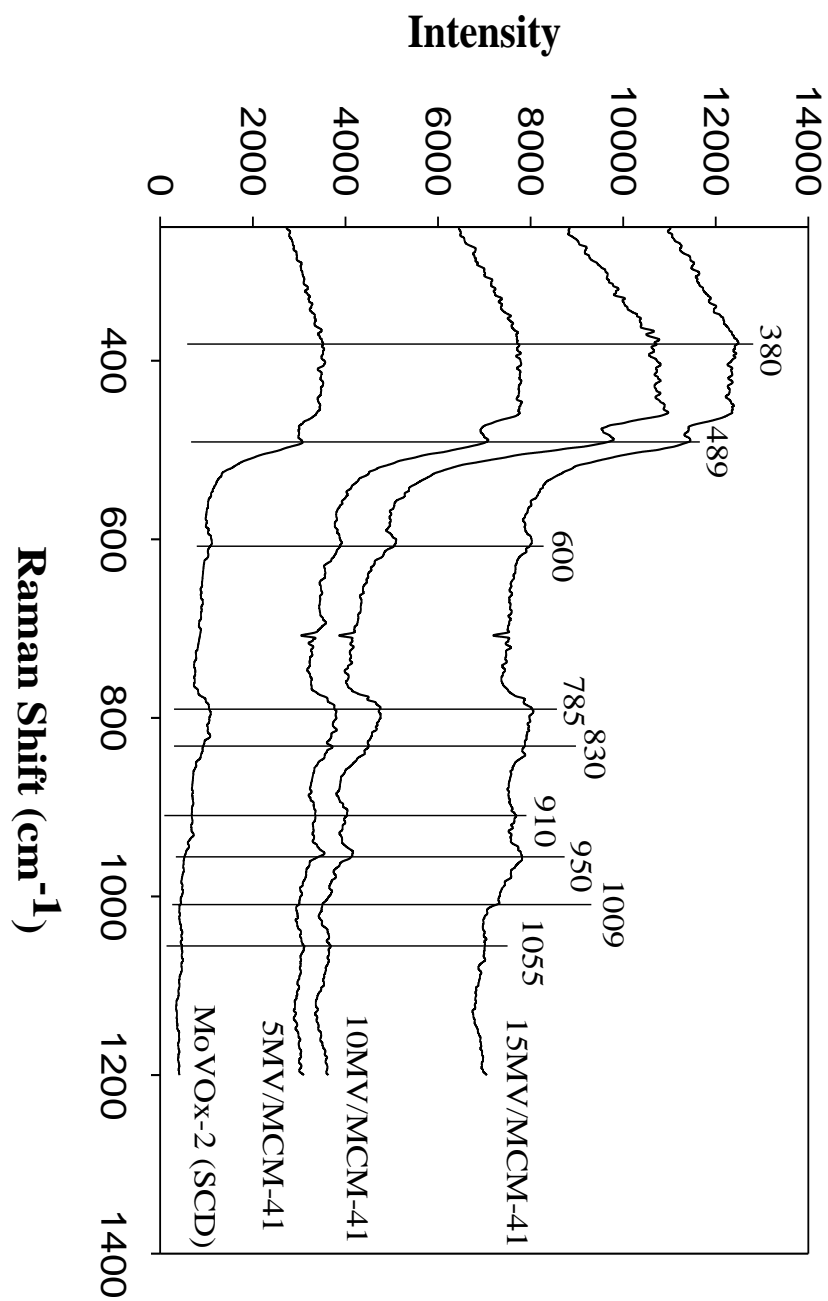
Figure 4.14 Raman spectroscopy of MCM-41, 5MV/MCM-41, 10MV/MCM-41 and 15MV/MCM-41.

4.2 Performance Evaluation of Catalysts

In the present study, the performances of unsupported (MoVOx-Y (SCD) where Y =2, 3, 4, and 5; MoVOx-1; and supported (xMV/MCM-41 where x=5, 10, and 15 catalysts were evaluated. The effects of varying the compositions of vanadium and molybdenum on the performance of unsupported catalysts that were prepared by a modified auto-combustion process of nitrate citrate gels method were investigated. Also, the effects of increasing metal loading percentage to the supported catalysts that were prepared by the impregnation method were studied. The effect of washing and super critical drying in the performance of MoVO-2 catalyst was evaluated. In addition, the life time of 15MV/MCM-41 was examined. The activity tests were carried out in a fixed bed reactor (FBR) system. The sample of feed mixture gases consisted of N_2, air, and propane, and they were introduced into the reactor with a ratio of 2:1 of propane and O_2, respectively, with a 100 ml/min total flow rate. The experiments were performed over a temperature range of 350 -600 °C. For all cases, the major products of the reaction were mainly propylene, H_2, CO_x, and other hydrocarbons. Throughout the present research, the following definitions will be used:

$$\text{Conversion (\%)} = \frac{\text{moles of propane reacted}}{\text{moles of propane in feed}} * 100 \qquad 4.1$$

$$\text{Selectivity (\%)} = \frac{\text{moles of propylene in product}}{\text{moles of propane reacted}} * 100 \qquad 4.2$$

$$\text{Yield (\%)} = \frac{\text{moles of propylene in product}}{\text{moles of propane in feed}} * 100 \qquad 4.3$$

4.2.1 Blank Runs

Figure 4.15 and Table 4.6 show, as a reference case, the propane conversion and product selectivity, as well as propylene yields in the reactor without any catalyst at different temperature. A higher temperature led not only to the start in propane conversion, but also to a drop in propylene selectivity due to thermal cracking. The effect of cracking began above 450 °C with approximately 1.7 % conversion of propane. The selectivity of propylene was 100% at 500 °C, and it decreased until reaching 14.3% at 600 °C due to combustion of propylene to CO_2, with selectivity near 85 % at 550 °C and 600 °C.

Table 4.6 Conversion, selectivity, and yield results of blank reactor (reaction conditions: F = 100 ml/min, $C_3H_8/O_2/N_2$ = 6/3/91).

Catalysts Code	Temperature °C	Propane Conversion %	Propylene Selectivity %	CO_2 Selectivity %	Propylene Yield %
Blank	350	0.0	0.0	0.0	0.0
	400	0.0	0.0	0.0	0.0
	450	0.0	0.0	0.0	0.0
	500	1.7	100.0	0.0	1.7
	550	0.9	14.7	85.3	0.1
	600	1.7	14.3	85.6	0.2
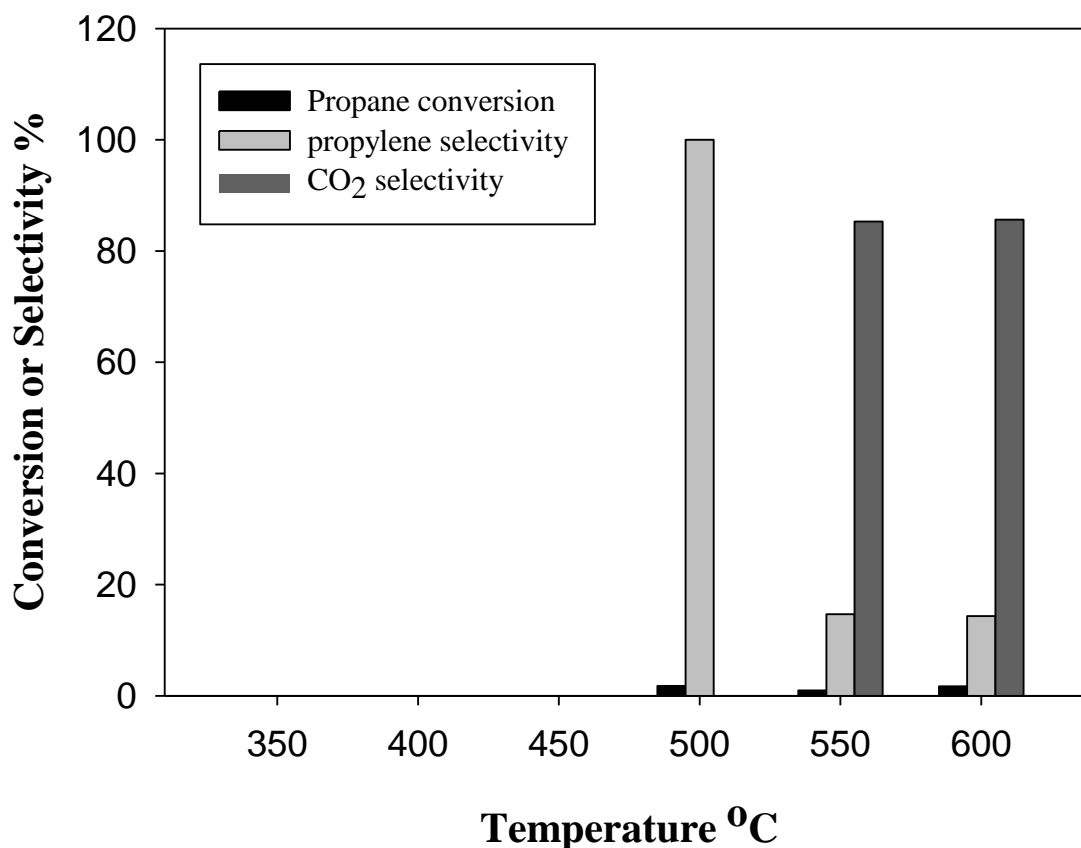
Figure 4.15 Conversion and selectivity as function of temperature of blank Runs (reaction conditions: F = 100 ml/min, $C_3H_8/O_2/N_2$ = 6/3/91).

4.2.2   Effects of washing and Super Critical Drying (SCD) on MoVOx-2 catalyst

The activity of MoVO-2 catalyst and MoVO-2 (SCD) catalyst were tested. Table 4.7 and Table 4.8 show propane conversion, propylene selectivity and yield, CO_2, and CO selectivity. The temperature range used in this work was 350 – 600 °C. The feed mixture gases rate was 100 ml/min, and it contained propane, nitrogen, and oxygen with a ratio of 2:1 of $C_3H_8:O_2$. There was marked improvement in the performance of MoVO-2 after washing and super critical drying (SCD). For MoVO-2, the propylene selectivity was

90

zero (0) until the temperate reached 450 °C. On the other hand, the propylene selectivity of MoVO-2 (SCD) was 100 % from 350 °C to 450 °C. Figure 4.16 shows conversion as a function of temperature for MoVO-2 catalyst and MoVO-2 (SCD) catalyst. The increase of the reaction temperature from 350 to 600 °C increased conversion from 4.0% to 13.1% for the MoVO-2 catalyst and from 2.7% to 12.8% for the MoVO-2 (SCD) catalyst because of increasing the temperature raised the amount of adsorbed propane and lifts up the propane conversion. In Figure 4.17, there is no propylene at 350 and 400 °C for MoVO-2 catalyst. The selectivity of propylene started at 450 °C, and it increased from 3.1% to 12.8%. The CO_2 selectivity was 100 at 350 and 400 °C, and it decreased at higher temperatures. In contrast, the propylene selectivity of the MoVO-2 (SCD) catalyst is 100% at 350, 400 and 450°C; it decreased along with the temperature until it reached 20.6%, as shown in Figure 4.18. Also, the CO_2 selectivity increased at higher temperatures for MoVO-2 (SCD) catalyst and it began producing at 550 °C. The selectivity of CO increased with an increase in the temperature, and it began producing at 500 °C for both catalysts. The production of CO_2 rather than propylene for MoVO-2 catalyst at low temperature could have been due to the formation of the Carbone-metal complexes during the self-ignition stage. The calcinations step did not remove all the Carbone that was formed. The O_2 that was introduced in the feed to the reactor preferred to react with the formation of Carbone. At higher temperatures, the selectivity of CO_2 decreased, and the selectivity of propylene increased because the Carbon was reduced, and the molybdenum and vanadium metal initiated their activity. This change in the catalyst activity for MoVO-2 (SCD) was due to the removal of the carbon that was produced in the self-ignition stage by using the washing and Super Critical Drying.

Table 4.7 Temperature, conversion, selectivity, and yield of MoVO-2 catalyst (reaction conditions: F = 100 ml/min, W= 0.5 g, $C_3H_8/O_2/N_2$ = 6/3/91).

Temperature °C	Propane Conversion %	Propylene Selectivity %	CO_2 Selectivity %	CO Selectivity %	Propylene Yield %
350	4.0	0	100	0	0
400	4.8	0	100	0	0
450	6.9	3.1	96.9	0	0.2
500	11.1	5.9	87.8	6.2	0.6
550	12.7	11.1	78.3	10.5	1.4
600	13.1	12.8	74.3	12.8	1.6

Table 4.8 Temperature, conversion, selectivity, and yield of MoVO-2 (SCD) catalyst (reaction conditions: F = 100 ml/min, W= 0.5 g, $C_3H_8/O_2/N_2$ = 6/3/91).

Temperature °C	Propane Conversion %	Propylene Selectivity %	CO_2 Selectivity %	CO Selectivity %	Propylene Yield %
350	2.7	100.0	0.0	0.0	2.7
400	2.9	100.0	0.0	0.0	2.9
450	3.4	100.0	0.0	0.0	3.4
500	7.6	31.6	0.0	68.3	2.4
550	9.8	26.6	23.0	50.3	2.6
600	12.8	20.6	30.5	48.8	2.6
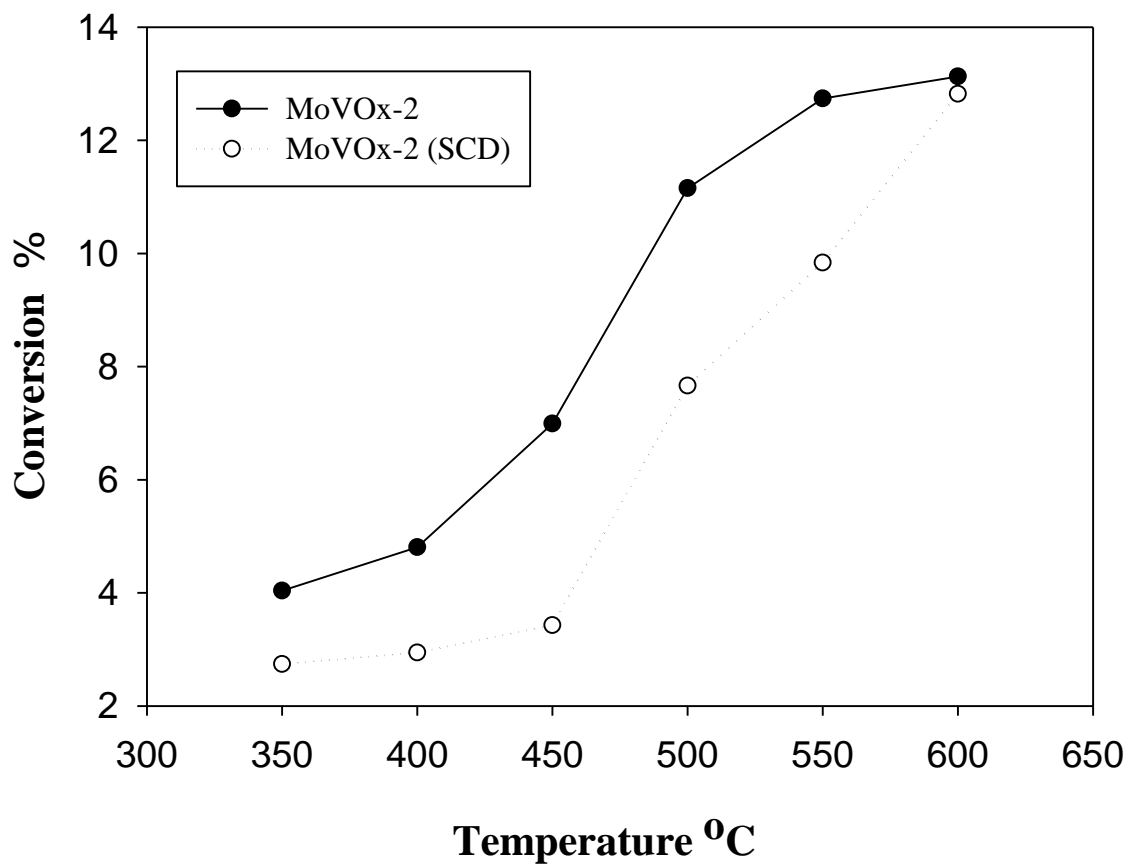
Figure 4.16 Propane conversion values as a function of temperature in propane ODH of MoVO-2 catalyst and MoVO-2 (SCD) catalyst (reaction conditions: F = 100 ml/min, W= 0.5 g, $C_3H_8/O_2/N_2 = 6/3/91$).
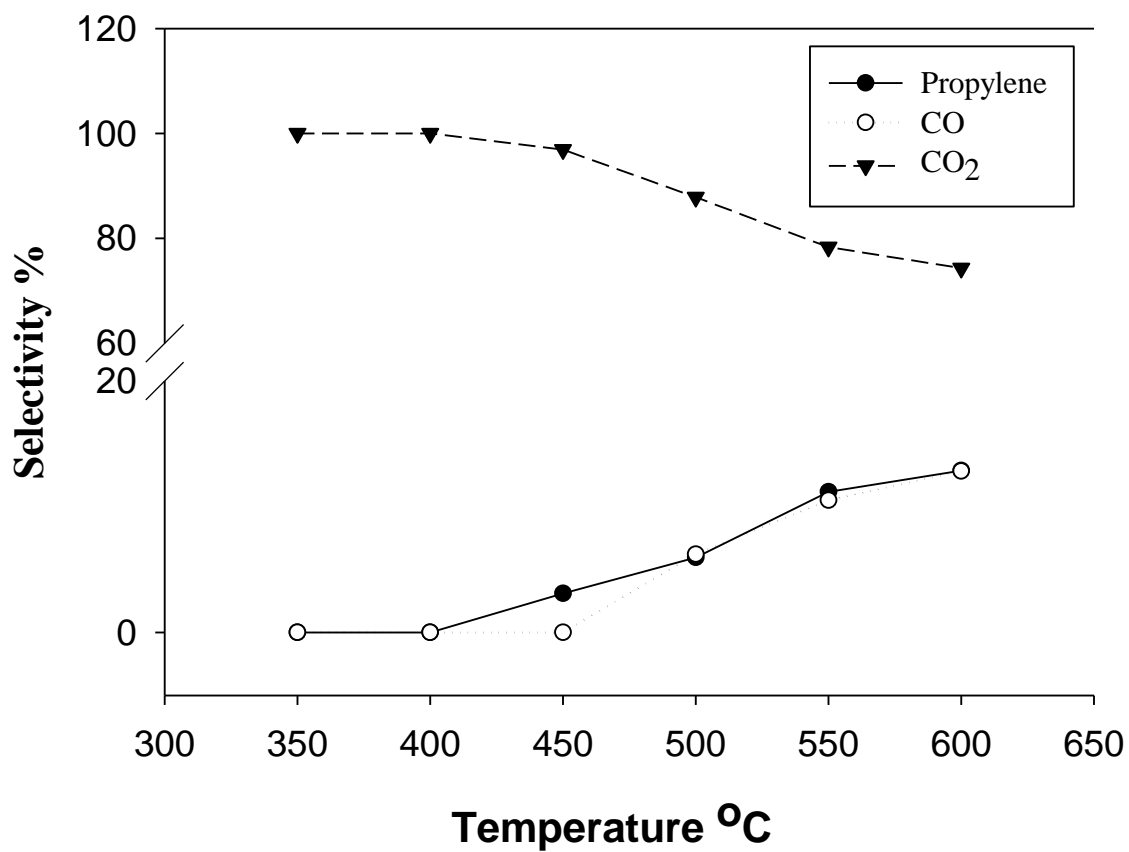
Figure 4.17 Selectivity values as a function of temperature in propane ODH of MoVO-2 catalyst (reaction conditions: F = 100 ml/min, W= 0.5 g, $C_3H_8/O_2/N_2$ = 6/3/91).
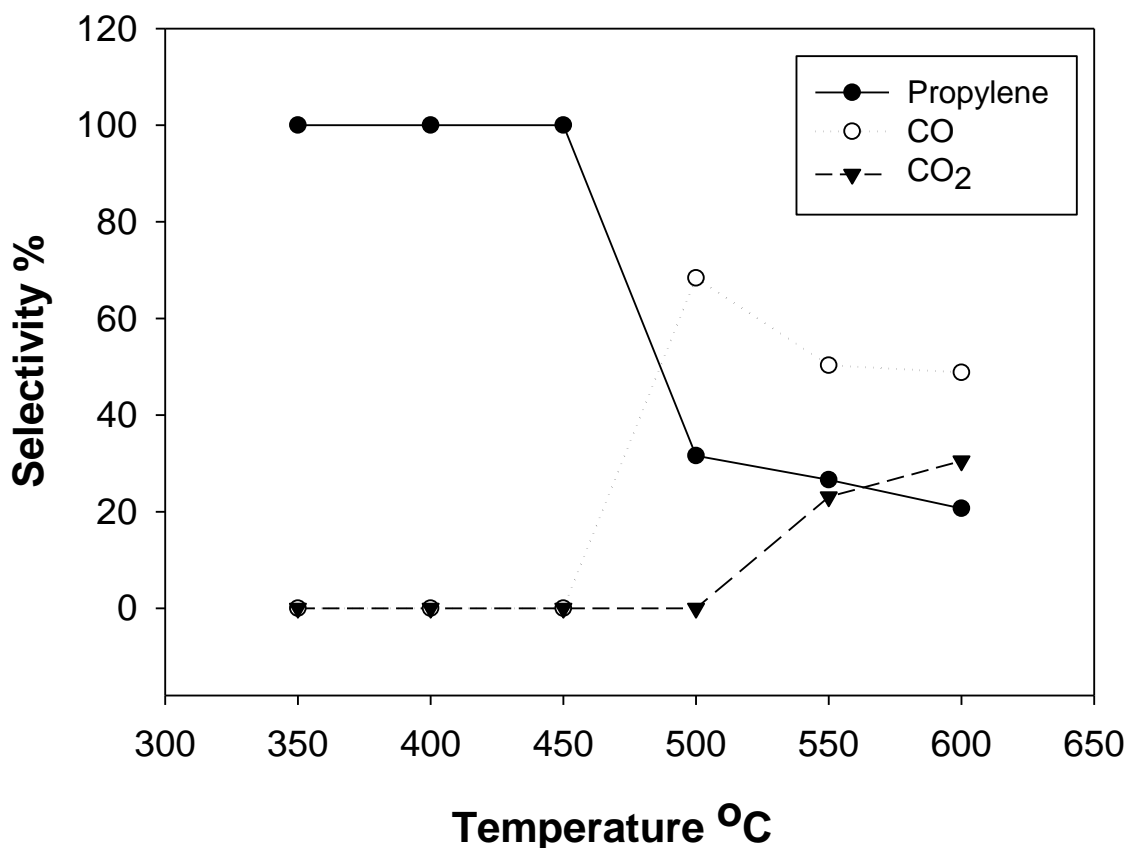
Figure 4.18 Selectivity values as a function of temperature in propane ODH of MoVO-2 (SCD) catalyst (reaction conditions: $F = 100$ ml/min, $W= 0.5$ g, $C_3H_8/O_2/N_2 = 6/3/91$).

4.2.3   Evaluation of unsupported catalysts

Table 4.9 shows the conversion, selectivity, and yield results of MoVO-2 (SCD), MoVO-3 (SCD), MoVO-4 (SCD), and MoVO-5 (SCD) catalysts. Figures 4.19 and 3.20 depict catalyst propane conversion as a function of the temperature and propylene selectivity as a function of the temperature, respectively, for MoVO-2 (SCD), MoVO-3 (SCD), MoVO-4 (SCD), and MoVO-5 (SCD) catalysts. For all catalyst, the propane conversion and the propylene selectivity observed for the reactions were strongly dependent on the reaction temperatures. The conversion of propane obviously increased

with increasing temperatures. The selectivity of propylene decreased with increasing temperatures. The product contained propylene, CO and CO_2 without any hydrocarbon or hydrogen, even at high temperatures. The inverse relationship between propane conversion and propylene selectivity is well known and commonly reported in the literature. This phenomenon is caused by the consecutive conversion of propane and propylene to CO and CO_2.

MoVO-2 (SCD) catalyst showed the best performance among the other catalysts, and the activity of the catalyst started at the low temperature of 350 ^{o}C with 2.7% propane conversion and 100 % propylene selectivity. The selectivity of propylene remained 100% until the temperature reached 500 ^{o}C to a show drop in the selectivity to 14% with propane conversion of 7.7 %. Between temperatures of 550 ^{o}C and 600 ^{o}C, propylene selectivity varied from 26.6 % to 20.6% at propane conversions of 9.8 % and 12.8 %, respectively. The CO selectivity began at 500 ^{o}C with 68.3 % and decreased at 600 ^{o}C to 48.8%. On the other hand, the CO_2 selectivity started at 550 ^{o}C and increased from 23.0 % to 30.5 at 600 ^{o}C.

The MoVO-3 (SCD) catalyst began its activity at 450 ^{o}C with 100% selectivity of propylene and 1.9% conversion. The propane conversion increased from 2.6% to 8.2%, and propylene selectivity dropped from 17.6% to 12.1% as the temperature increased from 500 to 600 ^{o}C. Meanwhile, the CO selectivity rose from 23.0% to 33.1, and CO_2 selectivity increased from 59.2 % to 54.7% as the temperature increased from 500 to 600 ^{o}C.

The MoVO-4 (SCD) was active at 400 ^{o}C but with extremely low propane conversion, 0.6%, with 100% propylene selectivity. This conversion rose from 2.1% to

8.1%, and also the selectivity of propylene lessened from 100% to 14.3% when increasing the temperature from 450 to 600 $^{\circ}$C. The CO and CO_2 selectivity ranged from 27.7% to 40.4% and from 55.8% to 45.1%, respectively, with temperature range from 500 to 600 $^{\circ}$C.

The MoVO-5 (SCD) showed 100% propylene selectivity at 450 $^{\circ}$C and 500 $^{\circ}$C with propane conversion of 2.7% and 4.8%, respectively. At 550 $^{\circ}$C, the propane conversion was 5.8, and propylene, CO and CO_2 selectivity were 15.0%, 48.6%, and 36.2%. The propylene selectivity at 600 $^{\circ}$C did not change significantly, but the conversion doubled the value at 550 $^{\circ}$C with CO and CO_2 selectivity 33.3% and 52.6%, respectively.

Significant differences in activity and selectivity to propylene can be achieved, depending on the vanadium-molybdenum content. All catalysts showed similar performances with high selectivity to propylene at low propane conversion. With increasing molybdenum content in the catalysts, the catalytic behaviors for propane ODH were improved. The presence of molybdenum in catalysts raised the amount of adsorbed propane, which, in line, lifts up the propane conversion to propylene (Nayak et al., 2010). The Raman detected a peak at 785 cm^{-1}, and this peak was assigned to polymolybdovanadate species V-O-Mo vibration which is the responsible for catalytic activity (Murgia et al., 2008). In oxidative dehydrogenation reaction, the mechanism is suggested to proceed via a redox type mechanism in two steps: reduction of the catalyst by the alkane with extraction of the lattice oxygen, after that reoxidation of the reduced catalyst with molecular dioxygen. In the TPR results, a correlation between the reducibility of active sites and the catalytic activity for oxidation reactions is generally

observed on unsupported catalysts. The lower catalytic activity of MoVOx-3 and MoVOx-4 samples could be explained by a decrease of both the number and the reducibility of the active sites. It is clear that Mo^{+6} ions show redox properties and they are also active sites in the activation of propane. The increased activity of MoVOx-2 sample (beside it contained higher amount of Mo) could be corresponded to the higher lability and consequently easier removal of lattice oxygen from VO_x moieties. The Tamman temperature of metal oxides can be used as a qualitative measurement of oxygen mobility. V_2O_5 has a lower Tamman temperature than MoO_3 (208 and 261 ∘C, respectively), indicating the higher lability of lattice oxygen in VO_x catalysts (Heracleous et al., 2005).

Table 4.9 Conversion, selectivity, and yield results of MoVO-2 (SCD), MoVO-3 (SCD), MoVO-4 (SCD), and MoVO-5 (SCD) catalysts (reaction conditions: F = 100 ml/min, W= 0.5 g, $C_3H_8/O_2/N_2 = 6/3/91$).

Catalysts Code	Temperature °C	Propane Conversion %	Propylene Selectivity %	CO Selectivity %	CO_2 Selectivity %	Propylene Yield %
MoVOx-2 (SCD)	350	2.7	100.0	0.0	0.0	2.7
	400	2.9	100.0	0.0	0.0	2.9
	450	3.4	100.0	0.0	0.0	3.4
	500	7.7	31.6	68.3	0.0	2.4
	550	9.8	26.6	50.3	23.0	2.6
	600	12.8	20.6	48.8	30.5	2.6
MoVOx-3 (SCD)	350	0.0	0.0	0.0	0.0	0.0
	400	0.0	0.0	0.0	0.0	0.0
	450	1.9	100.0	0.0	0.0	1.9
	500	2.6	17.6	23.0	59.2	0.4
	550	4.1	13.9	33.3	52.6	0.5
	600	8.2	12.1	33.1	54.7	1.0
MoVOx-4 (SCD)	350	0.0	0.0	0.0	0.0	0.0
	400	0.6	100.0	0.0	0.0	0.5
	450	2.1	100.0	0.0	0.0	2.0
	500	3.3	16.3	27.7	55.8	0.5
	550	4.7	24.4	37.6	37.9	1.1
	600	8.1	14.3	40.4	45.1	1.1
MoVOx-5 (SCD)	350	0.0	0.0	0.0	0.0	0.0
	400	0.0	0.0	0.0	0.0	0.0
	450	2.7	100.0	0.0	0.0	2.7
	500	4.8	100.0	0.0	0.0	4.8
	550	5.8	15.0	48.6	36.2	0.8
	600	10.4	15.9	33.8	50.2	1.6
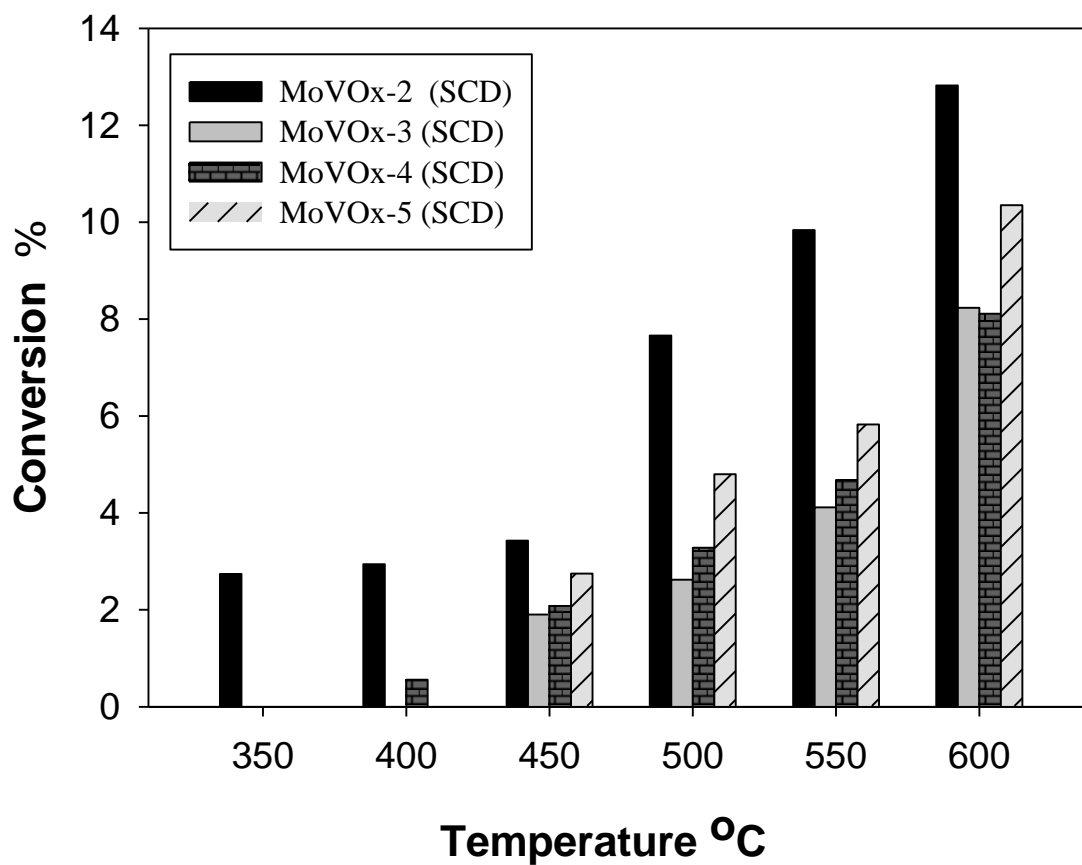
Figure 4.19 Propane conversions as function of temperature of MoVO-2 (SCD), MoVO-3 (SCD), MoVO-4 (SCD) and MoVO-5 (SCD) catalysts (reaction conditions: F = 100 ml/min, W= 0.5 g, $C_3H_8/O_2/N_2$ = 6/3/91).
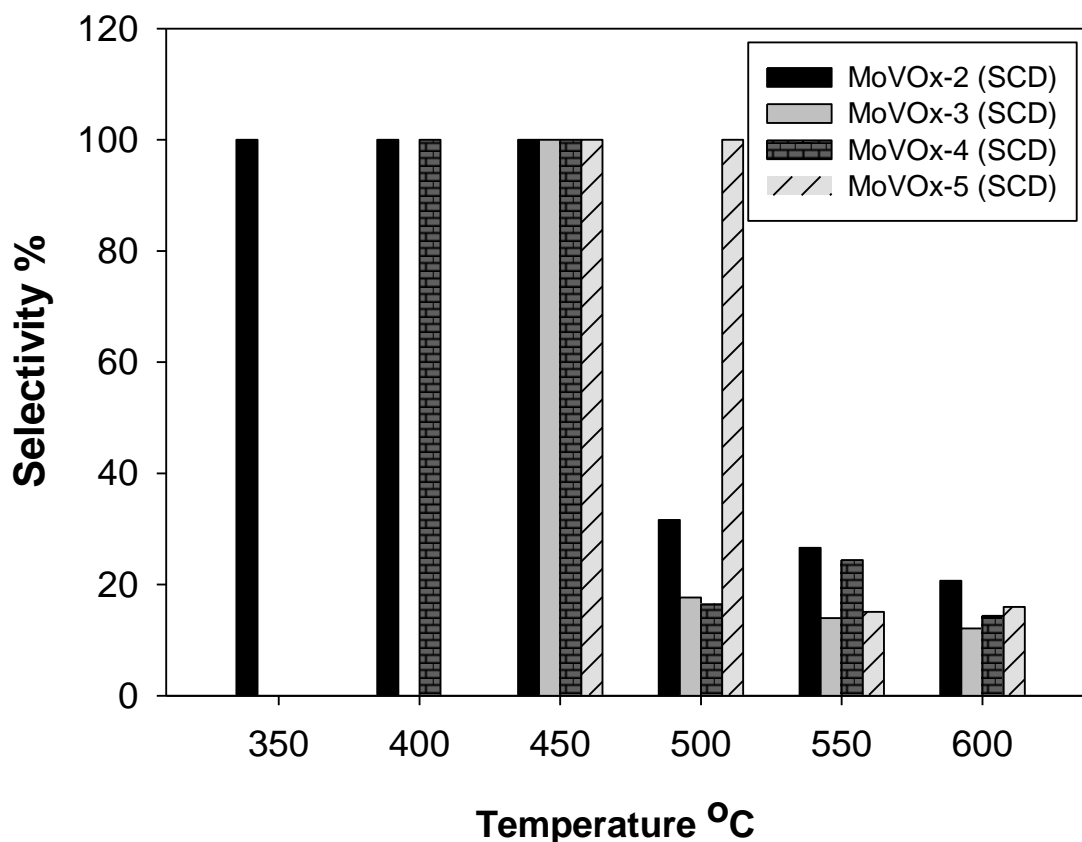
Figure 4.20 Propylene selectivity as function of temperature of MoVO-2 (SCD), MoVO-3 (SCD), MoVO-4 (SCD) and MoVO-5 (SCD) catalysts (reaction conditions: F = 100 ml/min, W= 0.5 g, $C_3H_8/O_2/N_2 = 6/3/91$).

Table 4.10 shows conversion, selectivity, and yield results of MoVOx-1. This catalyst was active at 350 ^oC with 1.9% propane conversion and 100% propylene selectivity. This 100% propylene selectivity was consistent until the temperature increased to 500 ^oC, and propylene selectivity reached to 40.5% with 6.0% propane conversion and 59.4% CO_2 selectivity. The propane conversion reached to approximately 14% at 550 ^oC and 600 ^oC. The propylene, CO and CO_2 selectivity varied from 11.5% to

14.6%, from 60.3% to 53.1% and from 28.1% to 32.1% respectively at 550 °C and 600

°C, respectively.

Table 4.10 Conversion, selectivity, and yield results of MoVOx-1(reaction conditions: F = 100 ml/min, W= 0.5 g, $C_3H_8/O_2/N_2$ = 6/3/91).

Catalysts Code	Temperature °C	Propane Conversion %	Propylene Selectivity %	CO Selectivity %	CO_2 Selectivity %	Propylene Yield %
MoVOx-1	350	1.9	100.0	0.0	0.0	1.9
	400	2.8	100.0	0.0	0.0	2.8
	450	3.2	100.0	0.0	0.0	3.2
	500	6.0	40.5	0.0	59.4	2.4
	550	14.7	11.5	60.3	28.1	1.6
	600	13.9	14.6	53.1	32.1	2.0

4.2.4   Evaluation of supported catalysts

Tables 4.11 and 4.12 show the propane conversions, propylene selectivity, and propylene yield results and methane, ethylene, CO, CO_2 and H_2 selectivity results, respectively, of MCM-41, 5MV/MCM-41, 10MV/MCM-41, and 15MV/MCM-41. Figures 4.21 and 3.22 depict catalyst propane conversion efficiency as a function of the temperature and propylene selectivity as a function of the temperature, respectively, for MCM-41, 5MV/MCM-41, 10MV/MCM-41, and 15MV/MCM-41 catalysts. The increase in propane conversion at the same time was higher than the decrease in propylene selectivity at higher temperatures. The inverse relationship between propane conversion and propylene selectivity is well known and commonly reported in literature; this phenomenon is due to the consecutive conversion of propane and propylene to CO and

102

CO_2, as discussed in the previous section. The propane conversion and the propylene selectivity observed for the reactions were strongly dependent on the reaction temperatures.

As a result of the MCM-41 support, the propane conversion increased from 5.2% to 14.8% while raising the temperature from 350 °C to 600 °C. Propylene selectivity varied from 8.7 % to 16.7% at propane conversions of 8.8% and 14.8%. The CO_2 selectivity at 350 °C, 400 °C and 450 °C was 100%, whereas at 600 °C, 37.4% selectivity was already obtained. In contrast, the propylene selectivity ranged from 33.8 % to 36.9% at 550 °C and 600 °C, respectively. There was no production of H_2 and methane at any temperature. At high temperatures, the ethylene selectivity varies from 4.7% to 8.8%. The propane conversion ranges from 5.4% to 26.7% at 450 °C and 600 °C respectively for 5MV/MCM-41 and ranged from 3.9% to 25.2% at 450 °C and 600 °C, respectively, for 10MV/MCM-41. The selectivity of propylene was 100% at 450 °C for 5MV/MCM-41 and 10MV/MCM-41, and it reduced to approximately 25% at 600 °C for both of them. The conversion of propane was estimated to be 1% of 15MV-MCM41 at 400 °C and rose to 28.4% at 600 °C. In fact, 15MV/MCM-41 catalyst showed 100% selectivity at temperature of 400°C and 450°C. As temperatures were increased above 450°C, selectivity continued to drop and reached 12.7% at 500°C. At 550°C and 600°C, selectivity was 23.2 % and 25.6%, respectively. For 5MV/MCM-41, 10MV/MCM-41 and 15MV/MCM-41 catalysts, the production of CO and CO_2 appeared at a range from 500 °C to 600°C. In addition, all catalysts presented selectivity to ethylene and H_2 at 550 °C to 600°C, and the catalysts also presented selectivity to methane at 600°C. For15MV/MCM-41 catalysts, the production of H_2 began at 500°C with 2.8% selectivity.

This production of hydrocarbon and H_2 at high temperatures was because of the cracking, coking, and consumption of O_2. At high metal loading, the catalysts showed improved selectivity to propylene at low propane conversion due to the selectivity of propane activation, and at high propane conversions, the selectivity to olefin was reduced. On the other hand, low selectivity to propylene was present at low metal loading. At high propane conversion, it was correlated to the $k_1/(k_2 + k_3)$ ratio, and the selectivity to propylene at low propane conversion is correlated to the k_1/k_3 ratio, as shown in the Figure1.1 (Solsona et al., 2001). Characterization of the supported catalysts showed that MoOx and VOx are dispersed on the support surface and this dispersion plays an important role in the catalysts activity. At low metal loading % (5 %), Mo and V were dispersed nicely on the support. When the metals loading were increased to 10 %, the active sites on the support and the surface area were decreased as it was shown in the surface area measurement results. This could be reducing the activity of the catalyst when metals loading % were increased from 5 % to 10 %. On the other hand, increasing metals loading to 15 % reduced the dispersion and increasing the metal crystal size on the surface of the catalyst (as it was presented in the XRD results) which increased the catalyst activity. In the Raman results, Mo-O-Mo (polymeric surface molybdenum oxide species) and V-O-V (polymeric surface Vanadium oxide species) stretch mode on the surface of the support were noted. The Mo=O stretching mode of the surface monooxo molybdenum oxide species and the monovanadate species V=O (stretching mode) were observed. The participation of Mo=O and V=O bands on the surface of the catalysts were found to be critical site for propane oxidative dehydrogenation, while Mo-O-Mo and V-O-V bonds were not critical for this reaction (Heracleous et al., 2005).

Table 4.11T Propane conversions, propylene selectivity, and propylene yield results of MCM-41, 5MV/MCM-41, 10MV/MCM-41, and 15MV/MCM-41 (reaction conditions: F = 100 ml/min, W= 0.5 g, $C_3H_8/O_2/N_2$ = 6/3/91).

Catalysts Code	Temperature °C	Propane Conversion %	Propylene Selectivity %	Propylene Yield %
MCM-41	350	5.2	0.0	0.0
	400	6.7	0.0	0.0
	450	8.5	0.0	0.0
	500	8.8	8.7	0.7
	550	9.7	17.6	1.7
	600	14.8	16.7	2.4
5MV/MCM-41	350	0.0	0.0	0.0
	400	0.0	0.0	0.0
	450	5.4	100.0	5.4
	500	8.8	22.5	2.0
	550	18.7	20.8	3.9
	600	26.7	25.1	6.7
10MV/MCM-41	350	0.0	0.0	0.0
	400	0.0	0.0	0.0
	450	3.9	100.0	3.9
	500	7.1	42.6	3.0
	550	20.2	23.8	4.8
	600	25.2	25.3	6.3
15MV/MCM-41	350	0.0	0.0	0.0
	400	1.0	100.0	1.0
	450	6.0	100.0	6.0
	500	11.5	12.7	1.4
	550	25.1	23.2	5.8
	600	28.4	25.6	7.2

Table 4.12 By products selectivity results of MCM-41, 5MV/MCM-41, 10MV/MCM-41, and 15MV/MCM-41(reaction conditions: F = 100 ml/min, W= 0.5 g, $C_3H_8/O_2/N_2$ = 6/3/91).

Catalysts Code	Temperature °C	Methane Selectivity %	Ethylene Selectivity %	CO Selectivity %	CO_2 Selectivity %	H_2 Selectivity %
MCM-41	350	0.0	0.0	0.0	100.0	0.0
	400	0.0	0.0	0.0	100.0	0.0
	450	0.0	0.0	0.0	100.0	0.0
	500	0.0	0.0	0.0	91.2	0.0
	550	0.0	4.7	33.8	43.7	0.0
	600	0.0	8.8	36.9	37.4	0.0
5MV/MCM-41	350	0.0	0.0	0.0	0.0	0.0
	400	0.0	0.0	0.0	0.0	0.0
	450	0.0	0.0	0.00	0.0	0.0
	500	0.0	0.0	40.9	36.5	0.0
	550	0.0	2.1	44.3	30.5	2.0
	600	1.9	4.3	37.0	21.9	9.5
10MV/MCM-41	350	0.0	0.0	0.0	0.0	0.0
	400	0.0	0.0	0.0	0.0	0.0
	450	0.0	0.0	0.0	0.0	0.0
	500	0.0	0.0	57.3	0.0	0.0
	550	0.0	2.1	48.0	21.6	4.2
	600	2.5	3.0	38.4	18.5	12.0
15MV/MCM-41	350	0.0	0.0	0.0	0.0	0.0
	400	0.0	0.0	0.0	0.0	0.0
	450	0.0	0.0	0.0	0.0	0.0
	500	0.0	0.0	36.8	47.5	2.8
	550	0.0	1.3	44.2	20.7	10.4
	600	1.5	1.6	36.1	22.0	12.9
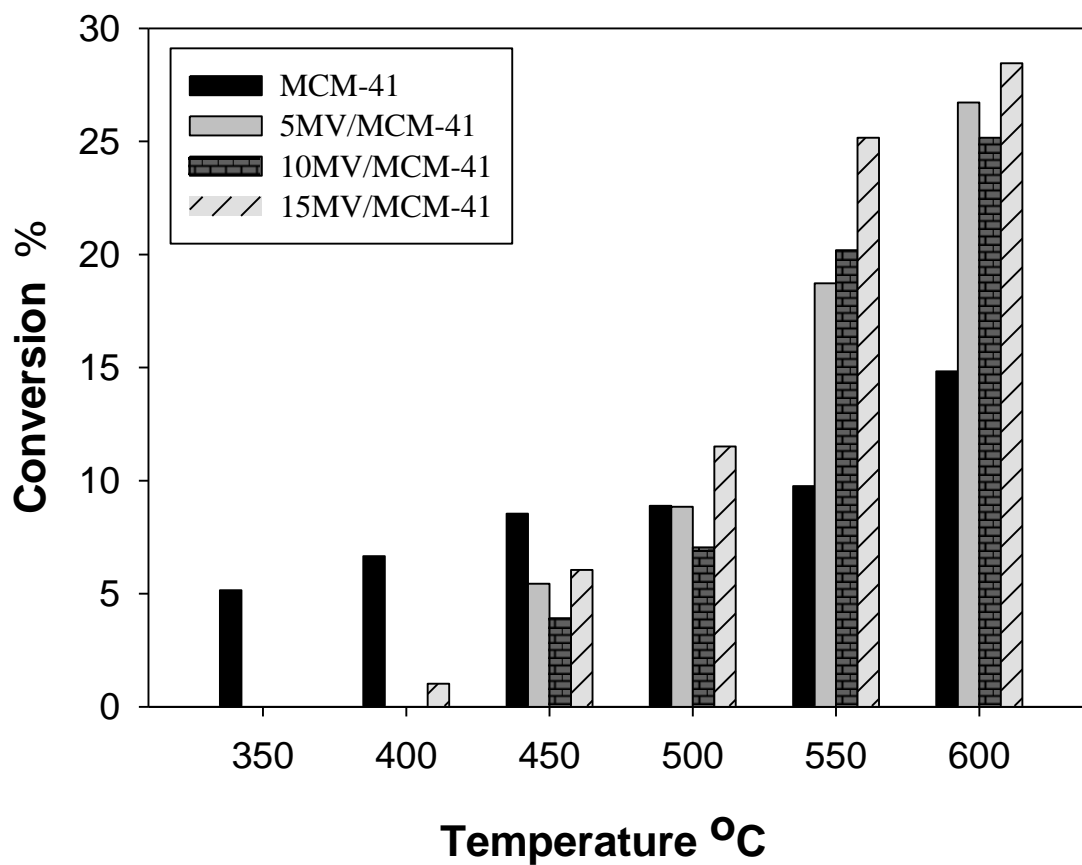
Figure 4.21 Propane conversions as function of temperature of MCM-41, 5MV/MCM-41, 10MV/MCM-41 and 15MV/MCM-41 (reaction conditions: F = 100 ml/min, W= 0.5 g, $C_3H_8/O_2/N_2$ = 6/3/91).
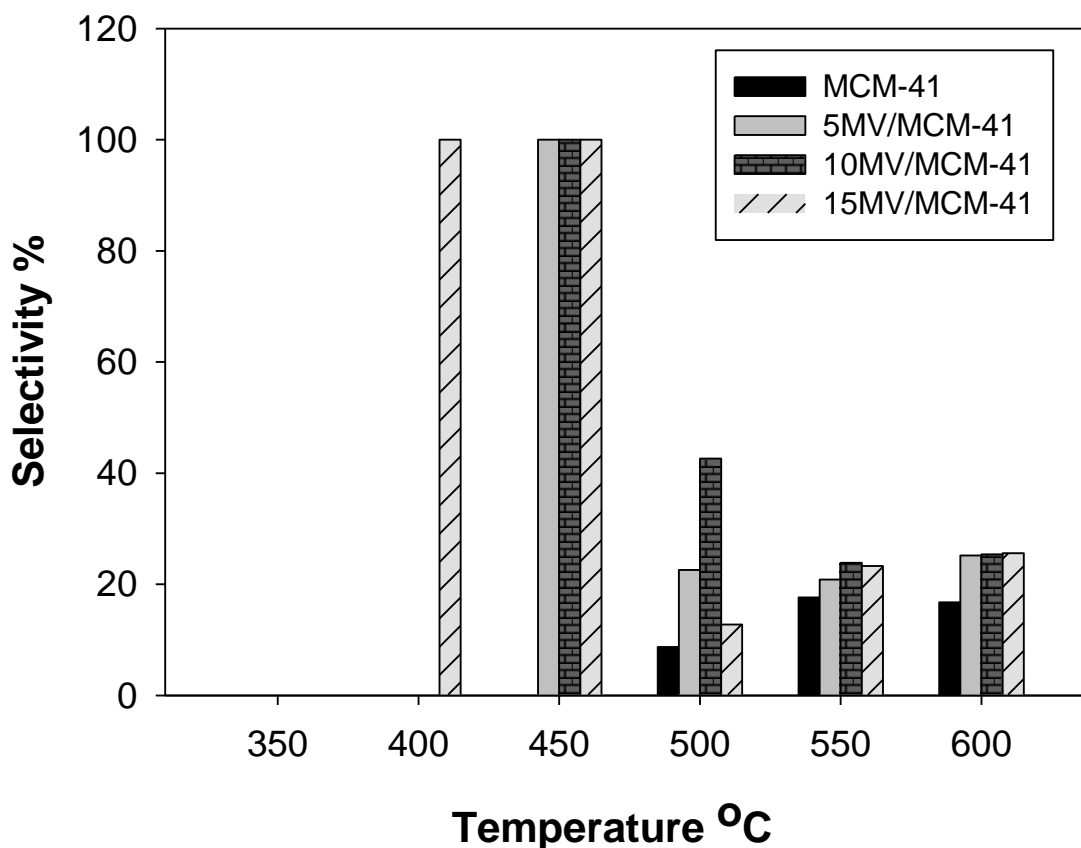
Figure 4.22 Propylene selectivity as function of temperature of MCM-41, 5MV/MCM-41, 10MV/MCM-41 and 15MV/MCM-41 (reaction conditions: F = 100 ml/min, W= 0.5 g, $C_3H_8/O_2/N_2$ = 6/3/91).

4.2.5   Comparison of unsupported and supported catalysts with Mo:V (1:1)

The comparison of unsupported and supported catalysts have a mole ratio of Mo:V 1:1. These catalysts were 5MV/MCM-41, 10MV/MCM-41, 15MV/MCM-41, MoVOx-1, and MoVOx-2 (SCD). The 5MV/MCM-41, 10MV/MCM-41 and 15MV/MCM-41 were prepared by the impregnation method. MoVOx-2 (SCD) was prepared by a modified auto-combustion process of nitrate citrate gels method, and the MoVOx-1 was prepared by physical mixing. Figures 4.23 and 4.24 depict, comparatively,

the catalytic results obtained propane conversions as a function of temperature and propylene selectivity as a function of temperature, respectively. MoVOx-1 and MoVOx-2 (SCD) catalyst were active at a low of temperature 350 °C with 100% propylene selectivity. The 5MV/MCM-41 and 10MV/MCM-41 catalysts began their activity at 450 °C, and 15MV/MCM-41 was active at 400 °C. All catalyst showed 100% propylene selectivity at 450 °C, and the selectivity decreased with increasing temperatures. The support catalysts showed greater activity and conversion of propane than MoVOx-1 and MoVOx-2 (SCD). Among the support catalysts, the highest rate of activity was from 15MV/MCM-41. The highest yield was 6.0% at 450 °C for 15MV/MCM-41, as illustrated in Table 4.11. The conversion of catalysts increased as follows:

15MV/MCM-41 > 5MV/MCM-41 > 10MV/MCM-41 > MoVOx-2 (SCD) > MoVOx-1

The supported catalysts showed higher activity than unsupported catalysts because of the following: the supported catalysts have higher surface area than unsupported catalysts. In the TPR results, the reduction temperature of the supported catalysts was lower than unsupported catalysts because the Mo and V were dispersed on the support and this dispersion allowed the metals to be more active. In the Raman results, Mo=O and V=O bands appear on supported catalysts and do not appear on unsupported catalysts and this Mo=O and V=O bands were found to be critical site for propane oxidative dehydrogenation as per discussed before.
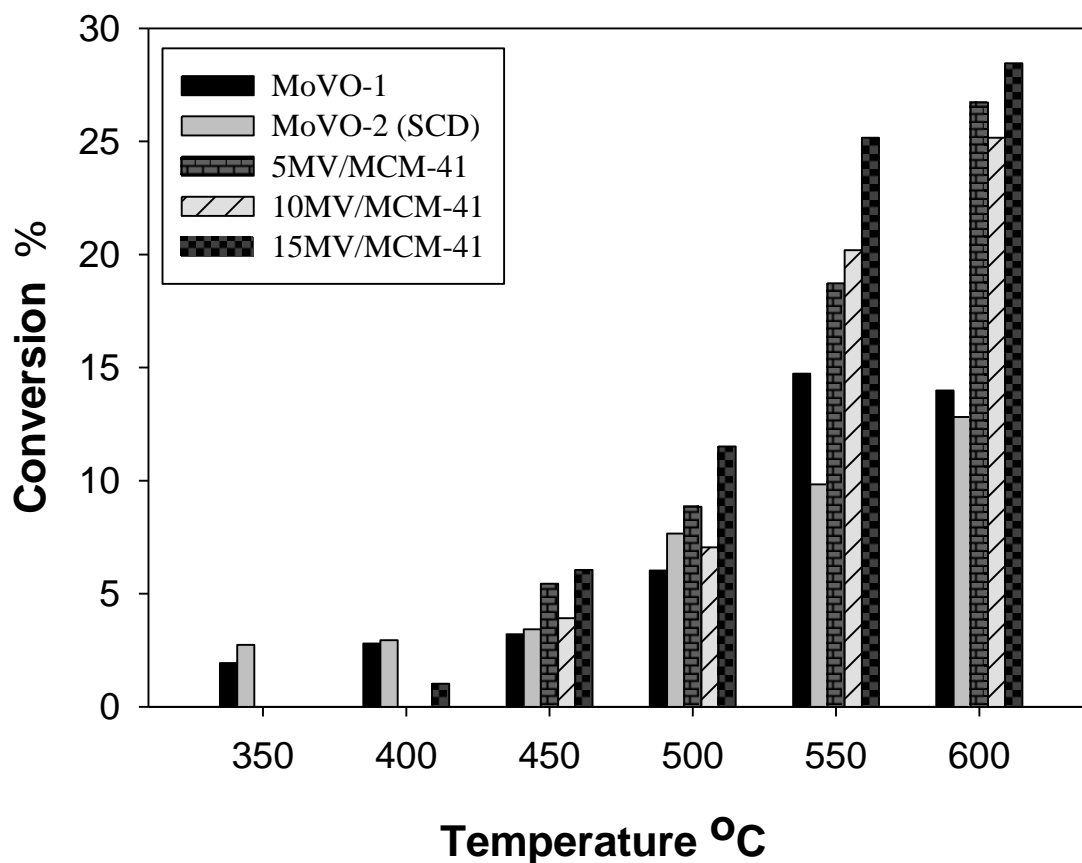
Figure 4.23 Propane conversions as function of temperature of 5MV/MCM-41, 10MV/MCM-41, 15MV/MCM-41, MoVOx-1 and MoVOx-2 (SCD) (reaction conditions: F = 100 ml/min, W= 0.5 g, $C_3H_8/O_2/N_2 = 6/3/91$).
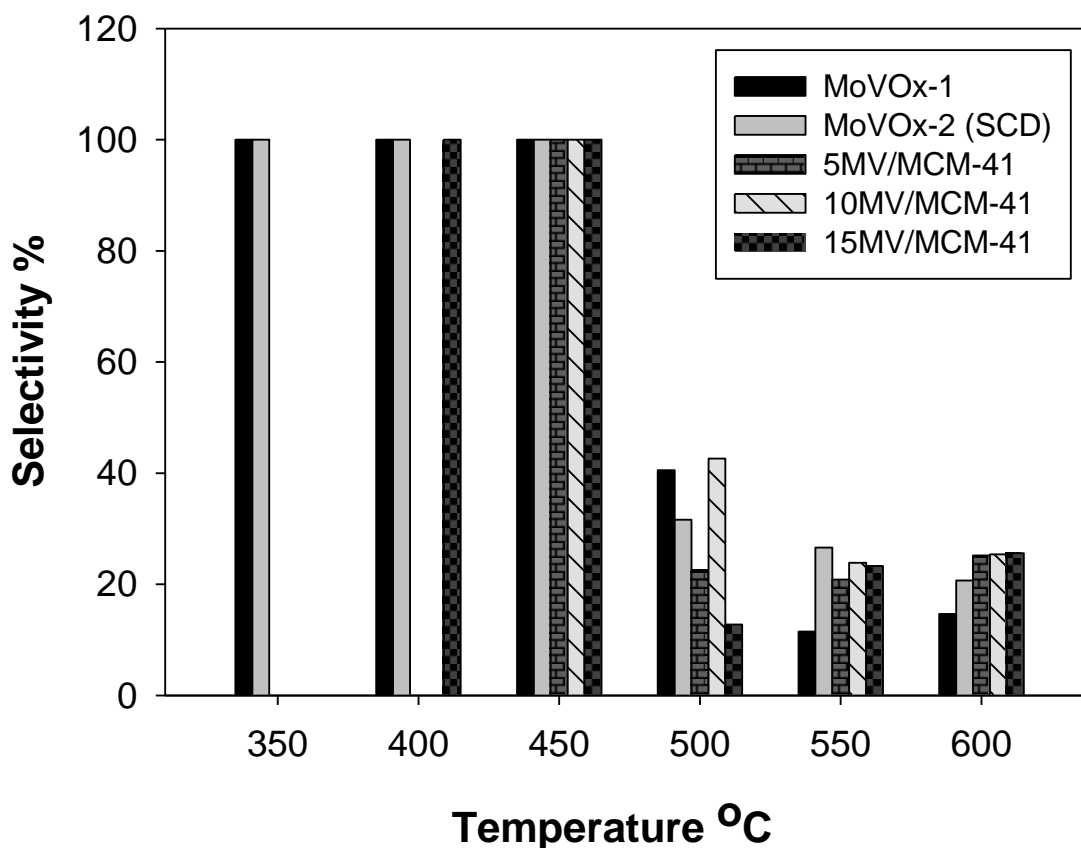
Figure 4.24 Propylene selectivity as function of temperature of 5MV/MCM-41,
10MV/MCM-41, 15MV/MCM-41, MoVOx-1 and MoVOx-2 (SCD) (reaction conditions:
F = 100 ml/min, W= 0.5 g, $C_3H_8/O_2/N_2$ = 6/3/91).

4.2.6   Life time performance of 15MV/MCM-41

Figure 4.25 depicts the propane conversions and selectivity of propylene and CO_2
as a function of the time of 15MV/MCM-41. The reaction was run for 29 hours at a
constant temperature of 475 °C to test the life time of the 15MV/MCM-41 catalyst. There
was no significant change in the propane conversion, and it averaged, approximately, 6%
during 29 hours. The selectivity of propylene reduced within the first three hours from

111

100% to remain constant at approximately 25%. During that time, the CO_2 selectivity

rose to remain constant at 75% with increasing time.
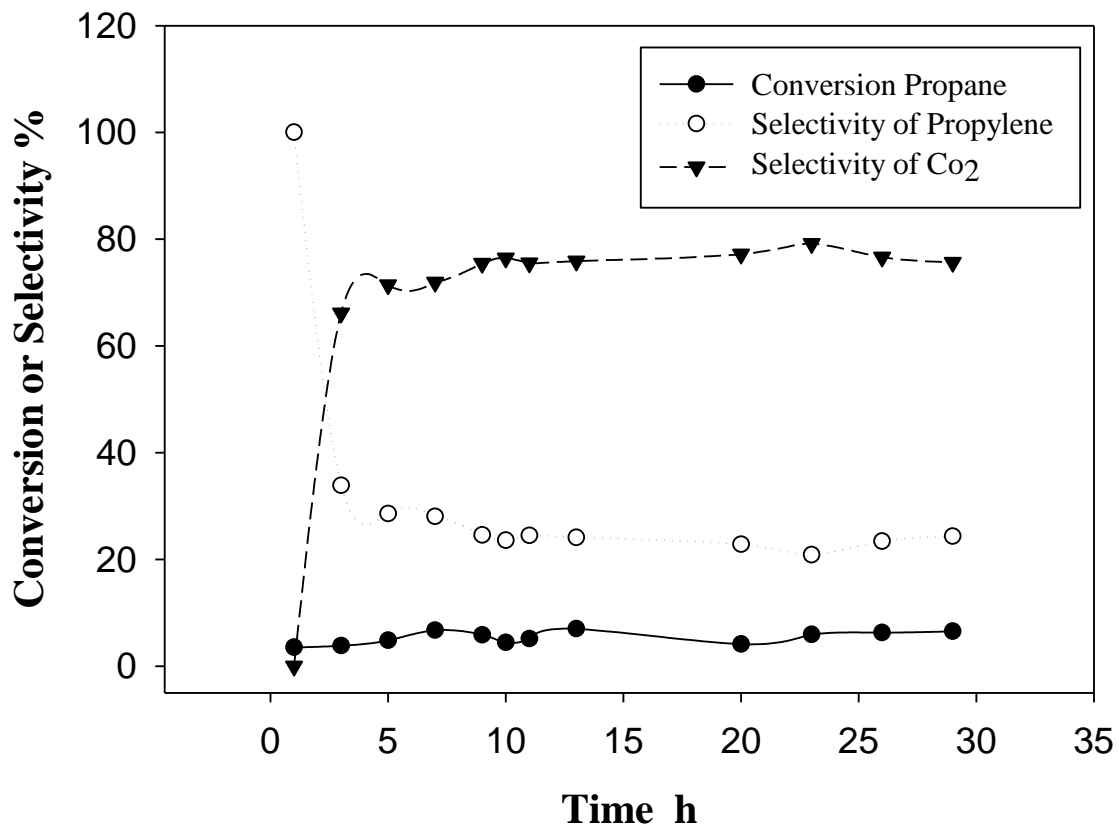
Figure 4.25 Propane conversions and product selectivity as function of time at 475 °C for 15MV/MCM-41 (reaction conditions: F = 100 ml/min, W= 0.5 g, $C_3H_8/O_2/N_2$ = 6/3/91).

CHAPTER 5

5. Conclusion and Recommendations

5.1 Conclusion

1. MoVOx catalysts were successfully prepared by a modified auto-combustion method and MoV/MCM41 catalysts were successfully prepared by using impregnation method.

2. The surface area of MoVOx-2 (SCD), MoVOx-3 (SCD), MoVOx-4 (SCD), and MoVOx-5 (SCD) catalysts were increased by increasing the mole ratio of Mo/V from 1 to 9. On the other hand, the surface area and pore volume of 5MV/MCM-41, 10MV/MCM-41, and 15MV/MCM-41 decreased with rising metal loading percentages from 5% to 15%.

3. In the TPR study, all catalysts had two peaks temperatures. For unsupported catalysts, the peak at 606 ^{o}C was reduced with the decrease of the vanadium content. On the other hand, the peak at 731 ^{o}C increased with the increase of the molybdenum content. For supported catalysts, the temperature of β_Z (Z = 5-7) peaks were increased, and the temperature of α_Z (Z = 5-7) peaks declined by increasing the metal loading percentages.

4. The UV spectroscope showed that the width of the band absorption of unsupported catalysts reduced with increasing molybdenum content, and the amount of absorption of supported catalysts rose with rising metal loading.

5. In the XRD and Raman study, the unsupported catalysts were crystalline catalyst, and the crystallization of the catalyst increased with increases of the molybdenum content. The supported catalysts were amorphous material. There was an interaction between the molybdenum and vanadium metal in all of the catalysis due to the presence of a peak at 785 cm^{-1} , which was assigned to polymolybdovanadate species V-O-Mo vibration in the Raman study. This interaction could be efficient for alkane activation.

6. Washing and super critical drying (SCD) produced dramatic improvement in the performance of MoVO-2.

7. For unsupported catalysts, the activity of the catalyst increased with the catalyst that had high molybdenum content, and the activity increased as follows:

   MoVOx-2 (SCD) > MoVOx-5 (SCD) > MoVOx-4 (SCD) > MoVOx-3 (SCD)
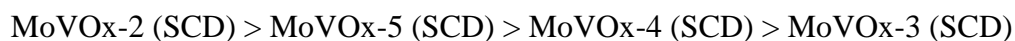
8. For the supported catalysts, the activity increased as follows:

   15MV/MCM-41 > 5MV/MCM-41 >10MV/MCM-41

9. The comparison between supported and unsupported catalysts that had the same ratio of Mo/V (1:1) was studied. The support catalysts were more active than unsupported catalysts, and the conversion of catalysts increased as follows:

   15MV/MCM-41 > 5MV/MCM-41 >10MV/MCM-41 > MoVOx-2 (SCD) > MoVOx-1

10. The best yield was obtained for 15MV/MCM-41: 6.05% with 100% propylene selectivity at 450 ^{o}C. However, the activity of 15MV/MCM-41 decreased when the life time was studied at 475 ^{o}C. The propylene selectivity dropped after three hours because of the production of CO_2.

5.2 Recommendations

1. Study the activity of unsupported catalysts to increase the vanadium and to decrease the molybdenum by the same method of preparation (modified citrate-nitrate auto-combustion).

2. Investigate the activity of supported catalysts with different Mo/V mole ratios with different metal loading percentages.

3. Improve the supported catalysis by adding alkali promoters, such as Li, K, and Na.

4. Test the activity of supported catalysts by using different support, such as MCM-48 and MCF.

APPENDICES

Appendix [A]

Adsorption-Desorption Isotherm of MV/MCM-41
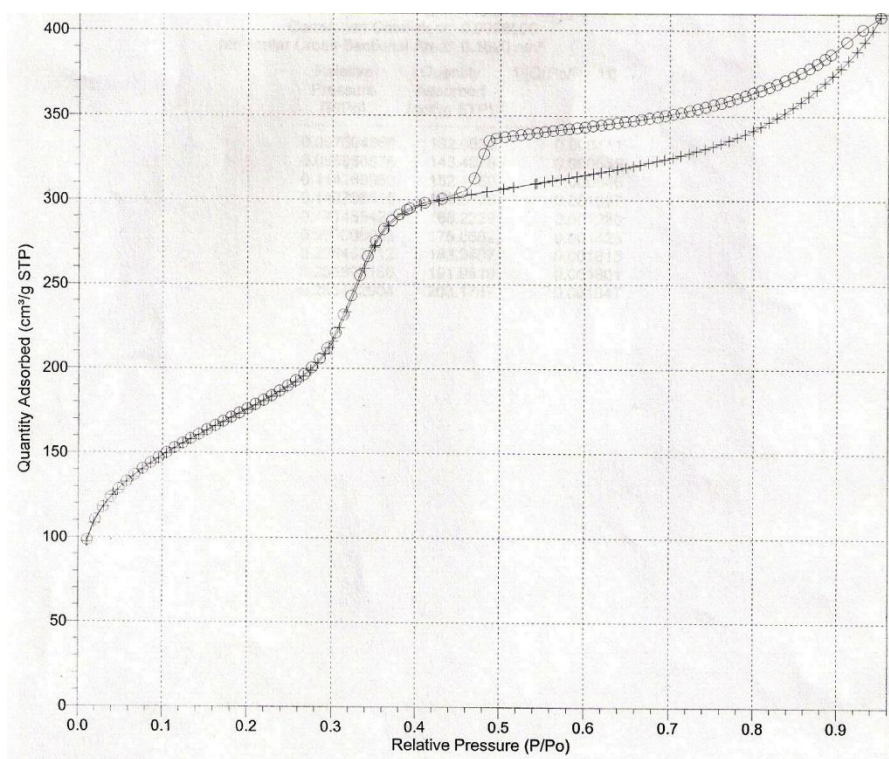
Figure A1 Adsorption-desorption isotherm of 5MV/MCM-41
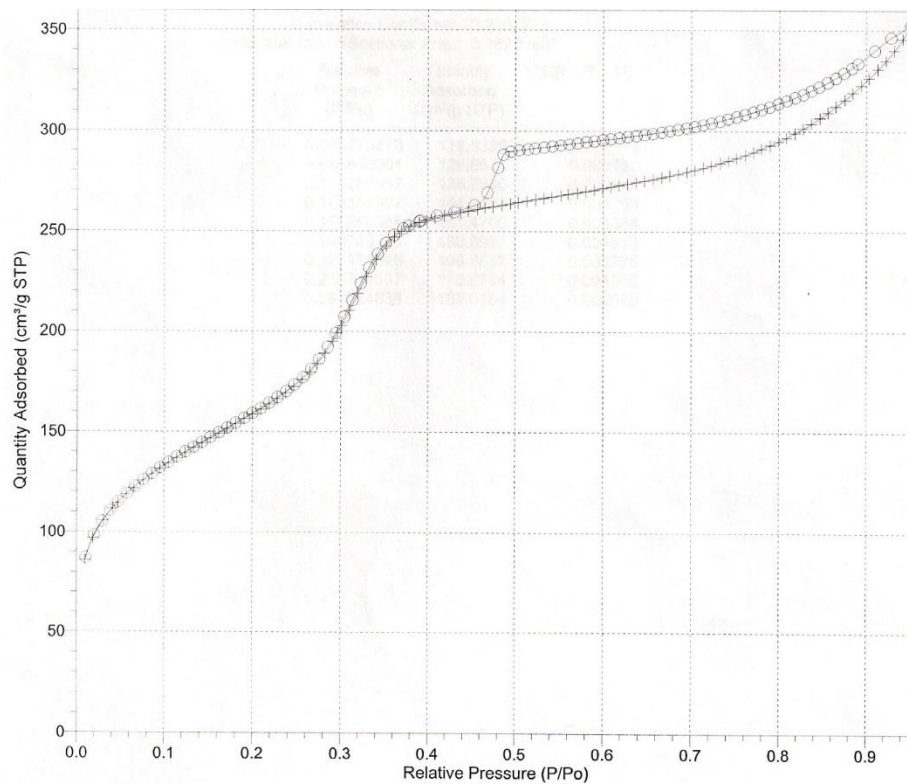
Figure A2 Adsorption-desorption isotherm of 10MV/MCM-41
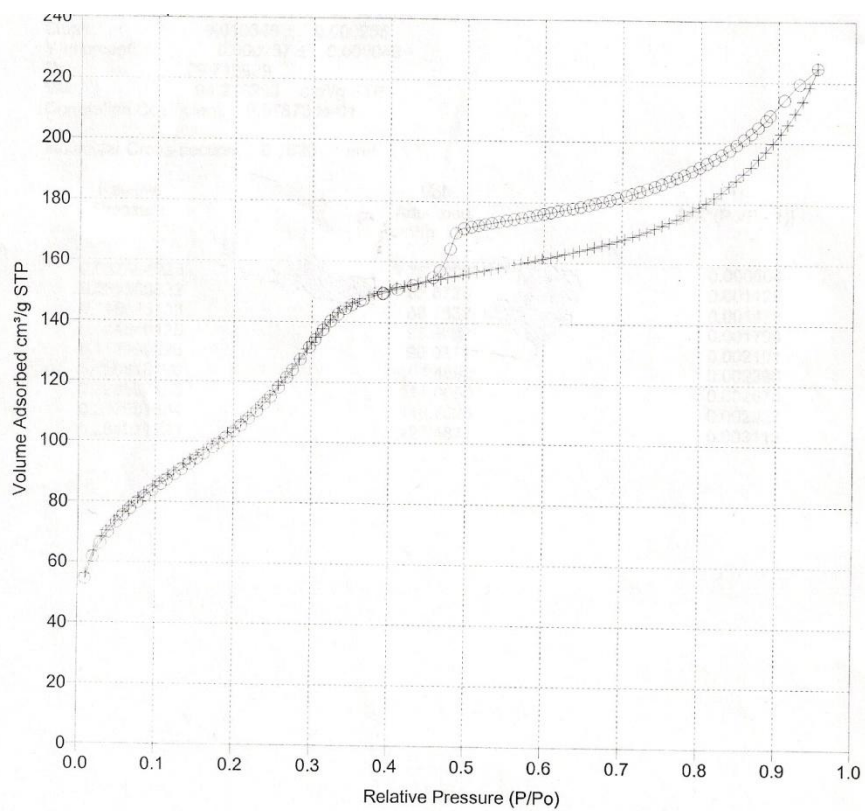
Figure A3 Adsorption-desorption isotherm of 15MV/MCM-41

Appendix [B]

Calculation of Feed Conditions and Composition

Taking 15MV/MCM-41 as an example for calculation:

Reactor diameter = 1 cm

Catalyst weight =0.5 g

Catalyst volume =1.4 ml

$$\text{Catalyst bed height} = \frac{\text{Catalyst volume}}{3.14 \times \left(\frac{\text{reactor diameter}}{2}\right)^2}$$

Catalyst bed height 1.78 cm

Feed gas temperature = 350 – 600 $^\circ$C

Reactor diameter = 1 atm

Total feed flow rate = 101.3 ml/min

Feed gas compositions from GC (mol/ml):

O_2 = 3.4, N_2 = 88.5,   propane = 6.8

O_2 flow rate = 100.0 * 3.4/100   = 3.5 ml/min

N_2 flow rate = 100.0 * 88.5/100 = 89.6 ml/min

Propane flow rate = 100.0 * 6.8/100 = 6.8 ml/min

Calculated feed flow rate = 3.5 + 89.6 + 6.8 = 100.0 ml/min

Space velocity = feed volume / catalyst volume = (101.3 / 1.4)*60 = 4342 s^{-1}

Appendix [C]

Calculation for Conversion, Selectivity and Yield

Taking 15MV-MCM41 as an example for calculation at 450 $^\circ$C:

$$\text{Conversion (\%)} = \frac{\text{moles of propane reacted}}{\text{moles of propane in feed}} * 100$$

$$\text{Selectivity (\%)} = \frac{\text{moles of propylene in product}}{\text{moles of propane reacted}} * 100$$

$$\text{Yield (\%)} = \frac{\text{moles of propylene in product}}{\text{moles of propane in feed}} * 100$$

Feed molear flow rate of propane $= 0.0002866$

Product molear flow rate of propane $= 0.0002692$

moles of propane reacted $= 0.0002866 - 0.0002692 = 1.74 * 10^{-5}$

moles of propane in feed $= 0.0002866$

moles of propylene in product $= 1.74 * 10^{-5}$

$$\text{Conversion (\%)} = \frac{0.0002866 - 0.0002692}{0.0002866} \times 100 \qquad = \quad 6.07\ \%$$

$$\text{Selectivity (\%)} = \frac{0.0000174}{0.0000174} \times 100 \qquad\qquad = 100\ \%$$

$$\text{Yield (\%)} = \frac{\text{Conversion} \times \text{Selectivity}}{100} \qquad\qquad = 6.07\ \%$$

Appendix [D]

Calculation for Preparation of Unsupported Catalysts

These conditions are fixed for all unsupported catalysts

- Citric acid/metal nitrates ratio (C/M) = 2

- Fuel/oxidant ratio (F/O) = 0.4

- pH= 9.0

Taking MoVOx-2 (SCD) as an example for calculation:

Basis 5 g of catalysis

Mole ratio Mo/V = 1/1

MW of MoVOx-2 (SCD) = 234.88 g/mol

Mole Mo = Mole V = 5/ 234.88 = 0.0212 mole

H(24)Mo(7)N(6)O(24) and NH(4)VO(3) are starting materials

Weight of H (24) Mo (7) N (6) O (24) = (0.0212 /7) * 1235.86 = 3.75 g

Weight of NH (4) VO (3) = 0.0212 * 116.98 = 2.49 g

Weight of Citric acid = 0.0243 * 0.2 * 192.43 = 9.36 g

Weight of ammonia nitrate (O) = (0.0312/ 0.4)* 80.04 = 6.25 g

Appendix [E]

Calculation for Preparation of Supported Catalysts

Taking 15MV/MCM-41 as an example for calculation:

Basis 2 g of catalysis

15% of Mo and V

Mole ratio Mo/V = 1/1

Mole of citric acid = mole of Mo

MW of 15MV/MCM-41 = 234.88 g/mol

Mass of 15MV/MCM-41 = 15 * 2/100 = 0.3 g

Mole of 15MV/MCM-41 = 0.3 /234.88 = 0.00127 mole = Mole Mo = Mole V

$H_{24}Mo_7N_6O_{24}$ and NH_4VO_3 are starting materials

Weight of H (24) Mo (7) N (6) O (24) = (0.00127 /7) * 1235.86 = 0.225 g

Weight of NH (4) VO (3) = 0.00127 * 116.98 = 0.149 g

Weight of Citric acid = 0.00127 * 192.43 = 0.245 g

REFERENCES

1.   Abello M., G.M., and Ferrett O., Oxidative conversion of propane over Al2O3-supported molybdenum and chromium oxides. Catalysis Letters, 2003. **87** p. 1–2.

2.   Argyle M., C.K., Bell A. and Iglesia E., Effect of Catalyst Structure on Oxidative Dehydrogenation of Ethane and Propane on Alumina-Supported Vanadia Journal of Catalysis 2002. **208** p. 139–149.

3.   Aruna S.and, M.A., Combustion synthesis and nanomaterials, . Current Opinion in Solid State and Materials Science 2008. **12** p. 44–50.

4.   Bahranowski K., G.R., . Grzybowska B., Kielski A., Serwicka E.M., Wcisło K., Wisła-Walsh E. and Wodnicka K., Synthesis and physicochemical properties of vanadium-doped zirconia-pillared montmorillonites in relation to oxidative dehydrogenation of propane. Topics in Catalysis 2000. **11/12**: p. 255–261.

5.   Banares M. and Khatib S., Structure–activity relationships in alumina-supported molybdena–vanadia catalysts for propane oxidative dehydrogenation. Catalysis Today 2004. **96** p. 251–257.

6.   Barbero B. , C.L., Vanadium species: Sm-V-O catalytic system for oxidative dehydrogenation of propane. Applied Catalysis A: General 2003. **244**: p. 235–249.

7.   Bin Y., D.T., Shi-Run Y., Yan Z., Ka-Ke Z., Jian-Feng P., Ji-Hua Z.and He-Yong H., Preparation of MoO3-V2O5 Nanowires with Controllable Mo/V Ratios inside SBA-15 Channels Using a Chemical Approach with Heteropoly Acid. Chinese Journal of Chemistry, 2005. **23** p. 32-36.

8.   Boizumault-Moriceau P., P.A., Grzybowska B. and Barbaux Y., Oxidative dehydrogenation of propane on Ni–Ce–O oxide: effect of the preparation method, effect of potassium addition and physical characterization. Applied Catalysis A: General 2003. **245** p. 55–67.

9.   Boucetta C., K.M., Ensuque A., Piquemal J., Bozon-Verduraz F. and Ziyad M., Oxidative dehydrogenation of propane over chromium-loaded calcium-hydroxyapatite. Applied Catalysis A: General 2009. **356** p. 201–210.

10.   Cadus L., A.M., Gomez M. and Rivarola J., Oxidative Dehydrogenation of Propane over Mg-Mo-O Catalysts. Ind. Eng. Chem. Res., 1996. **35**: p. 14-18.

11.   Caponetti E., M.A., Saladino M.L. and Spinella A. , Characterization of Nd–MCM-41 obtained by impregnation. Microporous and Mesoporous Materials 2008. **113**   p. 490–498.

12.   Cavani F., B.N., and Cericola A., Oxidative dehydrogenation of ethane and propane: How far from commercial implementation? . Catalysis Today, 2007. **127**: p. 113–131.

13.   Chao Z. , R.E., V–Mg–O prepared via a mesoporous pathway: a low-temperature catalyst for the oxidative dehydrogenation of propane to propene. Catalysis Letters 2004. **94** p. 3–4.

14.   Cherian M., R.M., Yang W., Jehng J., Hirt A. and Deo G., , Oxidative dehydrogenation of propane over Cr2O3/Al2O3 and Cr2O3 catalysts: effects of loading, precursor and surface area, . Applied Catalysis A: General, 2002. **233**: p. 21–33.

15. Concepcion P., B.P., and Nieto J., Catalytic and FT-IR study on the reaction pathway for oxidation of propane and propylene on V- or Mo–V-based catalysts. Applied Catalysis A: General 2004. **278** p. 45–56.

16. Cortez G., F.J., and Bañares M., Role of potassium on the structure and activity of alumina-supported vanadium oxide catalysts for propane oxidative dehydrogenation. Catalysis Today 2003. **78**: p. 219–228.

17. Dai H., B.A., and Iglesia E., Effects of molybdena on the catalytic properties of vanadia domains supported on alumina for oxidative dehydrogenation of propane. Journal of Catalysis, 2004. **221** p. 491–499.

18. Daniell W., P.A., , Kuba S., Anderle F., Weingand T., Gregory D. and zinger H., Characterization and catalytic behavior of VOx–CeO2 catalysts for the oxidative dehydrogenation of propane. Topics in Catalysis 2002. **20**: p. 1–4.

19. Davies T. and Taylor S., The oxidative dehydrogenation of propane using gallium–molybdenum based catalysts. Catalysis Letters 2004. **93**: p. 3–4.

20. Deganello F., M.G., and Deganello G., Citrate–nitrate auto-combustion synthesis of perovskite-type nanopowders: A systematic approach, . Journal of the European Ceramic Society 2009. **29** p. 439–450.

21. Dejoz A., N.J., MaÂrquez F. and VaÂzquez M., The role of molybdenum in Mo doped V-Mg-O catalysts during the oxidative dehydrogenation of n-butane,. Applied Catalysis A: General 1999. **180** p. 83-94.

22. Dury F., G.E., and Ruiz P., The active role of CO2 at low temperature in oxidation processes: the case of the oxidative dehydrogenation of propane on NiMoO4 catalysts. Applied Catalysis A: General 2003. **242** p. 187–203.

23. Fujdala K. and Tilley T., Thermolytic molecular precursor routes to Cr/Si/Al/O and Cr/Si/Zr/O catalysts for the oxidative dehydrogenation and dehydrogenation of propane. Journal of Catalysis 2003. **218** p. 123–134.

24. Grabowski R., Kinetics of Oxidative Dehydrogenation of C2-C3 Alkanes on Oxide Catalysts. Catalysis Reviews 2007. **48** (2): p. 199 — 268.

25. Guerrero-Perez M., H.M., Malpartida I., Larrubia M. and Alemany L., Effect of tellurium addition to supported Mo-V-O catalysts for the ammoxidation of propane to acrylonitrile. Catalysis Today 2008. **133–135**: p. 919–924.

26. Heracleous E., M.M., Lemonidou A. and Vasalos I., Oxidative dehydrogenation of ethane and propane over vanadia and molybdena supported catalysts. Journal of Molecular Catalysis A: Chemical 2005. **232**: p. 29–39.

27. Higashimoto S., H.Y., Tsumura R., Iino K., Matsuoka M., Yamashita H., Shul Y., Che M. and Anpo M., S, synthesis, characterization and photocatalytic reactivities of Mo-MCM-41 mesoporous molecular sieves: Effect of the Mo content on the local structures of Mo-oxides. Journal of Catalysis 2005. **235** p. 272–278.

28. Jibril B., Propane oxidative dehydrogenation over chromium oxide-based catalysts. Applied Catalysis A: General 2004. **264** p. 193–202.

29. Jibril B., A.S., Abasaeed A. and Hughes R., Oxidative dehydrogenation of propane over supported chromium–molybdenum oxides catalysts. Catalysis Communications 2003a. **4** p. 579–584.

30. Jibril B., A.S., Abasaeed A. and Hughes R., Effects of reducibility on propane oxidative dehydrogenation over Al2O3-supported chromium oxide-based catalysts. Catalysis Letters 2003b. **87**: p. 3–4.

31. Jibril B., S.A., Oxidative dehydrogenation of propane over Co, Ni and Mo mixed oxides/MCM-41 catalysts: Effects of intra- and extra-framework locations of metals on product distributions. Catalysis Communications 2006. **7** p. 990–996.

32. Karakoulia S., T.K., Tsilomelekis G., Boghosian S. and Lemonidou A., Propane oxidative dehydrogenation over vanadia catalysts supported on mesoporous silicas with varying pore structure and size Catalysis Today 2009. **141** p. 245–253.

33. Katou T., V.D., and Ueda W., , Structure dependency of Mo-V-O based complex oxide catalysts in the oxidations of hydrocarbons Catalysis Today 2004. **91–92** p. 237–240.

34. Khatib S., G.R., Pena M., Fierro J. and Banares M., Alumina-supported V–Mo–O mixed oxide catalysts, the formation of phases involving aluminum: AlVMoO7. Catalysis Today 2006. **118** p. 353–359.

35. Kim J., K.J., Jun S. and Ryoo R., Ion Exchange and Thermal Stability of MCM-41. J. Phys. Chem. , 1995. **99**: p. 16742-16747.

36. Koc S., G.G., Geisslerb S., Gurayab M., Orbay M. and Muhler M., , The oxidative dehydrogenation of propane over potassium-promoted molybdenum oxide/sol–gel zirconia catalysts. Journal of Molecular Catalysis A: Chemical 2005. **225** p. 197–202.

37. Kornelak P., B.B., Prokop C., Litynska-Dobrzynska L., Wagner J., Su D., Camra J. and Wesełucha-Birczynska A., The physicochemical properties of rutile-supported V-O-Mo catalyst. Catalysis Today 2007. **119** p. 204–208.

38. Kubacka A., W.E., Sulikowski B., Valenzuela R. and Cortés Corberán V., , Oxidative dehydrogenation of propane on zeolite catalysts, . Catalysis Today 61 343–352, 2000. **61** p. 343–352.

39. Kumar C., G.S., Muller T. and Lercher J. , Oxidative Dehydrogenation of Light Alkanes on Supported Molten Alkali Metal Chloride Catalysts Top Catal, 2008. **50**: p. 156–167.

40. Lemonidou A., N.L., and Vasalos I., Oxidative dehydrogenation of propane over vanadium oxide based catalysts Effect of support and alkali promoter. Catalysis Today 2000. **61**: p. 333–341.

41. Liu C., W.R., and Ozkan U., Spectroscopic characterization of Cl modified Mo/Si:Ti catalysts for oxidative dehydrogenation of propane. Topics in Catalysis 2006. **41**: p. 1–4.

42. Liu Y., F.W., Li T., He H., Dai W., Huang W., Cao Y. and Fan K., Structure and catalytic properties of vanadium oxide supported on mesocellulous silica foams (MCF) for the oxidative dehydrogenation of propane to propylene, . Journal of Catalysis 2006. **239**: p. 125–136.

43. Liu Y., F.W., Wang L., Cao Y., Dai W., He H. and Fan K., , Chromium supported on mesocellular silica foam (MCF) for oxidative dehydrogenation of propane. Catalysis Letters 2006. **106** p. 3–4.

44. Liu Y., W.L., Chen M., Xu J., Cao Y., He H. and Fan K., Highly Selective Ce–Ni–O Catalysts for Efficient Low Temperature Oxidative Dehydrogenation of Propane. Catal Lett 2009. **130**: p. 350–354.

45.   Machli M. , L.A., Optimization of V2O5–MgO/TiO2 catalyst for the oxidative dehydrogenation of propane effect of magnesia loading and preparation procedure Catalysis Letters 2005. **99**: p. 3–4.

46.   Malleswara Rao T., V.E., Baoares M. and Deo G., Obtaining the best composition of supported V2O5–MoO3/TiO2 catalyst for propane ODH reaction. Journal of Catalysis 2008. **258** p. 324–333.

47.   Mattos A., S.R., Rocco M. and Eon J., Zinc-modified alumina supported vanadium oxides as catalysts for propane oxidative dehydrogenation. Journal of Molecular Catalysis A: Chemical 2002. **178**: p. 229–237.

48.   Mishakov I., V.A., Bedilo A., Zaikovskii V. and Klabunde K., Aerogel VOx/MgO catalysts for oxidative dehydrogenation of propane. Catalysis Today 2009. **144**: p. 278–284.

49.   Moggi P., D.M., Ruiz P., Predieri G., Cauzzi D., Morselli S. and Ligabue O., Oxidative dehydrogenation of propane on pure and silica-dispersed multimetallic oxides based on vanadium and niobium prepared via hydrolytic and non-hydrolytic sol–gel methods. Catalysis Today 2003. **81**: p. 77–85.

50.   Murgia V., T.E., Gottifredi J. and Sham E., , Influence of concentration and order of aggregation of the active phases in V–Mo–O catalysts in the oxidative dehydrogenation of propane. Catalysis Today 2008. **133–135** p. 87–91.

51.   Nayak S., S.D., and Deo G., The Promotion of Vanadia–Alumina and Vanadia–Titania Catalysts by Surface Molybdenum Oxide for the Propane ODH Reaction. Catal Lett 2010. **136**: p. 271–278.

52. Patil K., A.S., and Mimani T., Combustion synthesis: an update. Current Opinion in Solid State and Materials Science 2002. **6** p. 507–512 .

53. Pless J., B.B., Kim H., Ko D., Smith M, Hammond R., Stair P. and Poeppelmeier K., Catalytic oxidative dehydrogenation of propane over Mg–V/Mo oxides. Journal of Catalysis 2004. **223**: p. 419-431.

54. Sarzi-Amade M., M.S., Moggi P., Maione A., Ruiz P. and Devillers M., The effect of sol–gel promoters on the characteristics of mixed V–Nb oxides and their catalytic properties in propane oxidative dehydrogenation Applied Catalysis A: General 2005. **284**: p. 11–20.

55. Selvaraj M., L.T., A novel route to produce phthalic anhydride by oxidation of o-xylene with air over mesoporous V-Mo-MCM-41 molecular sieves. Microporous and Mesoporous Materials 2005. **85** p. 39–51.

56. Solsona B., B.T., Lopez Nieto J., Pen M., Rey F. and Vidal-Moya A., Vanadium Oxide Supported on Mesoporous MCM-41 as Selective Catalysts in the Oxidative Dehydrogenation of Alkanes. Journal of Catalysis 2001. **203**: p. 443–452.

57. Solsona B., L.J., and Dıaz U., Siliceous ITQ-6: A new support for vanadia in the oxidative dehydrogenation of propane. Microporous and Mesoporous Materials 2006. **94**: p. 339–347.

58. Stark, W. How to make catalysts. 2005 [cited 2010 02 Oct.]; Available from: http://www.fml.ethz.ch/education/CatalReactEngin/Catalyst_Preparation.pdf.

59. Stelzer J., C.J., and Fait M., Oxidative dehydrogenation of propane on TiO2 supported antimony oxide/vanadia catalysts. Catalysis Communications, 2005. **6**: p. 1-5.

60. Sugiyama S., O.T., Hirata Y. and Sotowa K., Enhancement of the activity for oxidative dehydrogenation of propane on calcium hydroxyapatite substituted with vanadate. Applied Catalysis A: General 2006. **312**: p. 52–58.

61. Sugiyama S., O.T., Hashimoto T. and Sotowa K., Oxidative Dehydrogenation of Propane on Calcium Hydroxyapatites Partially Substituted with Vanadate. Journal of the Japan Petroleum Institute, 2008. **51**(1): p. 50-57.

62. Takehira K., S.N., Shimomura J., Kajioka H., Hamakawa S., Shishido T., Kawabata T. and Takaki K., Oxidation of C2–C4 alkanes over MoO3–V2O5 supported on a YSZ-aided membrane reactor. Applied Catalysis A: General 2004. **277** p. 209–217.

63. Taylor M., C.A., Davies T. and Taylor S., The Oxidative Dehydrogenation of Propane Using Vanadium Oxide Supported on Nanocrystalline Ceria. Top Catal 2009. **52**: p. 1660–1668.

64. Viparelli P., C.P., Lisi L., Ruoppolo G., Russo G. and Volta J., Oxidative dehydrogenation of propane over vanadium and niobium oxides supported catalysts. Applied Catalysis A: General   1999. **184**: p. 291-301.

65. Vuk A., O.B., Drazic G. and Colomban P., Vibrational Spectroscopy and Analytical Electron Microscopy Studies of Fe–V–O and In–V–O Thin Films. Monatsh. Chem. , 2002. **133**: p. 889–908.

66. Wang W., L.X., Gao F. and Tian C., Synthesis of nanocrystalline Ni1Co0.2Mn1.8O4 powders for NTC thermistor by a gel auto-combustion process, . Ceramics International 2007. **33** p. 459–462.

67.   Wang Y., Z.O., Ohishi Y., Shishido T. and Takehira K., Synthesis of V-MCM 41 by template-ion exchange method and its catalytic properties in propane oxidative dehydrogenation. Journal of Catalysis, 2005. **235** p. 272–278.

68.   Wolf D., D.N., Smejkal Q. and Buyevskaya O. , Oxidative dehydrogenation of propane for propylene production - comparison of catalytic processes. Chemical Engineering Science, 2001. **56** p. 713-719.

69.   Yang S., I.I., and Bell A., Oxidative Dehydrogenation of Propane over V2O5/MoO3/Al2O3 and V2O5/Cr2O3/Al2O3: Structural Characterization and Catalytic Function. J. Phys. Chem. B, 2005. **109**: p. 8987-9000.

70.   Zhang J., S.M., Cao C., Zhang Q., Wang Y. and Wan H., Effects of acidity and microstructure on the catalytic behavior of cesium salts of 12-tungstophosphoric acid for oxidative dehydrogenation of propane. Applied Catalysis A: General 2010. **380** p. 87–94.

71.   Zhao Z., G.X., and Wachs I., Comparative Study of Bulk and Supported V-Mo-Te-Nb-O Mixed Metal Oxide Catalysts for Oxidative Dehydrogenation of Propane to Propylene. J. Phys. Chem. B, 2003. **107**: p. 6333-6342.

72.   Zhaorigetu B., L.W., Xu H. and Kieffer R., Correlation between the characteristics and catalytic performance of Ni–V–O catalysts in oxidative dehydrogenation of propane. Catalysis Letters 2004. **94** p. 1–2.

73.   Zhou R, C.Y., Yan S. and Fan K., Rare earth (Y, La, Ce)-promoted V-HMS mesoporouscatalysts for oxidative dehydrogenation of propane. Applied Catalysis A: General 2002. **236**: p. 103–111.

74.   Zhou R., C.Y., Yan S., Deng J., Liao Y. and Hong B., Oxidative dehydrogenation of propane over mesoporous HMS silica supported vanadia. Catalysis Letters 2001. **75**: p. 1–2.

VITA

Name: Hassan Saeed ALAsiri

Date & Place of Birth: December 22, 1982, Tabuk (Saudi Arabia)

Nationality: Saudi

Religion: Islam

Marital Status: Married

Educational Qualification:

- B.Sc. degree in Chemical Engineering King Fahd University of Petroleum and Minerals, Dhahran, Saudi Arabia (2006).

- M.Sc. degree in Chemical Engineering King Fahd University of Petroleum and Minerals Dhahran, Saudi Arabia (2011).

Present Address: Flat No 5110, Qatif Street, Al-Frduce Court, King Fahd University of Petroleum & Minerals, Dhahran, Saudi Arabia

Permanent Address: Al-Aoulaia Street, Al-Madena Road, Tabuk, Saudi Arabia

Email Address: has4u2@gmail.com or alasiri@kfupm.edu.sa

Telephone Number: 0504797960